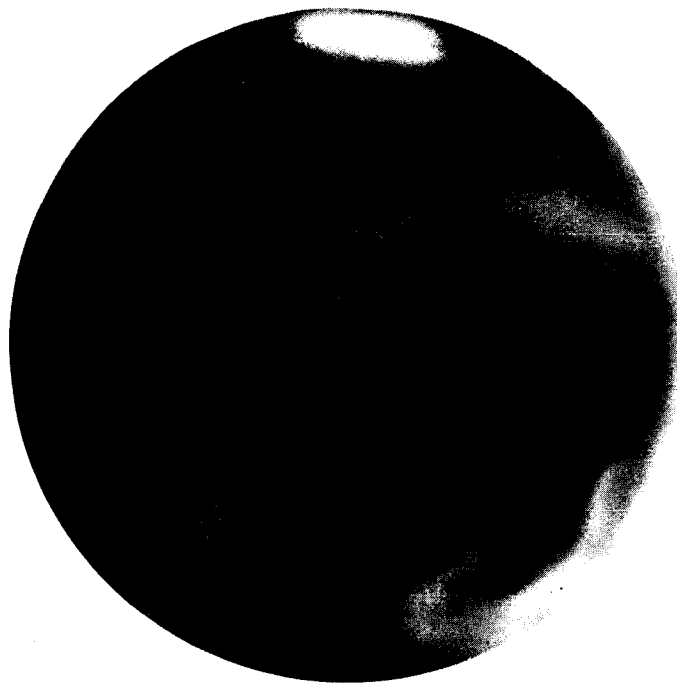


WOLF TRAP

MARS MICROBE DETECTOR

FINAL REPORT PREPARED FOR **The University of Rochester**



FACILITY FORM 802

N67-30742

(ACCESSION NUMBER)

98

(PAGES)

CR-85589

(NASA CR OR TMX OR AD NUMBER)

(THRU)

1

(CODE)

431

(CATEGORY)

B B R C



BALL BROTHERS RESEARCH CORPORATION

SUBSIDIARY OF BALL BROTHERS COMPANY INCORPORATED

BOULDER, COLORADO

FINAL REPORT

WOLFTRAP MARS MICROBE DETECTION DEVICE

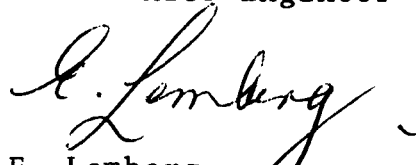
F66-09

Prepared for
UNIVERSITY OF ROCHESTER
Contract No. Nsg209-AG1
20 March 1967

Prepared by



L. Ried, Jr.
Electronics Engineer

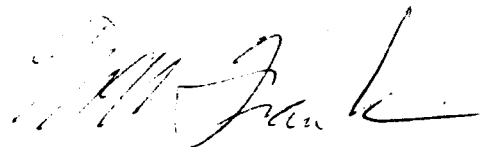


E. Lemberg
Research Engineer



D. E. Buckendahl
Project Physicist

Approved by



M. W. Frank
Project Engineer

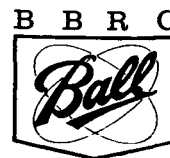


BALL BROTHERS RESEARCH CORPORATION

SUBSIDIARY OF BALL BROTHERS COMPANY INCORPORATED

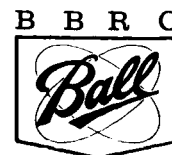
BOULDER, COLORADO

PRECEDING PAGE BLANK NOT FILMED.



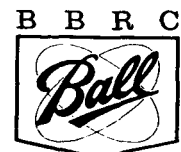
FOREWORD

This report is produced for the University of Rochester under agreement NsG-209 AG-1 entitled "Wolf Trap Microbe Detection Device" and constitutes the final report on tasks C and D, the Engineering Model and Checkout Console for the Engineering Model.



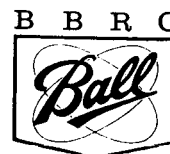
ABSTRACT

This report describes an engineering model of a microorganism detection device, intended eventually for a Mars landing. The model optically monitors turbidity resulting from organism growth in each of five separate enrichment cultures. A sensitive pH system provides corollary information on the acidity changes in each of the cultures. An aerosolized dirt inoculum is collected by a gas operated suction pickup located at the end of two spring ejected tubes. Electronic circuit design has been directed toward a typical assumed spacecraft interface. With few exceptions, overall design specifications required that the instrument withstand a strenuous launch environment. Ability of the overall device to withstand dry heat sterilization at 145°C is shown and, recommendations for engineering improvements in subsequent models are made in this final report.



CONTENTS

Section		Page
	FOREWORD	iii
	ABSTRACT	v
	ILLUSTRATIONS	ix
	TABLES	x
1	INTRODUCTION	1-1
2	STRUCTURE	2-1
3	PNEUMATIC SYSTEM	3-1
	3.1 System Description	3-1
	3.2 Pneumatic System Components	3-5
4	TURBIDITY DETECTOR	4-1
5	THE pH SYSTEM	5-1
	5.1 pH Measurement Errors	5-1
	5.2 Thermal Coefficient of Field Effect Transistors	5-3
	5.3 Electrometer Amplifier	5-5
	5.4 pH Probes	5-7
6	ELECTRONICS	6-1
	6.1 Data Format	6-1
	6.2 Data Transmission	6-3
	6.3 Event Sequence	6-3
	6.4 System Description	6-4
	6.5 Component Selection	6-12
7	CHECKOUT CONSOLE	7-1
	7.1 Console Description	7-1
	7.2 Console Control Description	7-3
	7.3 Automatic Data Recording	7-6
8	SYSTEM TEST	8-1
	8.1 Common Environmental Tests	8-2
	8.2 Electronics System	8-3
	8.3 pH System	8-10
	8.4 Structure and Pneumatic System	8-12
	8.5 Biological Testing	8-15
9	CONCLUSIONS AND RECOMMENDATIONS	9-1
	9.1 Conclusions	9-1
	9.2 Engineering Recommendations	9-2
10	REFERENCES	10-1
Appendix		
A	DETERMINATION OF NOZZLE CHARACTERISTICS	A-1
B	THE pH AMPLIFIER BIAS SAMPLE CALCULATION	B-1
C	VIBRATION TEST LEVELS AND TRANSMISSIBILITIES	C-1



ILLUSTRATIONS

Figure		Page
1-1	Wolf Trap Engineering Model - Front View	1-3
1-2	Wolf Trap Engineering Model - Back View	1-4
2-1	Experiment Structure	2-1
3-1	Pneumatic System Schematic	3-2
3-2	Pneumatic System - Front View	3-3
3-3	Pneumatic System - Back View	3-3
3-4	Gas Reservoir Assembly	3-5
3-5	Nozzle Assembly	3-6
3-6	Bellows Assembly	3-7
3-7	Pilot Reservoir System	3-8
3-8	Hopper Assembly	3-9
3-9	Manifold Assembly	3-10
4-1	Turbidity Detector	4-1
4-2	Turbidity Optics Diagram	4-2
5-1	Constant Temperature pH Probe Response	5-2
5-2	pH Probe Response with Temperature	5-2
5-3	pH Electrometer Amplifier Schematic	5-5
5-4	pH Probes	5-8
6-1	Event Sequence	6-3
6-2	Electronics System Block Diagram	6-5
6-3	Turbidity Amplifier Schematic	6-6
6-4	Lamp Regulator Schematic	6-10
7-1	Wolf Trap and Checkout Console	7-2
7-2	Console Interior	7-3
7-3	Console Front Panel	7-4
7-4	Data Recording Rack	7-7
8-1	Experiment in Vibration Test Fixture	8-2
8-2	Temperature Probe Calibration	8-6
8-3	Turbidity Channels 6, 8 and 9 Temperature Variation	8-7
8-4	Turbidity Channels 7 and 10 Temperature Variation	8-8
8-5	Nozzle Assembly Test Setup	8-12
8-6	Nozzle Test Results	8-13
C-1	Wolf Trap Vibration Notation	C-2
C-2	Sine Sweep Input Level to Bottle; Transverse X Axis	C-3
C-3	Transmissibility Plot of Bottle Bracket; Transverse X Axis; Input Level 2 g's	C-4
C-4	Transmissibility Plot of Bottle Bracket; Transverse X Axis; Input Level 10 g's	C-5
C-5	Sine Sweep Input Level to Hopper; Transverse X Axis	C-6
C-6	Transmissibility Plot of Hopper; Transverse X Axis, Input Level 2 g's	C-7
C-7	Sine Sweep Input Level to Hopper; Transverse Y Axis	C-8
C-8	Transmissibility Plot of Hopper; Transverse Y Axis, Input Level 2 g's	C-9
C-9	Transmissibility Plot of Hopper; Transverse Y Axis, Input Level 10 g's	C-10
C-10	Sine Sweep Input Level to Hopper; Thrust Z Axis	C-11
C-11	Transmissibility Plot of Hopper; Thrust Z Axis; Input Level 2 g's	C-12
C-12	Sine Sweep Input Level to Hopper; Thrust Z Axis	C-13
C-13	Transmissibility Plot of Hopper; Thrust Z Axis; Input Level 10 g's	C-14



TABLES

Table		Page
6-1	Data Format	6-2
6-2	Data Format	6-2
8-1	System Power Requirements	8-4
8-2	Housekeeping Data Temperature Stability	8-5
8-3	Environmental Test Effects on Turbidity Slide Measurements	8-9
8-4	pH System Temperature Stability with Nonautoclaved Probes	8-11
8-5	pH System Zero and Calibration Temperature Effects	8-11
8-6	pH System Temperature Stability with Autoclaved Probes	8-11
8-7	Biological Sensitivity Test Results	8-17



Section I INTRODUCTION

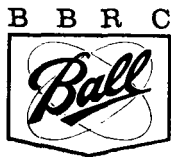
The instrument described herein represents the second generation instrument developed during an effort initiated in mid 1963. The device is a microbial life detection instrument intended for operation on the Martian surface. It has been dubbed "Wolf Trap" for the cognizant scientist, Dr. Wolf Vishniac, Professor of Microbiology, at the University of Rochester, New York. Dr. Vishniac has suggested that exploration of this form of life on Mars could be accomplished by a culture tube device containing suitable nutrient media, which could be monitored for changes in acidity and turbidity.

A conceptual breadboard model was constructed and tested (Section 10.1). This model demonstrated the feasibility of the detection concept. An extendable vacuum cleaner nozzle operated by a pressure gas source and venturi vacuum generator acquired a surface soil sample. Turbidity monitoring was provided by an optics train utilizing a miniature incandescent lamp and lens system which permitted only the light scattered by soil particles and the microorganisms to produce an electrical signal in a photodetector. The breadboard instrument was field tested in the Mohave Desert (Section 10.2) and showed promising microbial detection capabilities. The weaknesses detected appropriately altered the design approach to the second generation instrument.

At the start of the second development of the engineering model, there was no specific spacecraft interface specifications, although the model was to demonstrate the adaptability of the concept to flight hardware. Various NASA centers suggested guidelines for levels of environmental testing, and design specifications were established defining a device adaptable to a flight configuration with minimum modification, yet still flexible enough for extensive laboratory testing.

The broad objectives defined for this overall development are listed as follows:

- The instrument would be as small and light weight as possible to fit into a Martian lander.
- Minor deviations from true flight configuration would be allowed if they would facilitate repeated testing.
- The instrument would survive the anticipated long transit time from Earth to Mars.
- The instrument would have a fourteen day mission life after impacting the Martian surface.
- A common sample acquisition system would provide five separate culture cells. However, the concept would be extendable to as many as twenty culture cells.



- The instrument would survive twenty-four hour dry heat sterilization at 145°C.
- The device would withstand a harsh launching and landing environment.
- The sample acquisition system would provide the maximum amount of surface dust. This model would not limit the sample quantity distributed to each cell.
- Distribution of the dirt sample collected would be reasonably uniform between all culture cells.
- Range of the pH system would be from 5 to 9 pH units, but emphasis would be placed on producing a system having an overall stability of better than 0.1 pH units.
- The instrument, excluding electronics and optics, would withstand steam sterilization as much as possible.

The instrument produced as a result of the total development effort is shown in Figs. 1-1 and 1-2. This report discusses all subsystems of the engineering model and companion equipment used for instrument checkout and data presentation. Instrument performance during qualification testing is compared with design objectives, and recommendations for engineering improvements are offered.

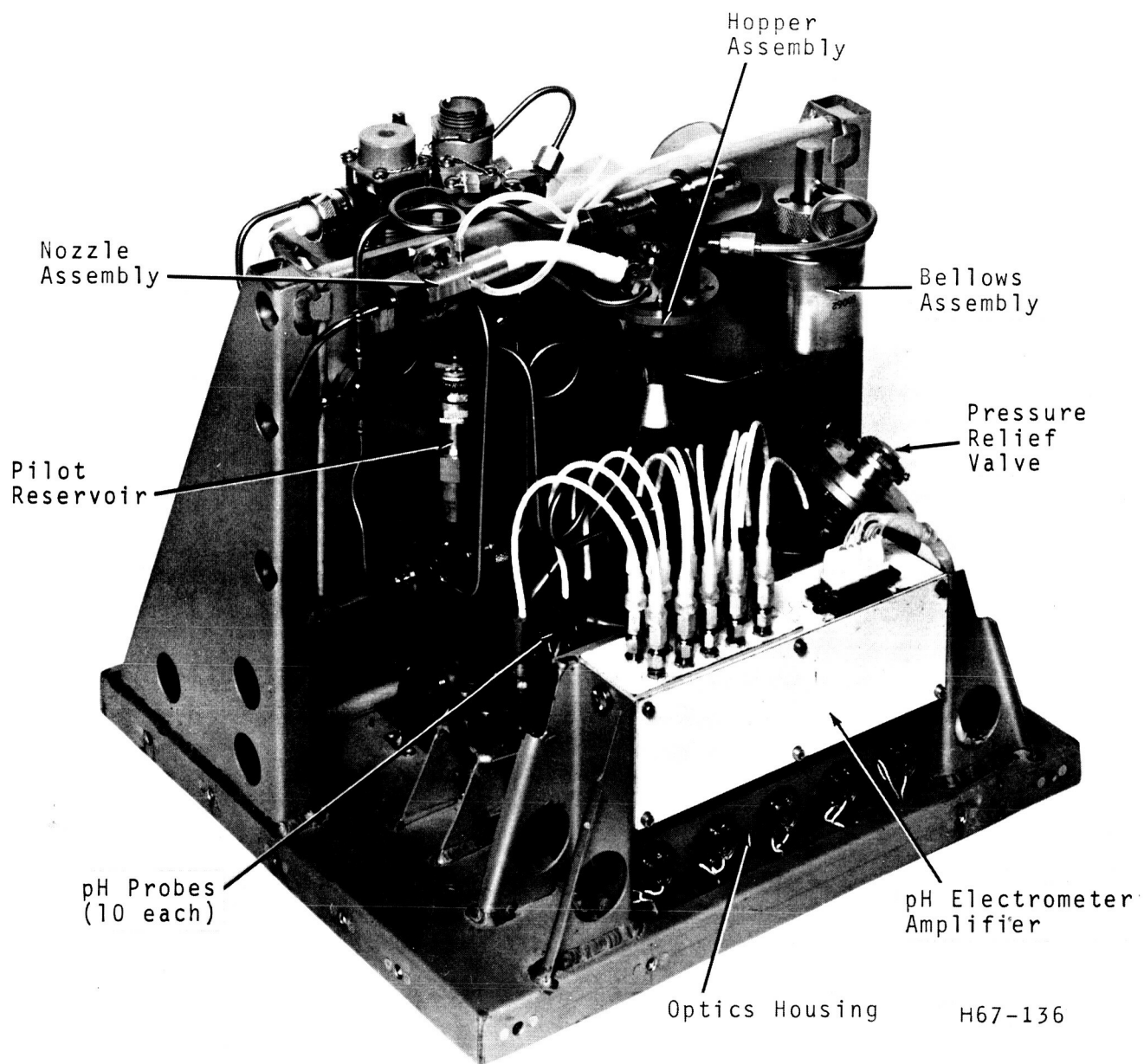


Fig. 1-1 Wolf Trap Engineering Model - Front View

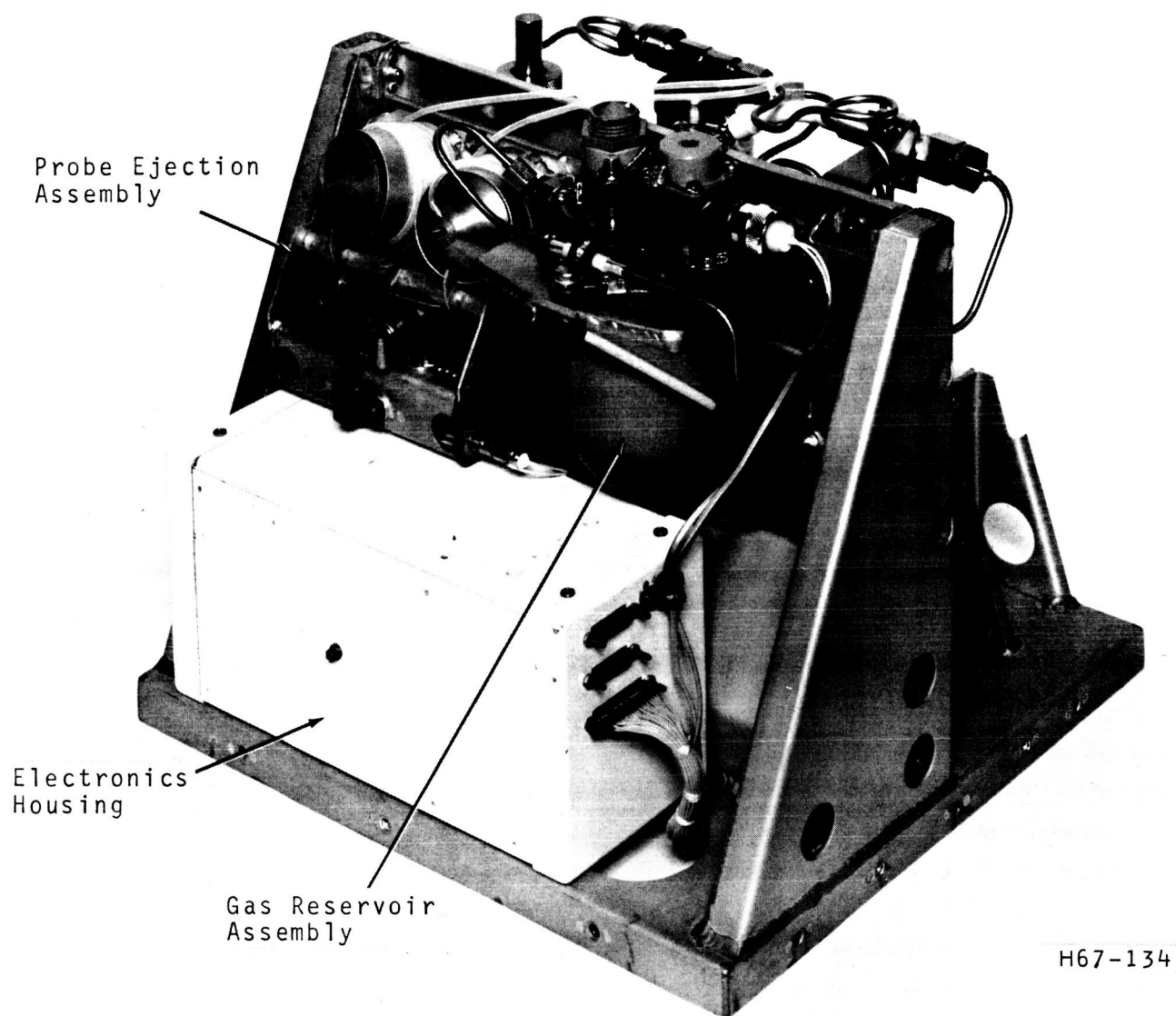


Fig. 1-2 Wolf Trap Engineering Model - Back View

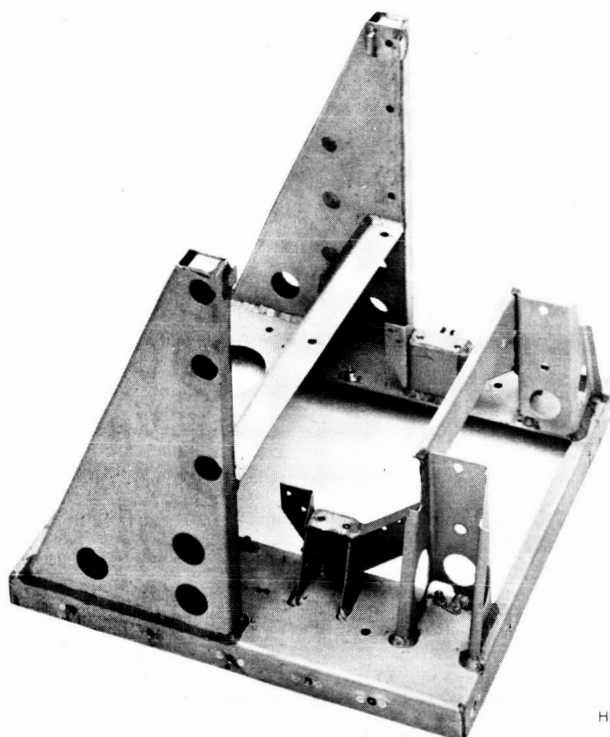
Section 2 STRUCTURE

The purpose of this second experiment structure is:

- (1) To integrate various experiment functional subassemblies into a compact overall package
- (2) To furnish a convenient attachment for spacecraft mounting

This experiment is composed of a number of self-contained subsystems, each capable of independent operation outside the structure. The design permits removal of any one subsystem without disturbing the others. The welded aluminum frame structure is designed to withstand the anticipated severe launch and landing loads. Design specification calls for axial loads of 200 g's and transverse loads of 100 g's.

The structure shown in Fig. 2-1 is a flanged, stiffened aluminum sheet base plate fitted with anchor nuts for peripheral attachment to an assumed spacecraft. The pneumatics assembly described in Section 3 is attached between the two tallest upright members shown in the figure. These are hollow box sections welded to the base plate and interconnected by a slanting welded shearweb. The area above the web is open for installation of the flat pneumatics mounting plate. This plate is secured to the



H67-135

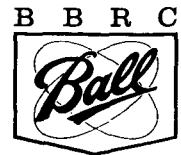
Fig. 2-1 Experiment Structure



uprights by three high-strength bolts per side. Close fitting pins pressed into the pneumatics plate transfer the horizontal shear to the shearweb. Guides in the upright members facilitate vertical removal of the entire pneumatics subassembly. To provide greater accessibility to the manifold assembly and the pH probes seen in Fig. 1-1, the upright members used for pneumatics attachment are not continued forward further than the pneumatics plate itself. The structure has sufficient redundancy to carry the transverse bending loads.

The main electronics control box is bolted directly to the base plate between the upright members and behind the fixed shearweb (Fig. 1-2). In front of the web are short, upright welded brackets which support the pneumatics manifold assembly. Further forward are raised brackets which support the pH electronics box. Both manifold and pH brackets straddle a large base plate cutout which accommodates the optical housing assembly attached underneath.

For maximum rigidity with minimum weight, all prime structure components and stiffeners are fabricated of formed welded aluminum alloy sheet. High strength screws and fixed anchor nuts attach all components and subsystems to the structure as well as attach the entire experiment to an assumed spacecraft adaptor. Although shear loads are not well distributed in riveted anchor nuts, these nuts are included to facilitate the removal and assembly of subsystems during laboratory testing.



Section 3

PNEUMATIC SYSTEM

This section describes the evolution of the pneumatic system and the components included therein. The terminology of component parts and subassemblies described here is continued in the following sections.

The pneumatic system collects surface soil particles and delivers these, together with water and suitable nutrients, into five bacterial culture cells. The entire system is dry heat sterilized to avoid contamination of the sample acquired for analysis. The system is operable on surfaces of varied characteristics and under conditions identical to those believed to exist on the Martian surface. The design specification calls for system operation in a 50 mb atmosphere which had been considered a reasonable value during the early stages of the program.

3.1 SYSTEM DESCRIPTION

The soil pickup concept is based on the miniature gas driven hypersonic nozzle-venturi combination which had been developed for the breadboard model (Section 10.1). This device generates a pressure considerably lower than ambient atmospheric pressure, which causes a flow of gas to be induced into the low pressure region at the nozzle efflux. This region is connected by flexible teflon tubing to collection probes ejected onto the surface to be sampled; consequently, the induced gases can carry dust particles through the probe orifices and into a collecting hopper for settling. The entire pneumatic system is shown schematically in Fig. 3-1. Figures 3-2 and 3-3 show the actual system components on the pneumatics mounting plate contained in the experiment structure. Previous experience with the breadboard model has indicated venturi sensitivity to back pressures when operating under Martian atmospheric conditions. Therefore, it is considered necessary to fully vent the hopper during times of sample induction even though some liquid is lost from boiloff.

Because a supply of compressed dry nitrogen gas is needed for nozzle operation, it is logical to utilize gas operated sequencing valves in other parts of the system. Each of the valves is spring-opposed to automatically return the valves to their original positions upon exhaustion of the gas supply. Valve reseating seals the entire system to prevent liquid boiloff.

Immersing the carrier tube outlet into sterilized water separates the induced dust from the gas carrier stream. This method is efficient and requires no elaborate baffling or filtering. The resultant bubbling in the water provides good mixing with uniform dust distribution throughout. Advantages gained by this separation method are somewhat offset by the rapid cooling resulting from the accelerated evaporation of water at Martian atmospheres. The fairly homogeneous volume of water-dust mixture is equally distributed into the five culture cells after percolating through separate dry nutrient media stored immediately above the cells.



Design specification requires equal distribution of water-dust into each cell with the instrument tilted in any direction from the vertical within 45 deg. Tests have been made on a gravity feed device providing five radially symmetric drain tubes at the bottom of a conical hopper which contains the dust-water mixture. The system was quite sensitive to orientation, so a secondary boost system has been developed to equalize the distribution. A dump valve at the bottom of the hopper opens rapidly, and gas pressure forces the water down the distribution tubes. The nutrient medium is inserted into each of the distribution tubes in teflon capsules; this offers some flow restriction to the water. Since all delivery tubes have approximately the same capacity and since the nutrient restricts the water flow, the pressurized system delivers equal volumes of metered water into the culture cells. Tests have shown that the system is still slightly attitude sensitive, but much less than before.

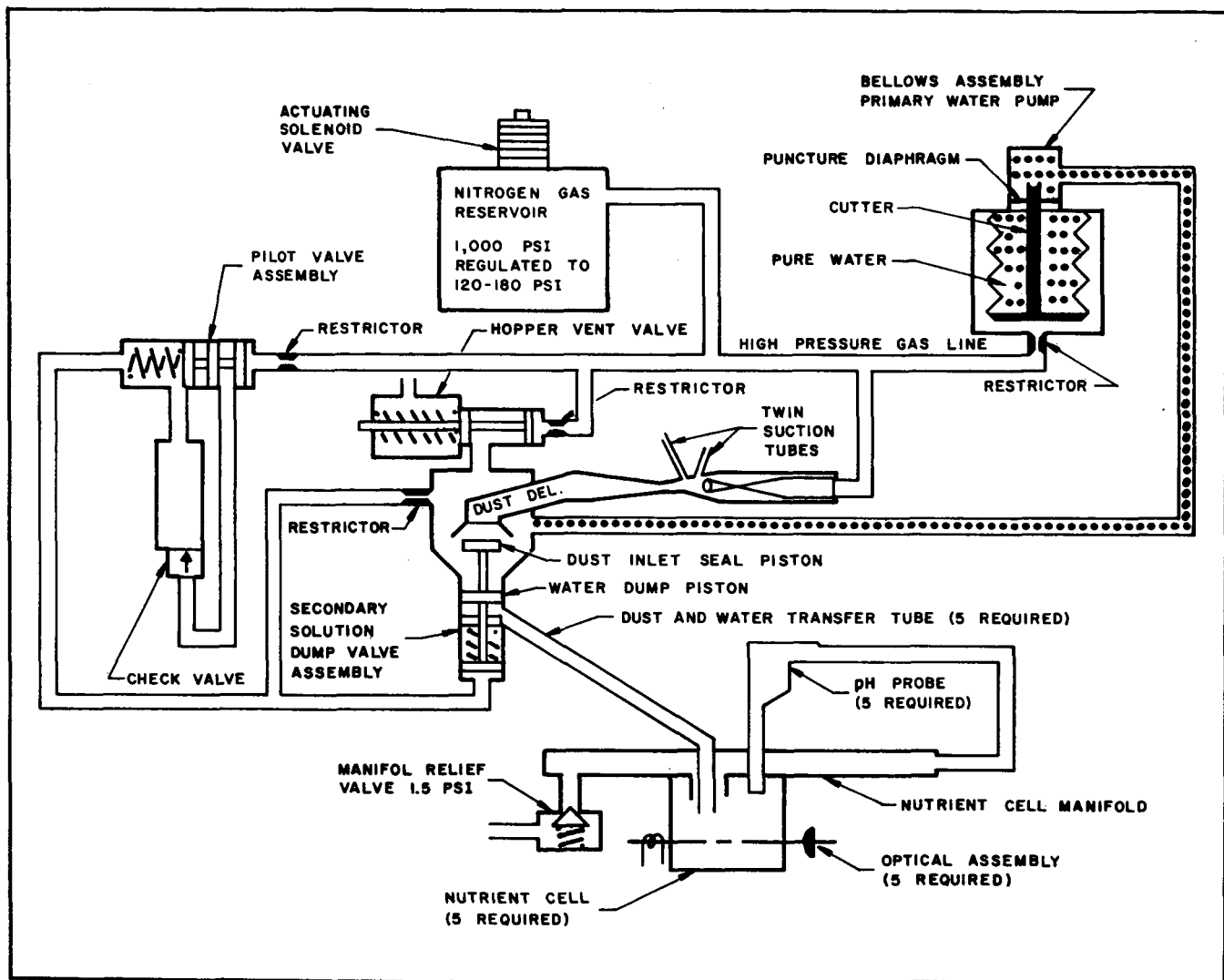


Fig. 3-1 Pneumatic System Schematic

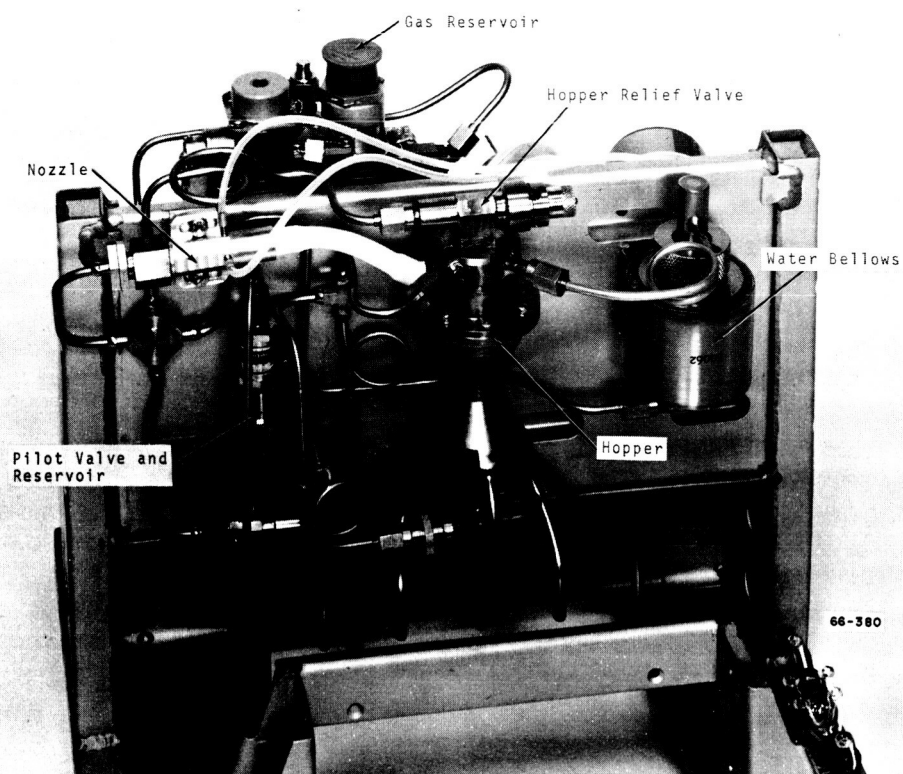


Fig. 3-2 Pneumatic System - Front View

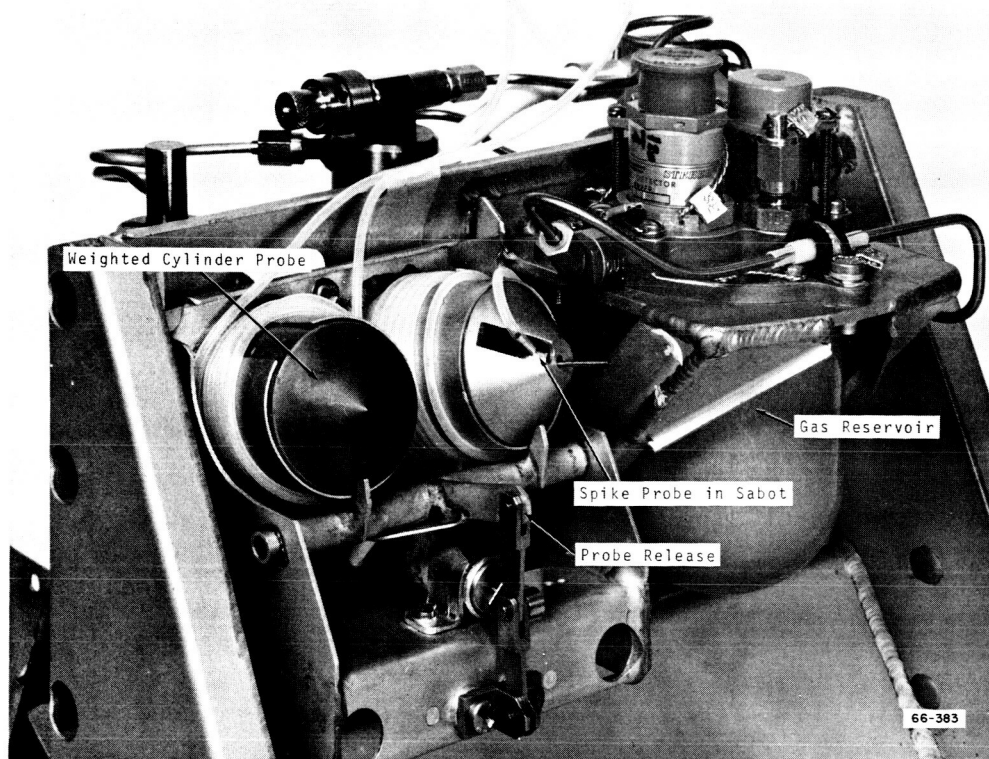


Fig. 3-3 Pneumatic System - Back View



An auxiliary pilot valve provides gas pressure for the booster system. Because the gas needed for this function is supplied after exhaustion of the main reservoir (after venturi operation) an auxiliary reservoir contains a portion of the pressurized gas until completion of the venturi induction period. The pilot valve then actuates and provides rapid activation of the water hopper dump valve; it also pressurizes the hopper interior to drive out the water.

System operation in a low pressure Martian atmosphere requires sealing to prevent water loss during the intended two-week mission life. Although water vapor pressure at the maximum operating temperature of 40°C produces low pressure differentials, every removable system joint must be sealed gas tight with "O" rings capable of withstanding the dry heat sterilization.

When the venturi nozzle depletes the gas supply, various venting valves are returned to their original positions to seal the system against water boiloff. The spring loaded valves, no longer held back by the high pressure gas, return to their sealing positions. By controlling spring rates and various metering orifices, it is possible to control the valve operation sequence. Figure 3-1 shows the function sequence as listed below:

- Hopper vent valve closed
- Bellows relaxed to original position
- Pilot valve closed to release high pressure gas stored during open period
- Auxiliary reservoir gas dumped into auxiliary pressure lines
- Hopper dump valve driven upward, sealing the dust delivery tube and permitting water-dust mixture flow into the culture delivery tubes
- Valve locked into the up position by a spring loaded latch which engages a groove in the piston shaft
- Gas pressure slowly supplied to the hopper to drive the water-dust mixture down the tubes

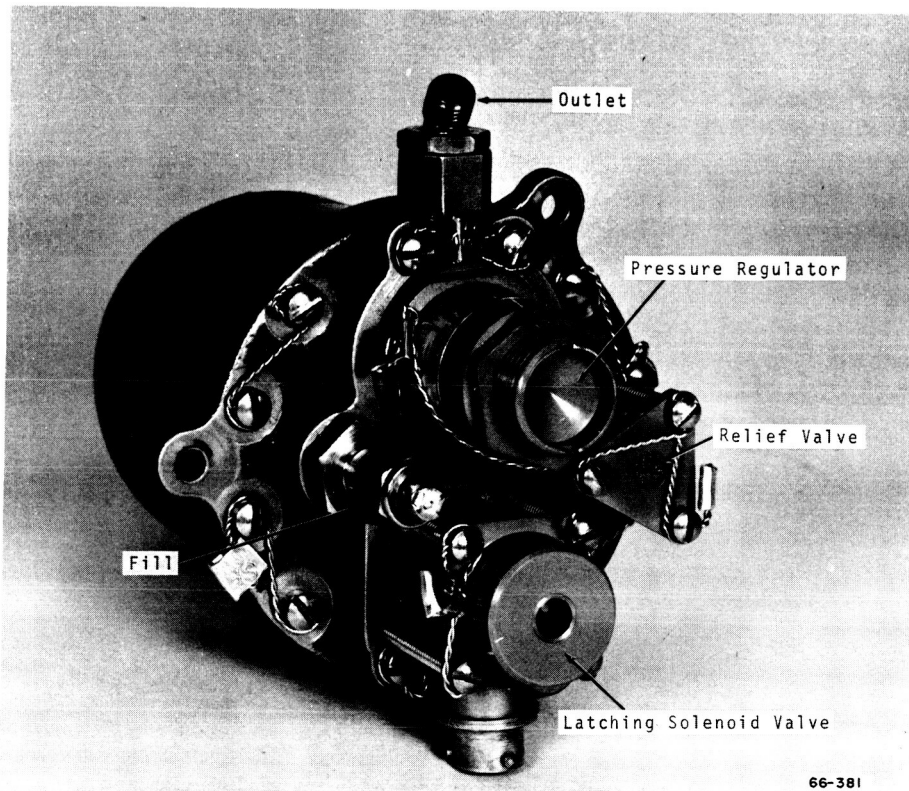
The corrosive nature of the specified nutrient media requires carefully selected material. A titanium alloy, 6Al-4Va, has been selected for the culture cells and hopper systems which closely contact corrosive materials. This alloy has both high strength, light weight (0.57 times the density steel), and remarkable inertness to many corrodents. Permanent joints are welded to provide reliable leak proof attachment. Other joints have "O" ring seals to facilitate disassembly for cleaning.

3.2 PNEUMATIC SYSTEM COMPONENTS

3.2.1 Gas Reservoir Assembly

The gas reservoir provides regulated high pressure gas for operation of the pneumatic system. The assembly, manufactured and tested by Sterer Engineering and Manufacturing Company to BBRC specifications, is shown in the Fig. 3-4. The package consists of a 13 in.³ cylindrical reservoir attached to an end plate which houses a filling check valve, a latching solenoid gas valve, an over-pressure relief valve, and an adjustable pressure regulator. The entire assembly weighs 1.28 lb. Adjustment from the gas regulator loading spring provides pressure outputs from 130 to 210 psig.

The reservoir volume provides 5 min nozzle operation at 130 psig, and about 3 min at 210 psig. The former pressure produces optimum venturi operation in Martian atmospheres, while the latter pressure produces an equivalent suction in earth atmosphere (Appendix A). Because experience with the bread-board model has shown that a 30 sec venturi operation is sufficient to produce a good sample, the lengthy operation times available from the reservoir are included only to allow ample time for laboratory evaluation between reservoir charges.



66-381

Fig. 3-4 Gas Reservoir Assembly



3.2.2 Nozzle Assembly

The nozzle assembly contains all components of the venturi which provide the low pressure for sample induction. The assembly shown in Fig. 3-5 consists of the nozzle, the nozzle mount, and the venturi block fitted with a locking sleeve to provide lateral adjustment for optimum suction. Twelve nozzles hand drawn from Pyrex glass provide a convenient method of experimenting with nozzle shapes. Derivation of the nozzle operating Mach number and mass flow rate were developed for the breadboard model (Section 10.4). The engineering model nozzle has orifice and exit diameters of 0.006 and 0.0315 in. respectively. The entrance/exit area ratio was 27.5:1 which produces a nozzle Mach number of 5.1.

Gas attachments to the nozzle assembly are seen in Fig. 1-1. High pressure input is supplied through titanium alloy tubing welded to the nozzle mount. Metal tubes pressed into the nozzle block provide two low pressure taps. Teflon tubing with an 0.07 in. diameter connects the assembly to the probe eject mechanism.



Fig. 3-5 Nozzle Assembly

3.2.3 Bellows Assembly

The bellows assembly contains pure water during the dry heat sterilization and during transit time to Mars; it also delivers the water to hopper during pneumatic system activation. The assembly shown in Fig. 3-6 contains a nested stainless steel bellows, hermetically sealed into an outer cylindrical pressure vessel. The innermost end of the bellows contains a removable hollow cutter shaft which high pressure gas within the containing vessel forces away from its seated position and forces through an aluminum puncture disc. The disc is sandwiched between two "O" rings and is secured by the cutter housing. Water flows through the hollow shaft and out to the hopper assembly through the coiled stainless steel tube.

The water storage portion of the assembly is designed to withstand the approximately 76 psi pressure generated during the 145 deg heat sterilization cycle. The nested metal bellows are built to withstand axial crushing at pressures up to 300 psi. Maximum water volume is 15cc with sufficient allowance for an internal air bubble which serves as an expansion cushion during heating.

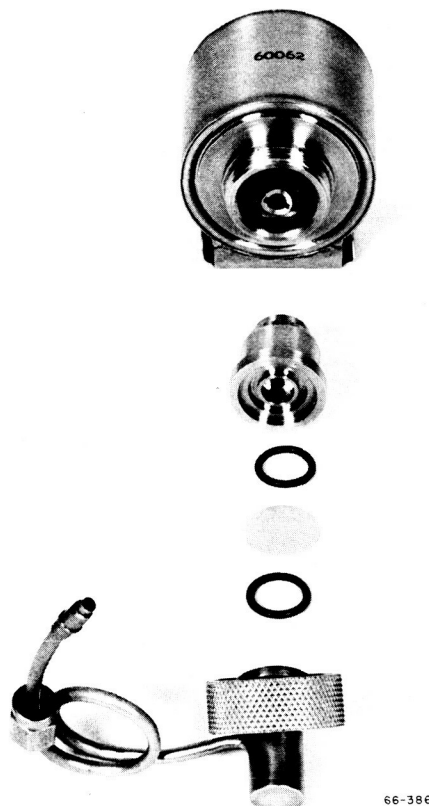


Fig. 3-6 Bellows Assembly

3.2.4 Pilot Reservoir System

The pilot reservoir system retains a small volume of high pressure gas until the main pressure reservoir is exhausted; the system then supplies the gas to the auxiliary water dump system. The pilot system shown in Fig. 3-7 consists of the pilot valve, the input check valve, and a pilot reservoir. The pilot spool valve has three annular grooves and operates within the valve body to open and close cross drilled ports. Port edges in the body are chamfered to prevent damage to the sliding "O" rings.

Upon input line pressurization from the main gas reservoir, the spool valve depresses the return spring and opens the inlet port to permit filling the pilot reservoir through the check valve. When the main gas reservoir is exhausted, the valve return spring moves the spool to its original position and opens the outlet port to release entrapped gas to the water dump system.

3.2.5 Hopper Assembly

The hopper assembly shown in Fig. 3-8 consists of split, matching upper and lower parts to which are attached the hopper vent valve, the water dump valve, and five water distribution tubes. The assembly is split to facilitate cleaning. All parts are made from the 6A1-4Va titanium alloy to minimize weight and to withstand possible high vibration acceleration loads caused by the hopper being far removed from the experiment point of attachment to the spacecraft. The hopper vent valve spring returns the valve and seals the hopper at about 40 psi. Also at that pressure, the pilot valve releases the stored gas into the

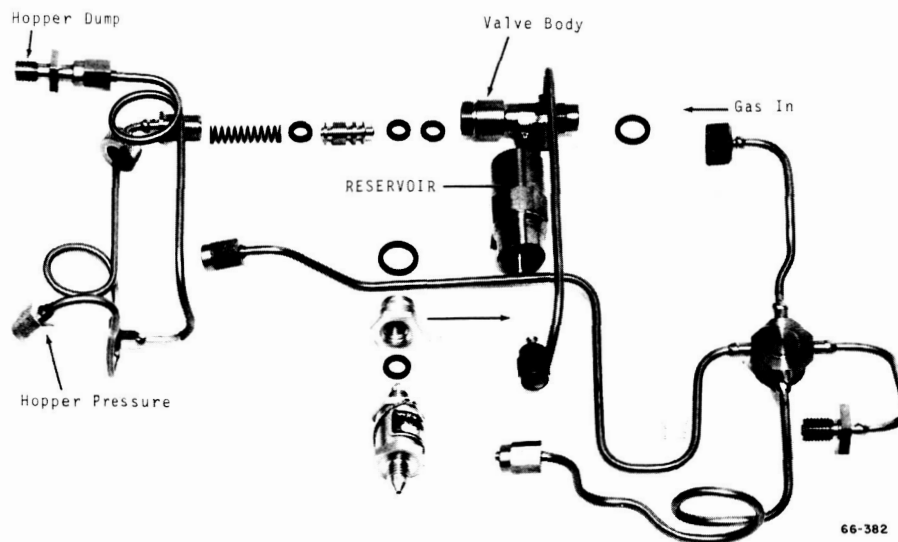


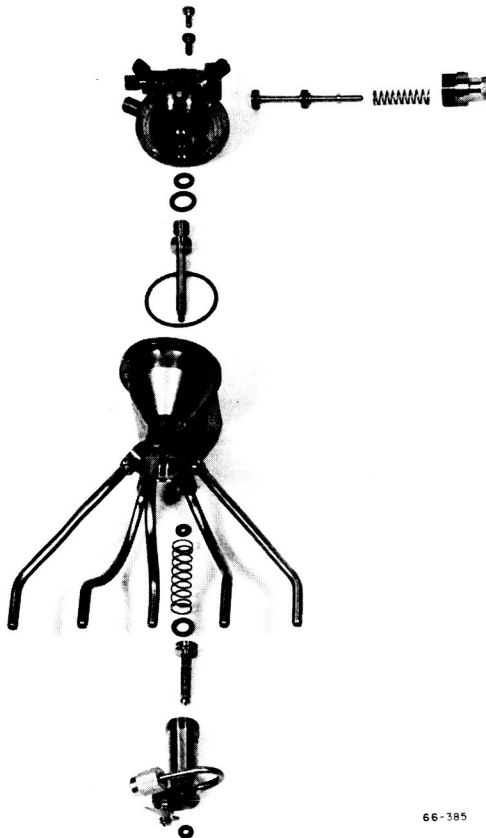
Fig. 3-7 Pilot Reservoir System

hopper to initiate liquid dump. The dump valve is spring loaded to hold the piston closed during launch vibration. Gas pressure forces the piston up, and a spring loaded latch retains the valve in the up position.

3.2.6 Valve Design

To insure gas tight seals at the relatively low system pressure differential of 1.5 psig, special design parameters for "O" ring grooves are necessary. Experimentation has shown an optimum design which provides a 0.004 in. internal and external ring compression. Too little compression causes unreliable sealing, while excessive compression produces piston jamming.

The "O" rings are used primarily for static application, while two-point contact quadrings are used for all moving pistons. Sealing rings are made of either Viton "A" (trademark) or silicon rubber to withstand the heat sterilization. All rings are lubricated with high vacuum silicon grease.



66-385

Fig. 3-8 Hopper Assembly

3.2.7 Manifold Assembly

The manifold assembly shown at the bottom of Fig. 3-9 provides attachment points for the hopper water transfer tubes from above and for the culture cells from beneath. The manifold provides common venting to each culture cell at a point much higher than the maximum culture liquid height. A silicon rubber diaphragm pressure release valve fixes the maximum system pressure at 1.5 psig. An "O" ring sealed plug at one end of the manifold and the removable elbow pressure tap at the other end provide convenient access for cleaning the manifold. The tap pressurizes the space above the electrolyte in the reference pH probes (Section 5) to the same pressure as that above the culture liquid.

The hopper water transfer tubes are sealed to the manifold by threaded sleeves containing "O" ring seals. The transfer tubes fit on the top of teflon capsules containing the nutrient media. The water-dust mixture from the hopper then has to percolate through the nutrient before passing into the culture cell. The water passed down through a small diameter tube to the cell which is vented through the annular space around the tube.

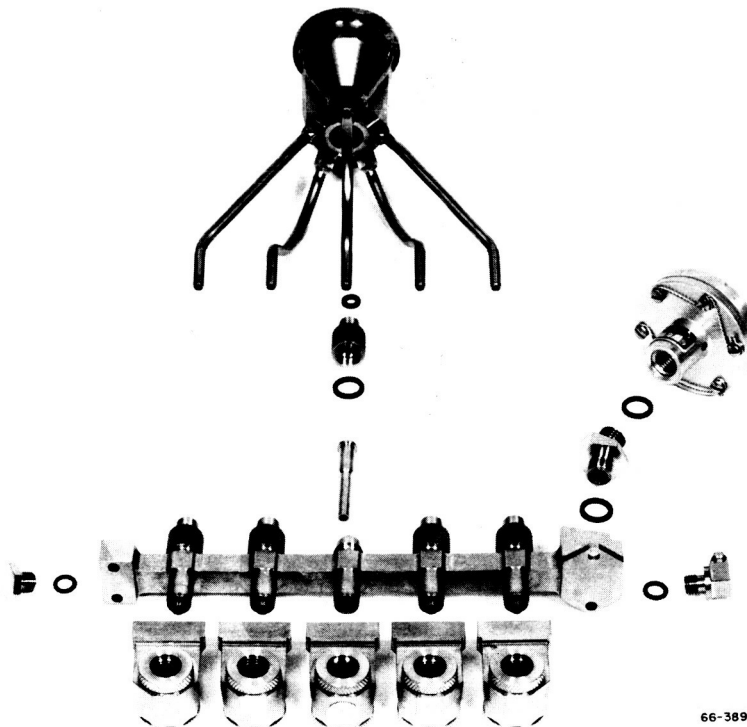
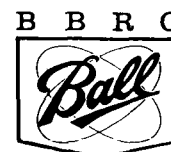


Fig. 3-9 Manifold Assembly



The titanium alloy culture cells provide cell attachment to the manifold, pH probes immersion in the culture liquid, and transparent end windows for optical determination of turbidity. Internal "O" rings in the three top holes provide pressure tight sealing against the pH probes and manifold. The transparent end windows are high quality fused quartz polished to minimize surface scratches. The windows are sealed by circumferential quadrings deformed by pressure loading of the screwon sleeves acting through spacer rings.

3.2.8 Probe Ejection System

The probe ejection system shown in Fig. 3-3 provides automatic ejection of two vacuum lines on to the surface to be sampled. The extended configuration of the probes is shown in Fig. 7-1. Two teflon tubes connected to the venturi nozzle assembly are coiled around the probe containing canisters. Weighted metal probes which place vacuum apertures close to the sampling surface (regardless of terrain characteristics) are fitted to the tube ends. Two types of probe fittings have been developed to assure better collection reliability.

The larger probe has a counter weighted cylindrical body which always rolls to the same position with the entrance apertures pointing downward. The four apertures are small holes, interconnected by a tangential tube which projects out the rear of the probe for attachment of the teflon suction hose. The counter-weight is designed so that its restoring couple on hard ground can overcome the torsional rigidity of the teflon hose.

The smaller probe consists of a symmetric four-armed spike made of small diameter stainless steel tube. At least one tube end is always in close proximity to the sampling surface regardless of contour. The probe is enclosed in a split sabot which provides a convenient spring loading surface for the awkward spiny probe.

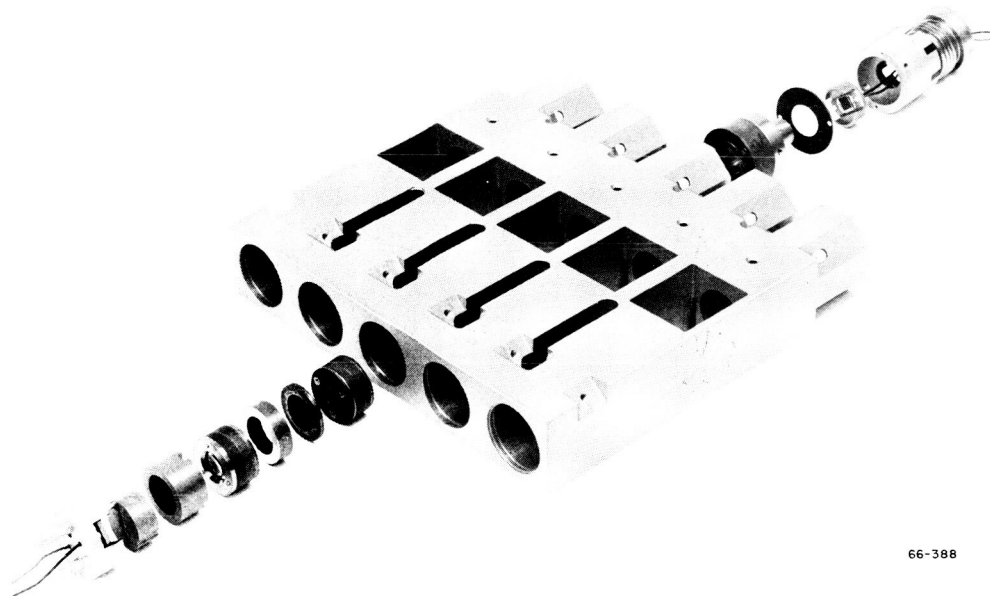
After the teflon suction hose has been coiled around the outside of the containing canister, both probes are installed into the canisters against a spring load. The probes are secured by an overtop dead-center latch linkage. Probe ejection is actuated by a centrally mounted release solenoid which kicks the latch mechanism over dead-center.

Section 4

TURBIDITY DETECTOR

The turbidity detector is an electrooptical device which produces an electrical signal when light passing through a turbid liquid is scattered by the small particles contained in that liquid. It has been shown (Section 10.3) that the nature of the scattered light (i.e., the direction and intensity with respect to the originating light rays) is highly dependent on such factors as illuminating light wavelength, particle size and index of refraction, and the index of the matrix containing the particles. However, the preferential scattering direction results in what can be called a forward lobe, for translucent organisms of about one micron size in an aqueous culture. Most of the scattered light in the lobe appears within a cone of 20 deg from the direction of the illuminating light. The engineering model turbidity detector is an arrangement of lamps, lenses, and photodetectors, all designed for maximum sensitivity.

The location of the turbidity detector in the overall instrument is shown in Fig. 1-1, and an exploded view of the optics housing is shown in Fig. 4-1. The complete assembly consists of the optics housing attached to a sheet shelf (not shown in the figure) which provides screw attachments to the main structure and which contains a wiring junction box to receive all electrical connections from the detector lamps and photodetectors. The five square holes in the center of the housing accommodate the cells containing the test cultures. Transparent end windows on each end of the culture cells permit straight through viewing of the inline optics train.



66-388

Fig. 4-1 Turbidity Detector



The optics housing is made from a single billet of aluminum; this provides maximum structural rigidity. Coaxial alignment of the optics systems must be maintained precisely with thermal variations. The reasonably symmetrical aluminum structure around each optics train prevents differential expansion of the housing. Because one of the design goals is to permit steam autoclaving of as much of the instrument as possible, the optics assembly, including wiring and connectors, is readily detachable from the main structure. Water condensation within the optics during autoclaving produces lens surface spotting and thus causes excess scattered light.

A diagram of the optics train used for each of the five cells appears in Fig. 4-2. The tungsten lamp, burning at approximately 2,100°K, provides illumination for both the lamp monitor photocell and the condenser lens system. The lamp photocell automatically maintains the lamp intensity at a fixed value determined by the input network of the regulator amplifier. The condenser lenses focus an image of the lamp filament on the aperture plate which contains a 0.011 in. diameter hole. The illuminated aperture serves as the source for the collimator which beams parallel light rays through the transparent end windows of the cell. The imaging lens system focuses undeviated light passing through the culture on to the image occulting disc that is the same size as the image aperture. The disc blocks the nonscattered light from the signal photocell located immediately behind the disc. Lens aberrations, scratched cell windows, and smudges lenses all produce stray light which appears as a fixed background signal. Light ray deviations within the culture cell, due to soil particulates and microorganisms, miss the occulting disc and are converted to an electrical signal in the photocell. The photocell electrical signal is then

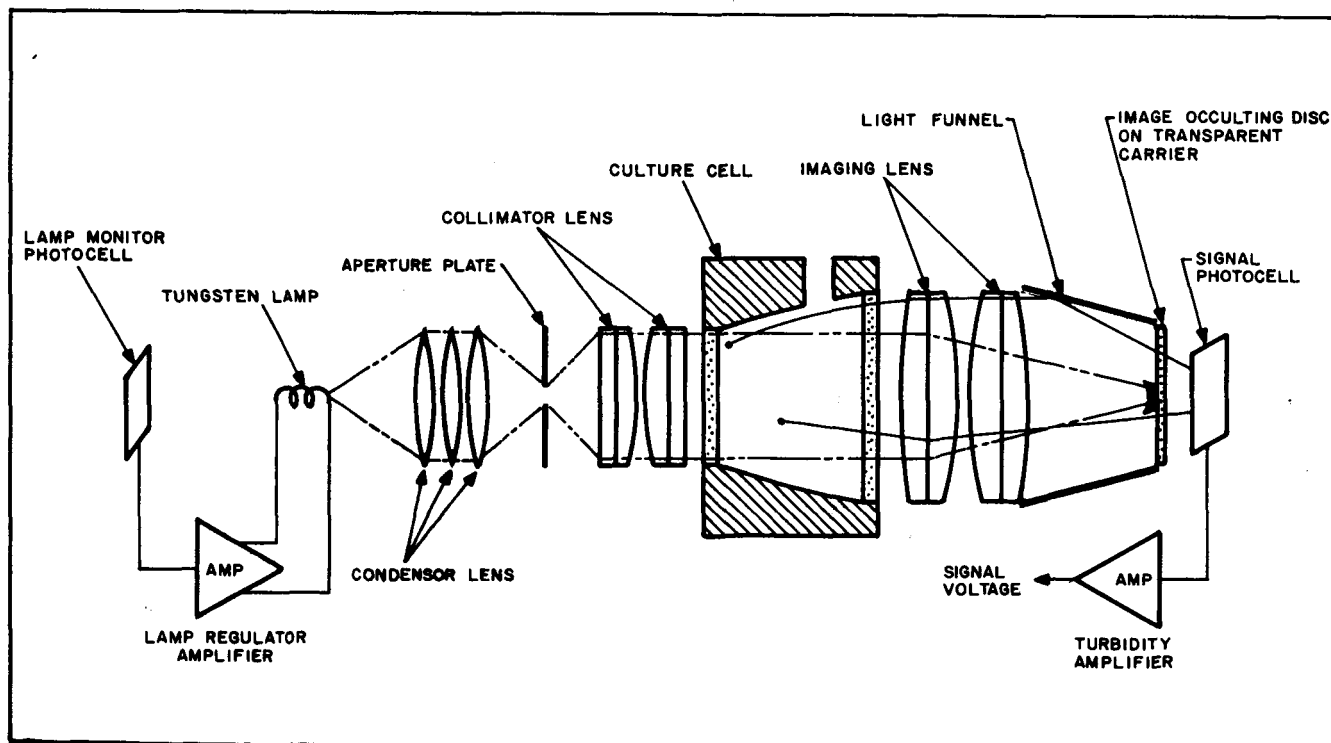
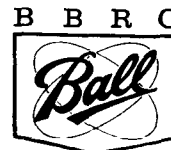


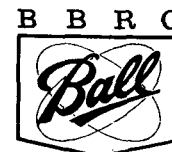
Fig. 4-2 Turbidity Optics Diagram



conditioned by the signal amplifier and made available as a voltage output. The actual optical components in the same orientation as the sketch are seen in Fig. 4-1. The three lens assemblies appear as cartridges held together with screws. The two cylinders on the left side provide the correct spacing for optimum focusing of condenser and collimator.

All lens systems are made from readily available commercial items, none of which are affected by heat sterilization. The condenser consists of three air spaced lenses and provides a lamp filament image 20 percent larger than the aperture hole. The lamp filament is a straight helix, tautly suspended between two upright posts. The condenser system views this obliquely to provide a nearly point source of light which, however, stretches out along the optic axis. The collimator is a symmetric pair of air spaced acromats. Interelement cement is a high temperature silicon jell which has been developed principally for optical coupling of photomultiplier tubes. The imaging system is also a symmetric pair of air spaced acromats, but they are larger in diameter and have a high temperature polymer cement. The large imaging lens, in conjunction with the polished light funnel, permits light scattered by organisms in all parts of the culture volume to be intercepted by the imaging system and reflected onto the signal photocell (Fig. 4-2). The conical interior of the culture cell is highly polished for good reflectivity, but considerations in the pH system require that the cell interior be coated with a less reflective insulating material (Section 5).

As has been previously stated, the lamp monitor photocell and associated circuitry are to keep a constant source illumination from the tungsten lamp. Because the red wavelength spectral response of the photocell (a diffused junction silicon solar cell) varies with temperature, the actual lamp brightness decreases as the system temperature is increased. This is due to the enhanced high temperature response of the photocell which requires that the lamp brightness be diminished to maintain the same current input into the regulator amplifier. Both signal and lamp monitor-photocell maintain at the same temperature by the heat conductivity of the aluminum used for the optical housing. Variation in lamp brightness with temperature does not affect the usable signal output from the system, because the signal photocell response changes identically with that of the lamp monitor. The absolute spectral response of a number of identical cells have been compared, and carefully selected pairs of cells have been chosen for use in each optics train. Cell response is between 4,000 and 12,000 Å, with peak response at about 8,500 Å.



Section 5

THE pH SYSTEM

This section describes the measurement technique required for pH monitoring and the circuitry developed to accomplish this. Also discussed are problems encountered in the performance of commercially available pH probes.

The purpose of the pH system is to monitor acidity changes in the bacterial cultures, thereby providing corollary information to turbidity data. The original design objectives required a system that had a total drift of less than 0.1 pH units, and which was capable of withstanding the dry heat sterilization. The required range of this original system was from 4 to 9 pH units with an accuracy of 0.25 pH units. But slight changes in acidity indicate changing conditions, so design emphasis is now based on stability rather than accuracy.

It was apparent early in the design that pH probes capable of dry sterilization are beyond the state-of-the-art. So the sterilization requirement has been modified. Probes are now sterilized by means other than heat. The use of nonflight qualified items also are allowed. Preliminary evaluation of commercially available silver-silver chloride probes indicated that these devices could survive stream autoclaving. Successive autoclaving during system testing seriously degraded probe performance.

There are no provisions for calibrating the pH probes against a standard buffer. Since the design now emphasizes stability rather than accuracy, offset voltage differences between probes are permissible. Nevertheless, system gain should be linear enough to provide the 0.1 pH unit stability.

The pH system is seen in Fig. 1-1 as ten glass probes interconnected to their electronic circuitry by white cabling. A probe set for each culture consists of the smaller diameter glass pH probe and the larger reservoir type reference probe. The system connects to the main electronics circuitry through the connector on top of the white pH circuit housing box (Section 6).

5.1 pH MEASUREMENT ERRORS

pH measurement is accomplished by measuring the voltage output out of the high source impedance probes. An electrometer amplifier conditions the signal and presents the amplified voltage to the data processing system. Measurement errors are caused by nonlinear effects in the probes and by thermal instabilities of probes and amplifier (Section 10.4). The amplifier effects are considered in following sections. The probe effects are discussed below.

A typical pH probe response curve at constant temperature is shown in Fig. 5-1. The linear curve is given by the expression

$$E(T) = E_0(T) + k(T) \text{ ph} \quad (5.1)$$

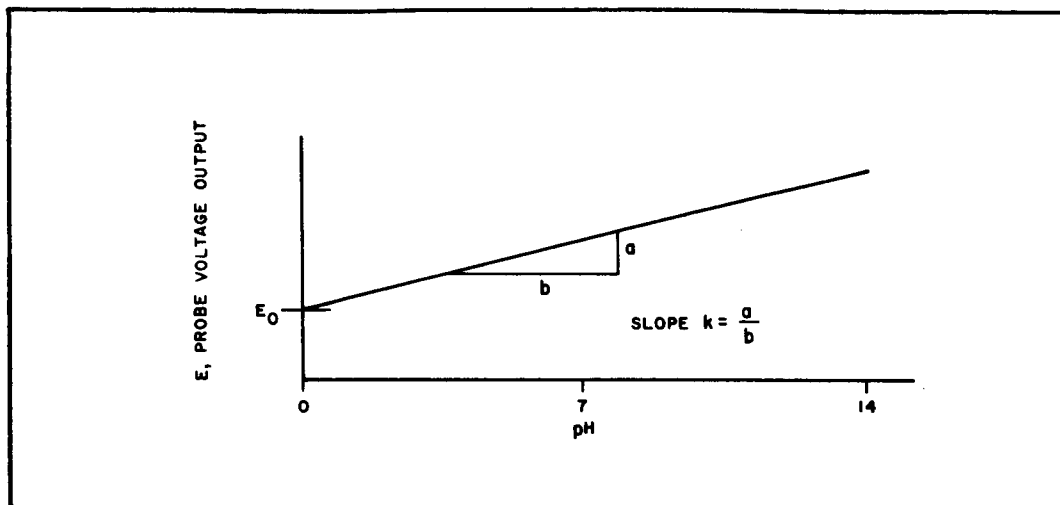


Fig. 5-1 Constant Temperature pH Probe Response

where

E is the indicated pH reading in millivolts

$E_0(T)$ is the standard reference potential of the electrode combination expressed in millivolts

$k(T)$ is the slope of the curve expressed in millivolts per pH unit

$k(T)$ and $E_0(T)$ are written as functions of temperature

$k(T)$ has a linear coefficient of about $+0.2 \text{ mv}/^\circ\text{C}$, while $E_0(T)$ is a quadratic function expressing internal cell voltage. The effect of these coefficients on actual pH curves is shown in Fig. 5-2.

Because $E_0(T)$ is a quadratic function and $k(T)$ is a linear function, the curves intersect at a loosely defined point called the pH isopotential (pH_{iso}). Temperature compensation of slope changes simply re-

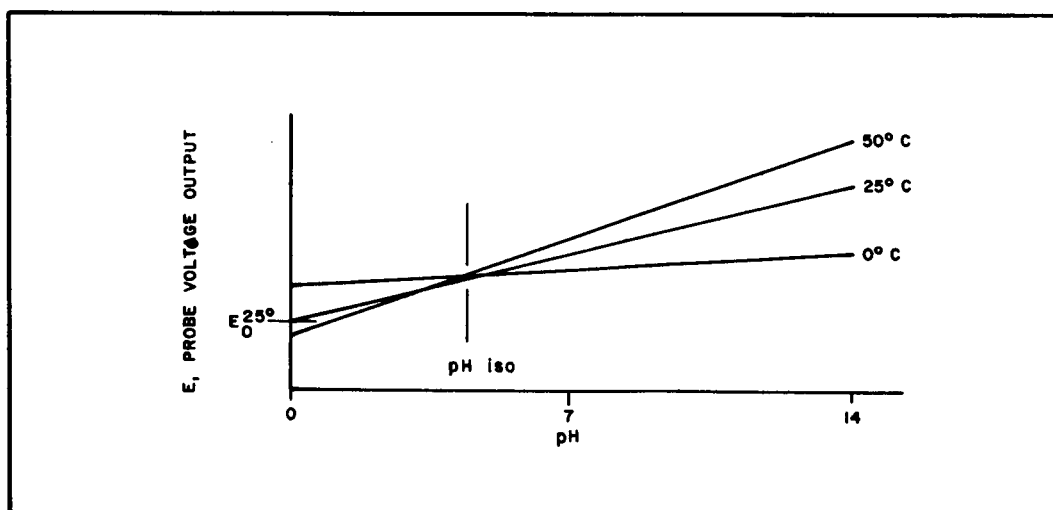


Fig. 5-2 pH Probe Response with Temperature



quires an offsetting linear coefficient in the amplifier. The nonlinear $E_o(T)$ is approximately corrected by biasing the amplifier so that the temperature stable pH_{iso} point becomes the offset, as shown by

$$E = K + k (pH - pH_{iso}) \quad (5.2)$$

where

K is a coefficient independent of temperature.

A linear coefficient may then be used to correct the offset change. Preliminary tests of commercial quality probes have shown considerable reference potential change with temperature, while the probes actually used have had very small change. However, these temperature effects are relatively small, so temperature compensation (to stay within the 0.1 pH stability requirement) is not necessary.

Another source of measurement error has been the IR drop caused by probe currents and the high internal impedance of the probes. To minimize the effect, the amplifier has an input resistance considerably higher than the source resistance of the probes. Since typical probe resistance ranges from 100 to 500 meg, the amplifier has an input resistance of about 10^6 meg; this maintains the loading effect at about 0.02 percent. The probe impedance also doubles at about every 7°C drop in temperature. A typical probe has a source impedance of 200 meg at 25°C but increases to 2,600 meg at 0°C . However, this effect is minimized by reducing the input transistor leakage with lowered temperature; this doubles the amplifier input resistance every 10°C (Section 5.2). The net IR drop changes with temperature are negligible.

5.2 THERMAL COEFFICIENT OF FIELD EFFECT TRANSISTORS

5.2.1 Preliminary Testing

During the early design of the pH system, the choice of probes had not been made, but work was started on amplifier development. Two types of field effect transistors (FET) were considered for the amplifier input stage: (1) junction type, and (2) P-channel enhanced metal oxide silicon (MOS). Parallel development effort commenced to evaluate both type devices for the specific application.

5.2.2 Test Results

MOS transistors have the apparent advantage in the application because of their greater than 10^{14} ohms input resistance. However, the devices are surface controlled, and charge perturbations with accompanying noise levels are very high. Considerable care must be taken to prevent input charge from breaking down the glass insulated input gate. Literature indicates that punch-through permanently destroys the device. More disturbing is the fact that some evaluation units experienced partial punch-through appearing



only as a loss in input impedance. This type of damage is likely when high source resistant devices are used. Input gate damage was experienced when the surface charge on a technician's hand exceeded the 60 v breakdown voltage that occurs with the use of a 10^8 ohms test source.

Furthermore, MOS FET's have unpredictable thermal coefficients. A negative compensating coefficient from the amplifier is needed to offset the positive coefficient of the pH probes. The MOS devices apparently have only a positive coefficient. The coefficient diminishes to near zero at 40°C; it depends on input bias at low temperatures.

Complete evaluation of the MOS devices was abandoned to permit development of the junction devices within the schedule constraints. At that time, there were only a few junction FET's commercially available with leakage currents sufficiently low to provide a 10^{12} ohms input resistance. A P-channel device, the 2N3112, was selected for the input stage. These transistors have low noise, stable operating parameters and a predictable thermal coefficient. The input gate junction coefficient is negative and fixed, while a positive coefficient exists because of drain channel resistance variation with temperature. The positive coefficient is a function of drain channel current and is adjustable by setting the input bias. Adjustment of the bias provides a convenient means of setting the overall required thermal coefficient.

The procedure for adjusting the overall thermal coefficient first requires an accurate determination of the manufacturer's literature to determine the coefficient of the input gate. The quiescent drain current value required for the offsetting positive drain coefficient can then be calculated. This drain current value establishes the DC bias required between input gate and source.

The required thermal compensation coefficient is determined by adding all error producing coefficients in the circuit. By omitting the probe reference potential E_o (which are negligible for the actual probes used) and by disregarding any IR drop in the probes, we achieve the following drift errors:

- | | |
|---|-------------|
| • Calculated closed loop amplifier drift caused by transistor junction potentials | +0.68 mv/°C |
| • Calculated FET gate-to-drain leakage with 10^8 ohm source resistance | +0.1 mv/°C |
| • pH probe slope change | +0.22 mv/°C |
| • Total estimated drift | +1.0 mv/°C |

The overall amplifier thermal coefficient required is -1.0 mv/°C. The calculations required to set the input bias to effect this compensation are shown in Appendix B. The measured bias in the amplifier is 0.95 mv; this closely agrees with calculations and provides good temperature compensation.

5.3 ELECTROMETER AMPLIFIER

The electrometer amplifier used to measure the pH probe output from each of the culture cells is a five stage amplifier (Fig. 5-3). The amplifier is a bridge measuring network which employs voltage feedback. The input field effect transistor (Q1) and R1, drain resistor RD, and voltage divider resistors R3 and R4 form the four branches of the bridge. Transistors Q2 through Q6 constitute the bridge measuring amplifier. Feedback is applied from the amplifier output to the node at "A"; this stabilizes closed loop gain and maintains circuit linearity and high input resistance.

Q1 is a P-channel low g_m FET selected for low leakage, and it is biased to produce a compensating thermal coefficient for drift caused in other parts of the amplifier and pH probes. Because the input terminal is referenced to ground, the FET gate-to-source negative bias is supplied at the source by the -10 v line through resistor R2. This is necessary in order to provide the required negative bias and simultaneously maintain an output quiescent voltage of +2.5 v (pH7) for mid scale spacecraft telemetry. To set bias and no-signal output voltage requires adjustment of both RD and R2.

Resistor R2 is part of the feedback network. If the input bias on Q1 is changed, the value of R2 must be recalculated to maintain the same amplifier gain. The resistor retains its large size so that no source resistance present in the 10 v line becomes part of the feedback ratio or alters the closed loop gain.

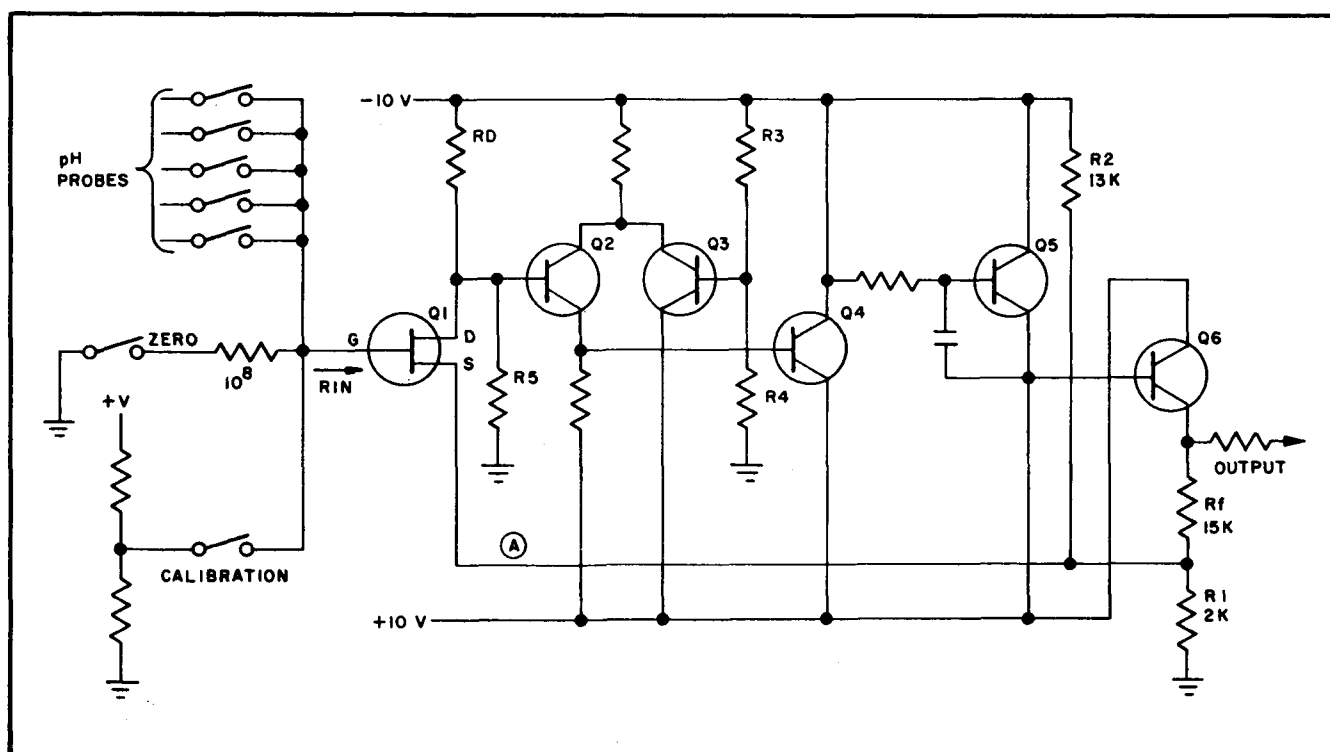
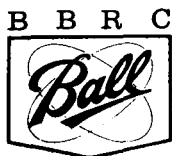


Fig. 5-3 pH Electrometer Amplifier Schematic



The closed loop gain is calculated by the well known voltage feedback expression

$$A_v = \frac{A_o}{1 - \beta A_o} \quad (5.3)$$

where

A_o = open loop gain

β = feedback ratio

A_v = gain with feedback

If $A_o \gg 1$

$$A_v \cong \frac{1}{\beta}$$

The open loop circuit gain A_o is approximately 90,000. The voltage gain of each stage from input to output is 3.6, 9.3, 10, 260, and 1. Loop gain is therefore

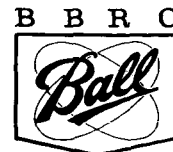
$$A_v = \frac{1}{\beta} = \frac{R_f + 11R_1R_2}{11R_1R_2} = \frac{R_f (R_1 + R_2)}{R_1R_2} \quad (5.4)$$

$$= 9.61$$

A relay commutator switches inputs into the electrometer amplifier. Terminal relay resistance is about 10^{14} ohms, which sufficiently avoids loading of the probes. In the zero mode of the data format, the amplifier input is shorted to ground through a 10^8 ohm resistor (Section 6). This permits a check on total electrometer leakage and establishes the zero input condition which produces 2.390 v output. During the calibration mode, a 0.221 v signal is impressed on the input through a 10^8 ohm resistor which produces an output of 4.516 volts. Measured circuit gain should always be the same as calculated gain and is determined by the relation

$$\frac{E_{cal} - E_{zero}}{0.221 \text{ v}} = 9.61$$

Any increase in the input circuit leakage results in a gain loss. Because the electrometer amplifier is adjusted to compensate for the thermal variations in the pH probes, the zero and calibrate readings have temperature coefficients close to those of the pH probes. This is due to the stable temperature of the purely resistive networks which develop the zero and calibrate inputs and the built in amplifier drift.



5.4 pH PROBES

Early correspondence with manufacturers of pH probes have indicated two things: (1) Existing probes do not withstand the dry heat sterilization; and (2) major changes in configuration from existing designs are prohibitively expensive. Consequently, the design requirements have been changed to permit probe sterilization by means other than dry heat as well as to permit the use of fairly conventional probes. Vibration and shock test requirements have been eliminated. The principal problem remaining was the selection of probes which can withstand steam autoclaving and which do not dilute the cultures with excessive electrolyte solution.

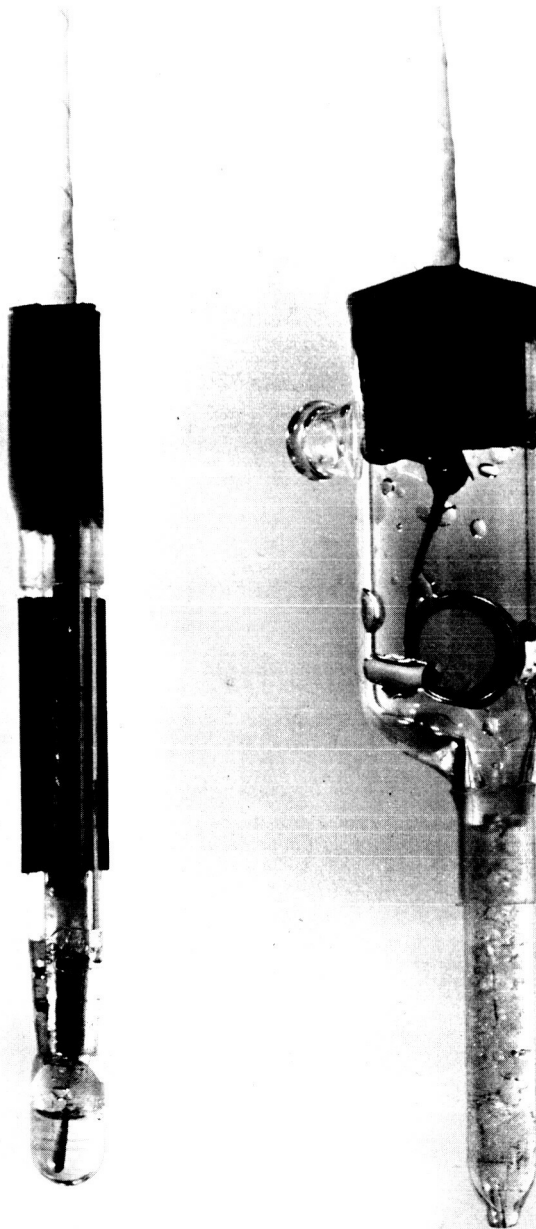
Discussion with Beckman Instruments about state-of-the-art probes has offered little encouragement. Their development groups were working on the problem for NASA and discovered that the special glass used in the potential measurement probe was subject to heat deterioration. Source impedance of the probes, present as the resistance of special glass used in the probe tip, would increase as much as 2 orders of magnitude after heat exposure. The increase would require an electrometer amplifier input impedance in excess of 10^{14} ohms, greater than considered practical for flight hardware.

Subsequent probe evaluation at BBRC has shown that steam sterilization of probes might be practical so high quality small probes were ordered as catalogue items and subjected to successive autoclavings at 15 psi steam pressure for 15 min. Glass impedance of both sets of probes tested did show marked increase, but less than expected. An internal glass-to-metal seal of one probe ruptured, but this was attributed to an excessively high heat up rate in the autoclave. Actual pH measurements between sterilizing cycles showed changes in reference potentials but both sets of probes stabilized after five heating cycles. The only apparent problems in adapting the commercial probe to the instrument were miniaturization and selection of a heat resistant insulation for the electrical leads.

The probes used in the instrument are shown in Fig. 5-4. A probe set for each culture consists of the smaller diameter measurement probe and the larger reference probe used to establish electrical contact with the test culture. The pH probes have silver-silver chloride internal electrodes. The glass measurement probe is hermetically sealed near the bottom by an internal glass-to-metal seal. The reference probe, filled with potassium chloride electrolyte, provides a low flow rate electrolyte bridge to the culture through a thin asbestos fiber at the bottom of the probe. Both probes use teflon insulated, shielded cable for connection to the electrometer amplifier. The air space above the reference probe liquid is vented so that it is at the same pressure as the culture cell interior. This assures good electrolyte flow rate established by the difference in liquid height between reference liquid and culture liquid.

The probes with the electrometer amplifier provide readings stable within 0.1 pH units over the range from 0°C to 50°C. This is the maximum error occurring at pH 9; it is attributed to sodium ion interference. Probe time response is about 1 sec (a much better time than that originally anticipated).

However, three autoclaving cycles during biological testing increased the response time to about 20 sec. Figure 5-4 shows a discoloration of the outer shield on the inner connecting braid. This is caused by the rupture of the internal on three of the five pH probes which permitted the hydrochloric acid reference solution to leak into the glass tube. Actual discoloration is the effect of the acid on the metallic conductors. The cable shielding is cut back to eliminate the electrical leakage caused by the acid.



H67-139

Fig. 5-4 pH Probes



Section 6 ELECTRONICS

This section describes the selected data format and circuitry developed to perform the required functions. Also included is an outline of component testing performed to assure compliance with the heat sterilization requirements.

The experiment electronics, housed in two separate enclosures, seen in Figs. 1-1 and 1-2 condition the turbidity and pH signals and present them along with internally generated housekeeping signals to an assumed spacecraft interface. The assumptions which guide this design approach are as follows:

- Power - Unregulated positive and negative power lines are to be available from central spacecraft power source.
- Programming - A central spacecraft programmer is to be available which provides synchronized signals for the experiment functions and presents a time base for data evaluation. Other anticipated functions include a single DC command at the moment of spacecraft impact on the Martian surface and a constant sampling rate drive for a data commutator.
- Data Sampling - A central spacecraft commutator is to provide fifteen positions for the experiment data at a constant sampling rate and provide five experiment commutator command lines activated three times in succession during experiment data sampling.
- Data Transmission - A 10-bit analog to digital converter is to be provided; it is to have a conversion time of 200 μ sec or less. Data transmission for the experiment would be at a rate of 1/2 bit sec without storage capability.

6.1 DATA FORMAT

The electronics system provides information as shown in the data format of Tables 6-1 and 6-2. One complete information cycle, called a main frame, is 160 min and consists of 32 subframes, each having the same format but representing different operating modes of the amplifiers. Mode 1 occurs during subframe 1 and provides zero amplifier input signals that determine the baseline level of the amplifiers. Mode 2 occurs during subframe 2 and provides calibration data for stability and gain checks on the circuits. Finally, Mode 3 is repeated through 30 subframes to provide 150 min of turbidity, pH, and housekeeping data.



Table 6-1
DATA FORMAT
(1 Subframe = 5 min)

Output Channel	Output Functions
1	Sync level 1
2	Sync level 2
3 Housekeeping channel	Amplifier mode ID (calib., zero level or data)
4	Temp monitor 1
5	Temp monitor 2
6	Turbidity detector 1
7	Turbidity detector 2
8 Turbidity channel	Turbidity detector 3
9	Turbidity detector 4
10	Turbidity detector 5
11	pH detector 1
12	pH detector 2
13 pH channel	pH detector 3
14	pH detector 4
15	pH detector 5

Table 6-2
DATA FORMAT
(Main Frame = 160 min)

Subframe	Amplifier Mode (Housekeeping Unchanged)
1	Zero levels and housekeeping
2	Calibration and housekeeping
3	Data - scatter, pH, housekeeping
-	-
-	-
-	-
32	Data - scatter, pH, housekeeping

6.2 DATA TRANSMISSION

Nominal spacecraft telemetry transmission rate is approximately 1/2 bit/sec. To conform with typical spacecraft design, the amplifier analog output signals to the spacecraft analog to digital converter are kept within 0 to 5 v DC. Based on experience with the earlier breadboard model, the desired resolution of the overall system is 0.2 percent (10 mv). Considering quantization error, the desired resolution requires a 10-bit analog to digital converter. The required time for data transmission at 1/2 bit/sec is as follows:

Function	Bits Required	Transmission Time
Data	10	20 sec
Subframe	150	5 min
Main frame	4800	160 min

6.3 EVENT SEQUENCE

The programmed event sequence of the experiment is shown in Fig. 6-1. A system reset command is

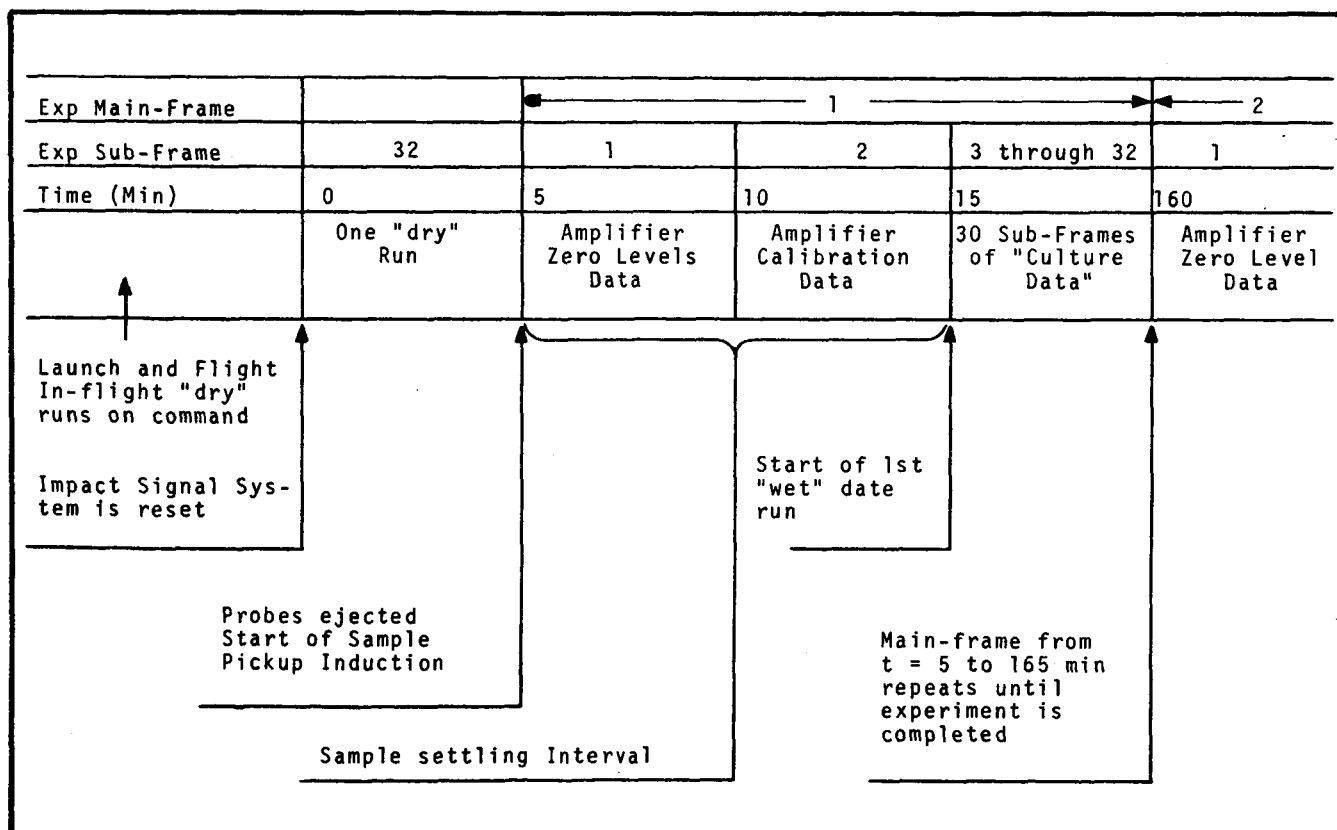
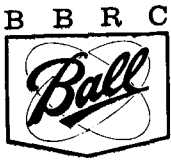


Fig. 6-1 Event Sequence



provided either by the single occurrence of a ground impact signal from the landing spacecraft or by a telemetered command line used for checkout during transit time. Either reset command automatically sets the experiment programmer at the beginning of subframe 32. The experiment then advances with the spacecraft clock to produce one dry run which provides turbidity data on empty culture cells. At the moment of reset, but only in the case of an impact signal command, the pickup device is ejected to the surface. However, sample acquisition does not start until completion of the dry run. At the beginning of subframe 1, the pneumatics gas system is activated, and the sample acquisition proceeds as the amplifier zero levels and calibration are being determined. First turbidity and pH data is available at the start of subframe 3 and continued for the balance of the main frame.

6.4 SYSTEM DESCRIPTION

The electronics system block diagram is shown in Fig. 6-2. Inputs from the spacecraft to the experiment are shown on the right, and data outputs from the experiment are shown at the left. Output data is presented on the three analog lines. The turbidity and pH amplifiers are connected directly to their respective lines and commutation is performed at the input of the amplifier. Housekeeping data is conventionally commutated; pH and housekeeping data are presented continuously, but turbidity data is available only during the allotted commutator position. This conserves power by turning on the relatively high power tungsten lamps in the optics only when turbidity information is scheduled. All commutation is synchronously advanced by the five commutator command inputs from the spacecraft source.

A clock pulse taken from the spacecraft commutator is assumed to have a period of 5 min; it advances the experiment subframe matrix. This matrix and associated selector logic provide the following functions:

- Inhibit turbidity lamp turnon during pH amplifier and housekeeping data readout
- Provide calibration signal control
- Inhibit calibration signal and zero suppression circuits during zero amplifier level readout
- Provide amplifier mode identification
- Provide power to the pneumatics system solenoids only during subframe 1

The pneumatics solenoids, which control ejection of the sample acquisition probe and the release of

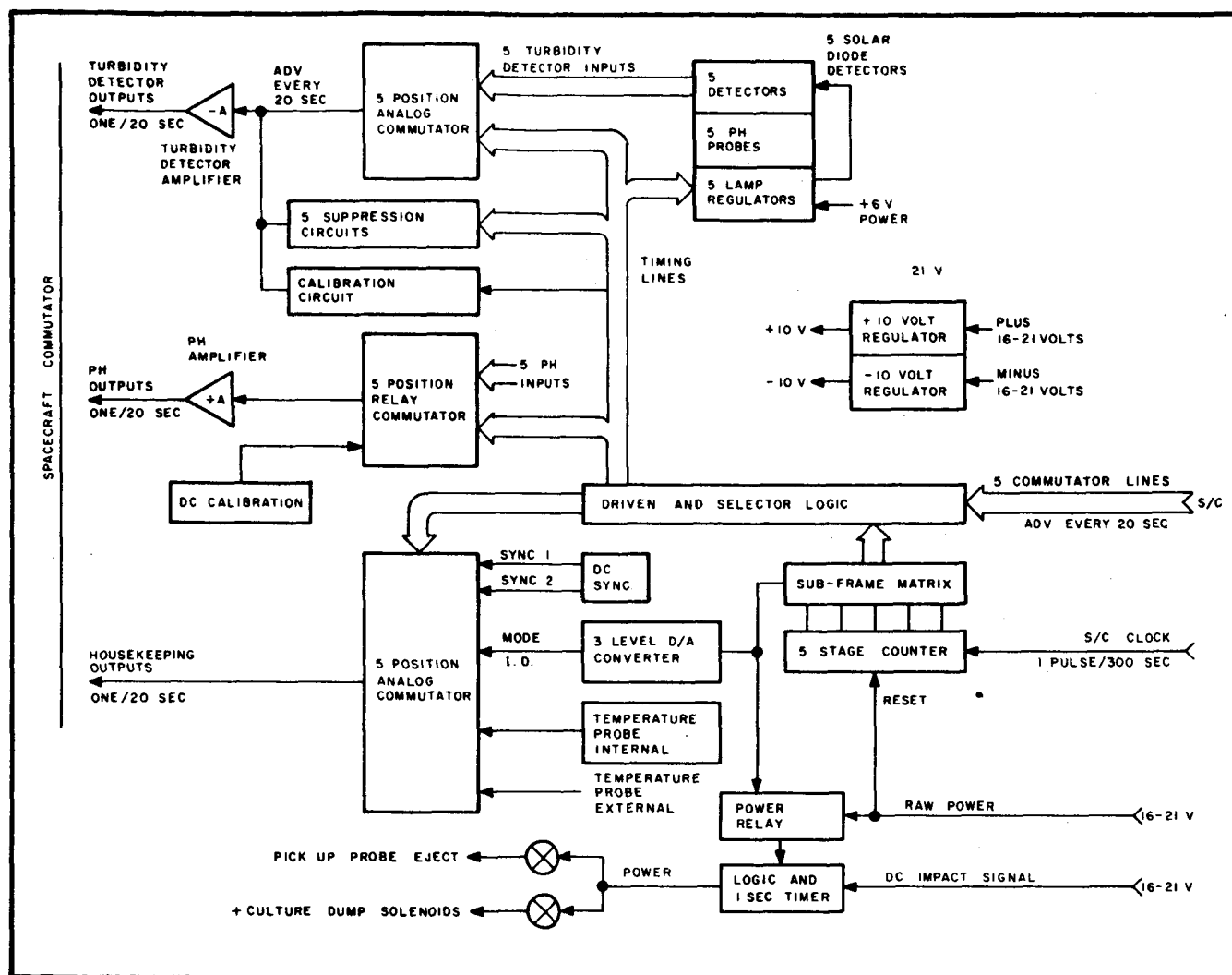


Fig. 6-2 Electronics System Block Diagram

high pressure gas, can be actuated only during the presence of the DC signal impact control from the spacecraft. Control solenoids within the experiment electronics provide 1 sec contact closure to activate the pneumatics solenoids. A safety feature of the circuit requires that additional raw power from the spacecraft, used for the actual energizing of the pneumatic solenoids, be provided by the spacecraft after the impact. Pulse currents as high as 1 amp are required for the pneumatic solenoids. Protection of the spacecraft power line (in case of timer circuit failure) is provided by a delay fuse which opens the experiment pneumatics solenoid power line.

6.4.1 Turbidity Amplifier and Analog Commutator

The turbidity circuitry commutates the five separate signal photocells in the turbidity optics, amplifies the low level signal, and provides suppression of the fixed level signal resulting from stray light in the



optics housing (Fig. 6-3). Previous evaluation of the breadboard model indicates that a maximum 10 namp drift current (referred to the input) is permissible. We have decided that a low level DC amplifier would be better than a chopper stabilized amplifier because of greater simplicity and lower power consumption.

The amplifier is a five stage negative shunt feedback circuit. Feedback provides a high degree of stability as well as low input and output impedances. Thermal variations depend largely on the feedback resistor R_f , which has 0.1 percent stability throughout the operating temperature range of 0 to 40°C. Input voltage changes are minimized by using matched input transistors which have a differential thermal coefficient of less than $10 \mu\text{V}/1^\circ\text{C}$. The collector current of the first stage is set at $1 \mu\text{A}$ bias. With a minimum current gain of 100 at the lowest operating temperature, the base current loading effect on

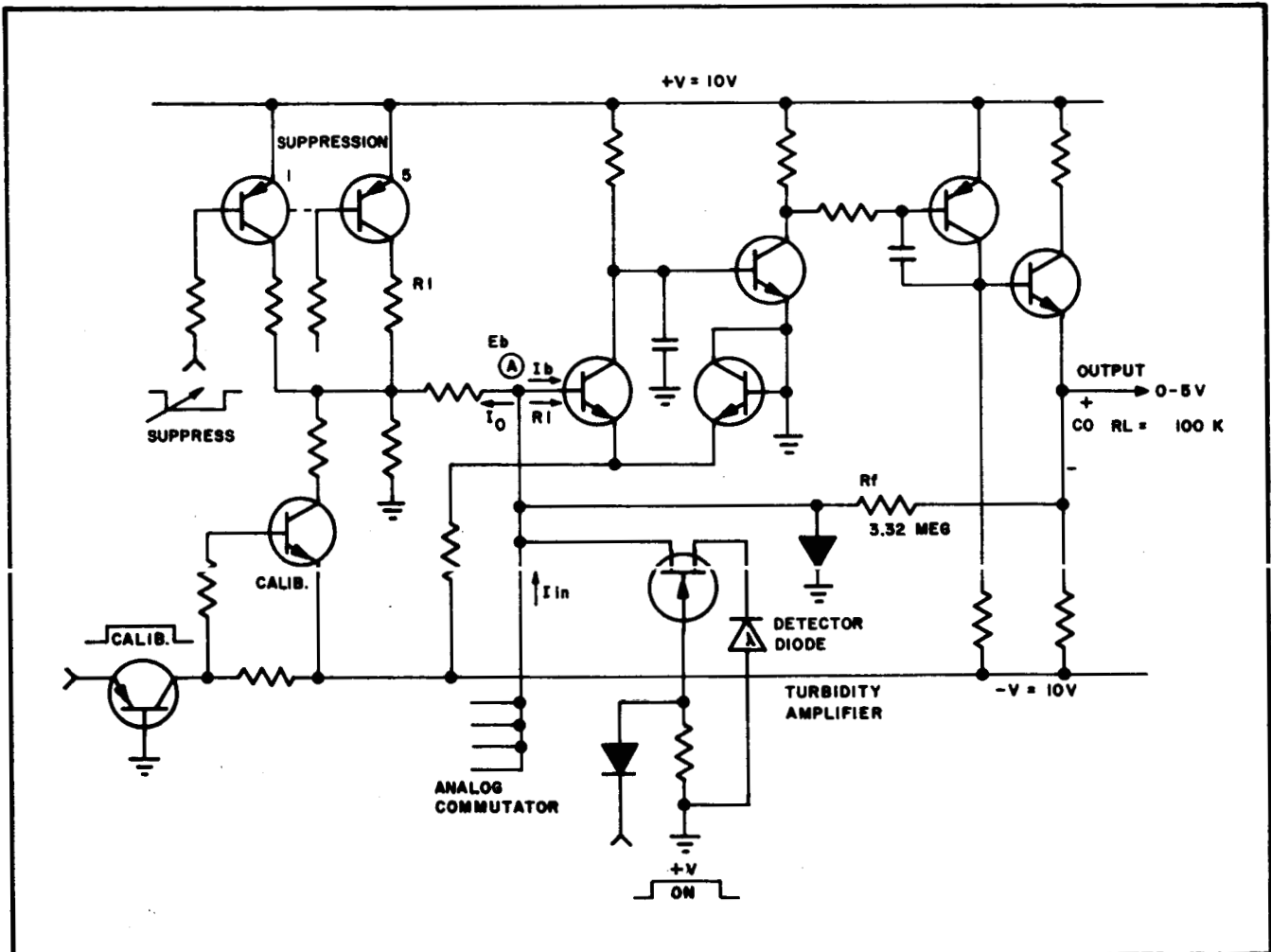


Fig. 6-3 Turbidity Amplifier Schematic



signal current is maintained at less than 0.005 percent at full output voltage of 5 v and at 50 K load resistance. Input collector-to-base junction leakage is negligible since the first transistor collector voltage is clamped at 0.5 v. Latching effects caused by loss of reverse bias of the input collector-to-base junction during power transients is eliminated by the input diode.

For optimum thermal stability, the detector silicon photocells require a resistive load of less than 100 ohms. The actual amplifier input resistance is given by the expression

$$R_{in} = \frac{R_f}{(1 + A_v)} = 3 \text{ ohms} \quad (6.1)$$

where A_v is the open loop voltage gain of about 1 million

Using summing currents at point A of Fig. 6-3, the input voltage and current, E_{in} , I_{in} and output voltage E are related by

$$e_{in} = I_b R_i \quad (6.2)$$

$$e_{in} = I_R R_f = e_o \quad (6.3)$$

$$e_o = -e_{in} A_v \quad (6.4)$$

$$I_{in} = I_b + I_{R_f} \quad (6.5)$$

where R_f = feed back resistor

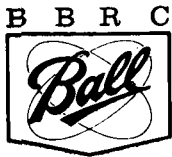
$$I_R = \text{feedback current}$$

$$I_b = \text{base input current}$$

$$R_i = \text{base input resistance}$$

Combining the above equations, we get

$$e_{in} = I_R R_f + (I_{in} - I_R) R_i A_v \quad (6.6)$$



$$\text{since } I_R = \frac{e_{in} - e_o}{R_f} = \frac{e_{in} (1 + A_v)}{R_f} \quad (6.7)$$

Combining Eqs. (6.6) and (6.7), we have

$$R_{in} = \frac{e_{in}}{I_{in}} = \frac{R_i}{1 + \frac{R_i}{R} (1 + A_v)}$$

If $R_i \gg 1$ and $A_v \gg 1$, then

$$R_{in} \cong \frac{R}{1 + A_v} = \frac{3.3 \text{ meg}}{1 + 10^6} \cong 3 \text{ ohms}$$

The amplifier, driven from the signal photocell current source, has a gain transfer impedance given by

$$e_o = -I_{in} R_f \quad (6.8)$$

if $A_v \gg 1$

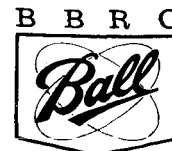
and $R_i \gg 1$

R_i is large because the bias current I_b is a maximum of 10 namp.

Designated maximum signal current above stray background is $1.5 \mu\text{amp}$ which sets R_f at 3.32 meg, thereby providing a maximum 5 v output. Overall amplifier gain linearity is a 1 percent deviation from a best straight line expressed as a percent of full scale.

The load resistance of each silicon photocell is limited to the "on" resistance of the N-channel field effect transistor commutator. Because the "on" resistance is approximately equal to $1/g_m$, high transconductance devices are used to provide a commutation "on" resistance of between 100 and 150 ohms. There is no detectable crosscoupling between the silicon detector cell signals over the temperature range of -25°C to $+70^\circ\text{C}$. The amplifier DC input voltage is held between 2 and 4 mv to minimize signal shunt leakage paths within the silicon photocells.

The fixed level signal current caused by stray light in the optics is suppressed by injecting an opposing current into the input of the amplifier. A constant but different suppression current for each of the five detectors is provided through resistors R_1 and R when the experiment programmer logic circuitry selectively



turns on the proper suppression PNP transistor. The five identical transistors have been selected for stable collector-to-emitter saturation voltage and provide suppression value variations of no more than 0.1 percent. The suppression current is given by

$$(V - V_{CES}) \frac{R_2}{(R_1 + R_2) R} \quad (6.9)$$

where V_{CES} is the PNP transistor saturation voltage.

Thermal stability of the amplifier depends on the value of R . Since the gain transfer impedance is

$$E_o = I_{in} R_f \text{ and } I_{in} = \frac{E_s}{R}$$

where E_s = suppression voltage at the input of R , we have

$$E_o = E_s \frac{R_f}{R} \quad (6.10)$$

The voltage gain A_v is given by

$$A_v = \frac{R_f}{R} \quad (6.11)$$

When there is a high level signal caused by stray light from scratched or smudged culture cells, R necessarily is small, and the amplifier voltage gain increases. The circuit then amplifies the equivalent input voltage drift and renders the circuit more temperature dependent. The performance of the final circuit configuration with temperature is shown in Section 8 (System Test).

A fixed value calibration current is provided to check the amplifier gain. This current is injected into the input of the amplifier in a way similar to that of the zero suppression circuit. The value of this current is given by

$$I_{cal} = (V_{CES}) \frac{R_2}{(R_2 + R_3) R} \quad (6.12)$$

6.4.2 Lamp Regulator

The lamp regulator is an amplifier which adjusts current through the tungsten lamp in the turbidity optics to maintain a constant output from the lamp monitor silicon photocell. The circuit shown in Fig. 6-4 is a high gain, negative feedback series regulator. The configuration is similar to the turbidity amplifier

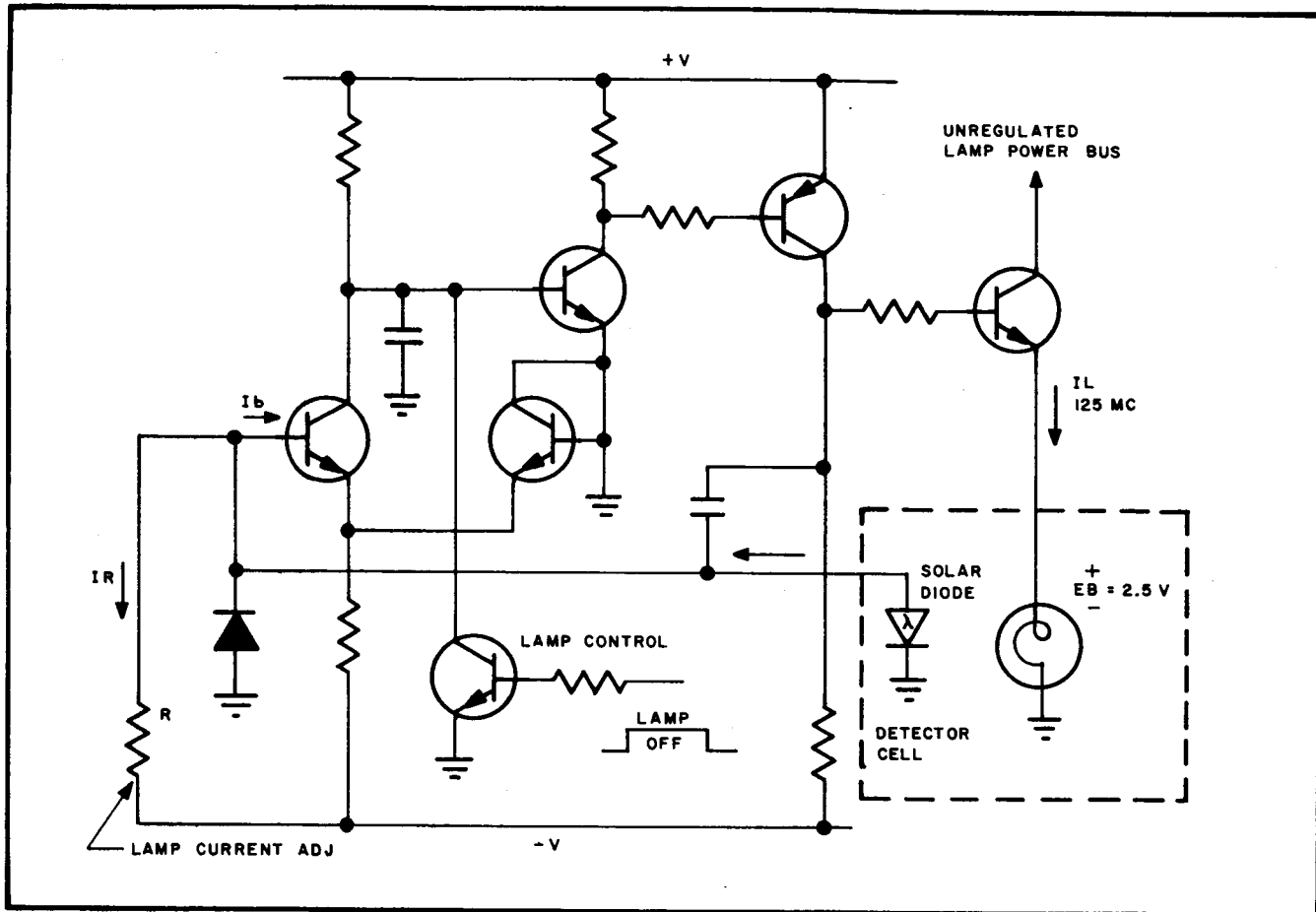
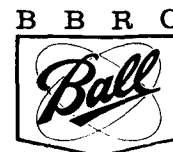


Fig. 6-4 Lamp Regulator Schematic

except that the feedback resistor R_f is replaced by the lamp monitor photocell. The separate regulator for each lamp is turned on when the lamp control transistor is turned off. Approximately 125 ma current is delivered to the lamp. The monitor photocell current I_s is about $300 \mu\text{a}$ for all five assemblies. Quiescent lamp current is selected by adjusting the value of R . Since the open loop current gain is about 1 million times I_b , the base drive current is about 0.02 percent of I_s , so I_R approximately equals I_s . Gain variation, therefore, hardly affects the performance of the regulator.

Regulator stability is appreciably affected by the stability of the monitor silicon photocell. The illumination ϕ is a function of the lamp voltage E_b , which is given by

$$E_b = -(S_s \phi) I_s \approx -S_s I_R \quad (6.13)$$



where S_s = sensitivity of the solar diode.

As stated previously, the sensitivity S_s of the silicon photocell is a function of temperature. Therefore, the illumination from the lamp varies with temperature, but the net change in turbidity signal is quite small since the signal photocell remains at the same temperature as that of the lamp monitor and the two cells tracked in temperature. The main disadvantage of this method is that failure of one photocell to track the other causes a net change in turbidity signal. Tracking deviations principally result from spectral mismatch between cells and from the differential cell degradation occurring during heat sterilization. Measured circuit thermal stability is not as good as expected (Section 8). We attribute this to a slight spectral mismatch between the photocell pairs rather than to sterilization. The circuit is quite insensitive to power supply variations, which produces a change in turbidity signal of only 0.2 mv for every volt change in the unregulated lamp voltage.

6.4.3 Housekeeping Commutator

The housekeeping commutator consists of five P-channel field effect transistors driven by the experiment programmer. Once every five minutes, the commutator provides the following information:

- Two successive synchronization words of fixed voltage used in computer analysis of data
- An operating mode identification to indicate whether the amplifiers are in the zero, calibrate or data mode
- The temperature within the electronics housing
- The temperature of the centralmost culture cell

The synchronization word signal is obtained from a resistive divider across a regulated power supply, and mode identification is obtained from an operational amplifier. Output impedance of the synch word circuit is about 10 kohms, and impedance of the mode channel is limited to 100 ohms by the field effect commutator resistance. Both temperature monitors are single transistor amplifiers having 15 kohm output impedances.

The transistor commutator operates effectively with any load resistance above 2 kohms. Loading the two synchronization word channels with 1 meg causes a 1 percent signal loss which remains fixed with a constant telemetry load. No cross coupling exists between channels with any load impedance.



6.4.4 Voltage Regulators

All signal amplifiers in the experiment operate from well regulated positive and negative voltage regulators. Both regulators are three transistor devices that are temperature compensated to provide 0.02 percent output variation over the temperature range of -25°C to $+70^{\circ}\text{C}$. All relays used in the experiment operate from the unregulated power source. Neither voltage regulator is damaged by momentarily shorting the output.

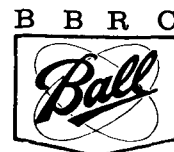
6.5 COMPONENT SELECTION

All electric components must be carefully selected prior to instrument assembly to assure that the instrument could withstand twenty-four hours of dry heat sterilization at 145°C . The instrument itself is not necessarily tested for resistance to ethylene oxide gas also used in the prelaunch spacecraft sterilization. However, a listing of component types and materials to be used in the end item was checked with the best available NASA (JPL) listing of qualified items. With the exception of possible long-term storage of the sterilant gas by silicon rubber, all component and material items could be safely used. In the early design stages, the intended components were checked against the listing of qualified components from the Ranger program. Consequently, it was decided to use qualified components wherever possible, but to allow new items as well if they passed stringent qualification screening.

Component testing required that items be subjected to temperatures far exceeding those required for the system test and that maximum acceptance limits be set for value changes caused by overstress. Allowable parameter absolute values and maximum changes from initial parameter values have been established for all components. All components were subjected to a four-hour thermal soak at 160°C , immediately followed by exposure to ambient laboratory air temperatures to produce thermal check. All components were then measured for conformance to parameter requirements, and all devices were subjected to an identical twenty-four heating and retested in the same manner.

The testing showed that some components were subject to parameter aging under heat stress and that others were subject to complete failure. Approximately 10 percent of all carbon composition resistors were out of tolerance. Deviation from initial value varied at random, from high to low. One percent of all transistors and diodes tested have been outside specification. Failures are excessive leakage in a P-channel transistor and channeling failure in a PNP transistor. One percent of all metal film resistors also have failed to meet specification. Over 30 percent of miniature transistor relay failures can be attributed to armature sticking and to apparent contact resistance increase. However, no capacitors have failed during testing.

Total system sterilization testing (Section 8) have produced two additional component changes. One electrolytic capacitor showed end cap cracking, but there was no change in parameter value. One qualified miniature relay showed intermittent contact closure.



Section 7

CHECKOUT CONSOLE

The checkout console for the experiment is an electrical device which performs the following functions:

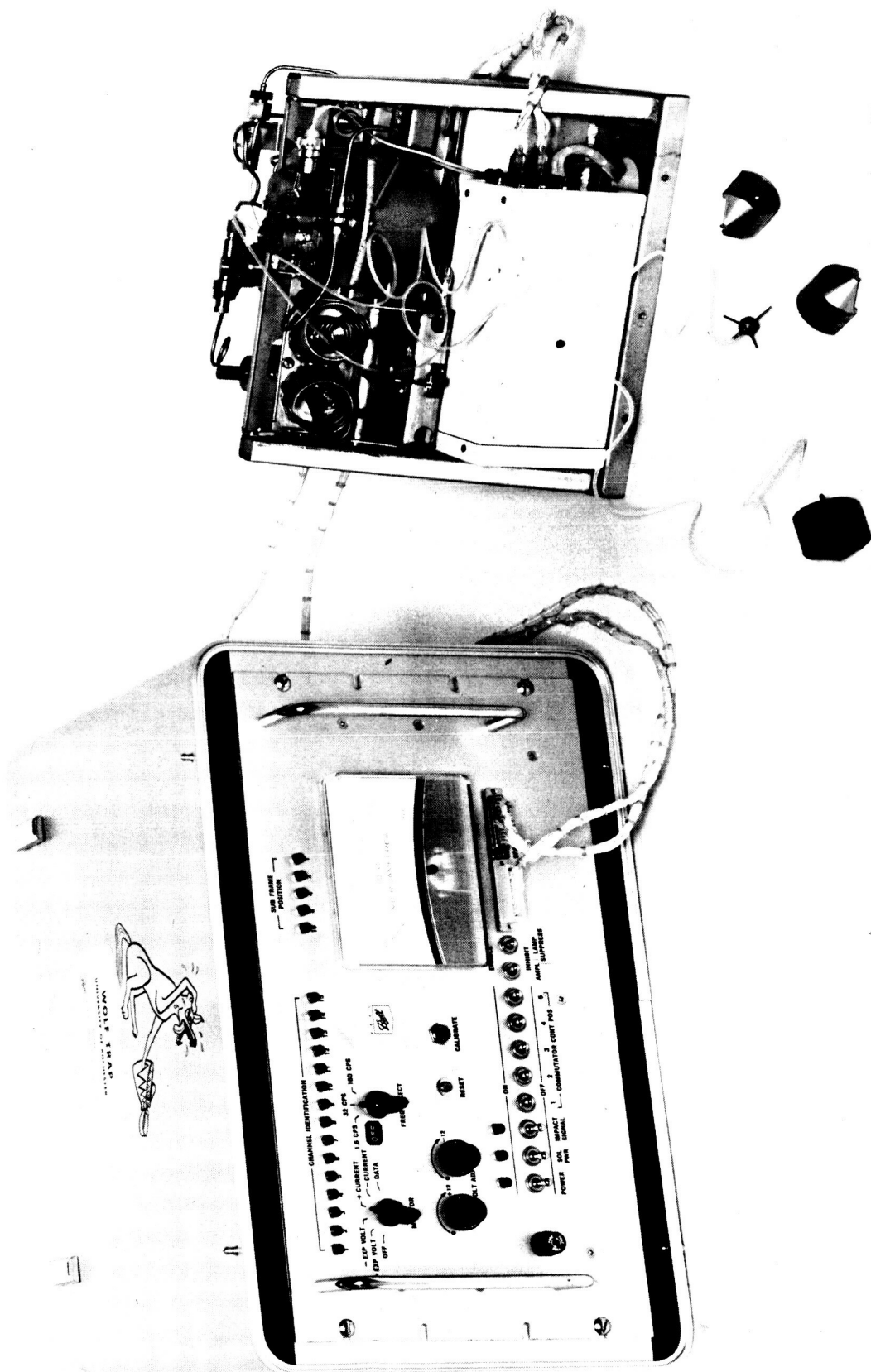
- Simulates the assumed spacecraft functions including power supply, clock timing, and automatic commands
- Provides a visual monitor meter for output data and also provides data in a manner suitable for automatic recording
- Provides manual control switches for ground checkout of experiment functions

The console is designed to be rack mounted in either a relay rack or in a protective carrying case suitable for field test operations. Figure 7-1 shows the console mounted in a portable aluminum case and interconnected to the experiment. One of the interconnecting cables would be the permanent connection between experiment and spacecraft, while the other would be a removable cable used only for pre-flight checkout. Not shown in the figure is the cable from the back of the console, which presents data to an automatic recording system.

7.1 CONSOLE DESCRIPTION

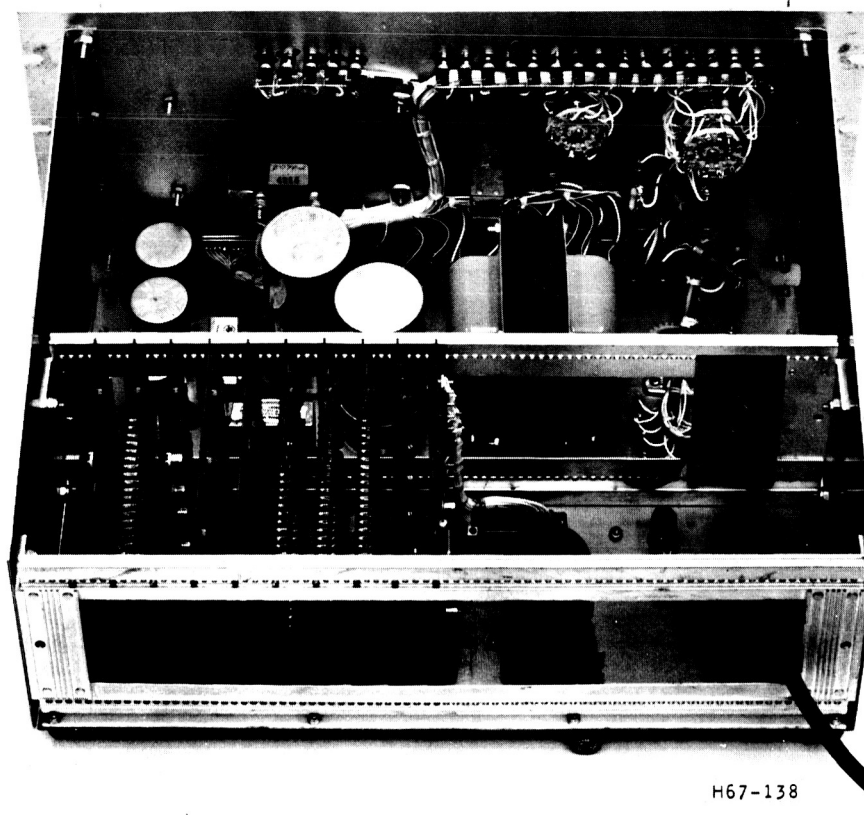
Figure 7-2 shows the relatively simple interior of the console. The front panel contains the meter monitor, manual control switches, and indicator lights for visual indication of experiment functions during checkout. Most of the chassis is given to the 110 v, 60 Hz power supply which simulates the positive and negative spacecraft power bus. An adjustable DC voltage regulator in the power supply provides wide range voltage inputs into the experiment used for checkout of the experiment precision voltage regulators. A rearward mounted connector provides data output to an automatic recording system.

All spacecraft simulation functions are provided by printed circuit plug-in cards at the back of the chassis. Experiment programming is synchronized by a clock circuit, stable to 1 percent over a wide operating temperature range. Clock timing is adjustable to facilitate rapid checkout of experiment functions. A three-position, dry-reed relay commutator simulates a spacecraft multiplexer. The commutator remains at each of the housekeeping, turbidity, or pH outputs from the experiment for 100 sec. During this time, the experiment programmer commutates the input to the amplifiers to produce five successive outputs of either housekeeping, turbidity, or pH. The experiment programmer is driven from the console clocking circuits, which synchronizes all commutation. During the 20 sec ON period of any single experiment commutator interval, the console clock initiates a command pulse at the end of 19 sec which permits external automatic data equipment to convert the analog signal to a printed record.



H67-132

Fig. 7-1 Wolf Trap and Checkout Console



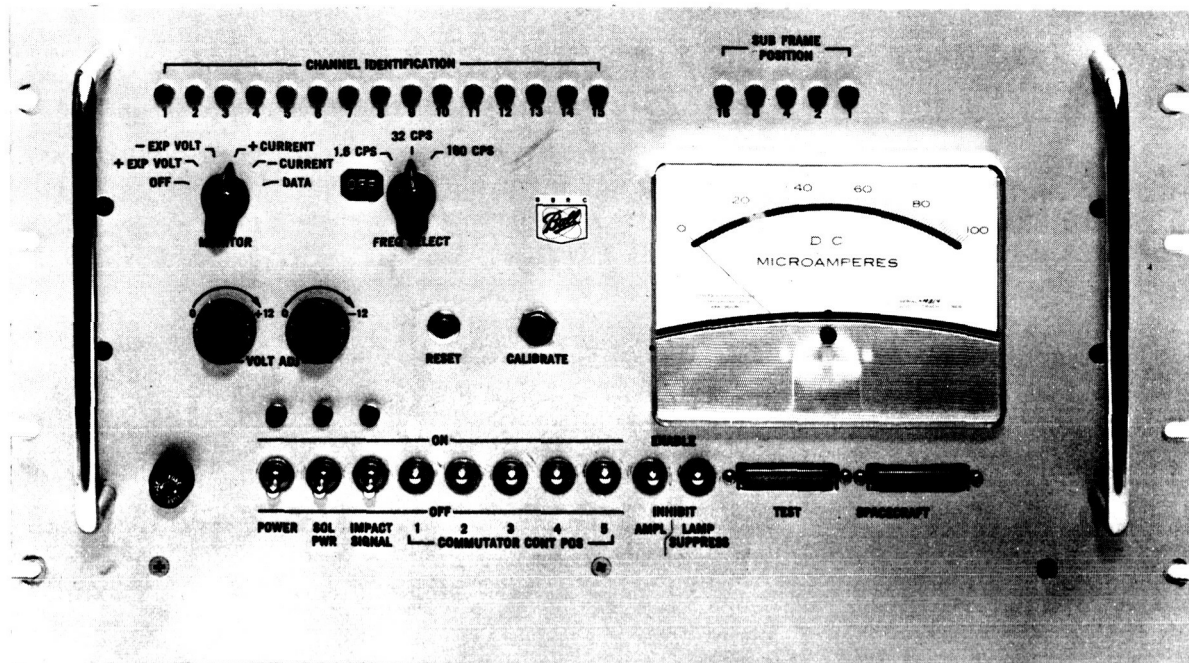
H67-138

Fig. 7-2 Console Interior

7.2 CONSOLE CONTROL DESCRIPTION

The front of the console panel is shown in Fig. 7-3. A brief description of all panel indicators follows with the panel designation in upper case letters.

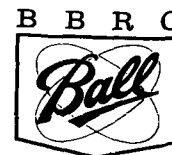
- CHANNEL IDENTIFICATION
 Fifteen red lights show which word, within each subframe, is being presented.
 In the normal operating mode, each light remains on for 20 sec.
- SUBFRAME POSITION
 Five red lights indicate in binary form which subframe is being presented.
- MONITOR
 (Information presented on panel meter)



H67-133

Fig. 7-3 Console Front Panel

- OFF
 Panel meter is shorted for maximum damping and protection during transport.
- +EXP VOLT
 Voltage input to the experiment positive precision voltage regulator.
- -EXP VOLT
 Voltage input to the experiment negative precision voltage regulator.
- + CURRENT
 Total experiment current drawn from the console positive voltage supply. All experiment relays excluding 1 amp solenoids were operated from the positive supply.
- - CURRENT
 Total current drawn from the console negative supply.
- DATA
 Data output voltage designated by the channel identification lights.



- **FREQ. SELECT**
Selects the frequency of the console synchronizing clock. An auxiliary position allows the clock to be stopped for a continuous presentation of any output. Additional speed-up positions are provided to facilitate fast advance of the commutators and checkout of the experiment functions.
- **VOLT ADJ**
Provides independent adjustment of both positive and negative console power supplies over the range of 16 to 21 v to facilitate checkout of experiment precision voltage regulators.
- **RESET**
Momentary press button which resets both console and experiment programmers to the beginning of subframe 32.
- **CALIBRATE**
Momentary push button which, in any experiment operating mode, would inject a present calibrate current into the turbidity and pH amplifiers for gain checks.
- **PANEL METER (not labeled)**
100 kilohm internal resistance, taut band panel meter for visual observation of current and voltage data.
- **FUSE**
1 amp fuse on the line input to the power supply which supplies both console and experiment.
- **POWER**
Main line power switch with red light indicator.
- **SOL PWR**
Indicator light and toggle switch which supplies main power to the probe eject and gas pressure release solenoids in the experiment. This switch simulates the spacecraft function of providing solenoid power only after impact.
- **IMPACT SIGNAL**
Indicator light and toggle switch which automatically resets console and experiment to the beginning of subframe 32 and initiates total automatic experiment sequence. This control simulates the acceleration switch which is activated by the impact of the spacecraft on the surface.



- **COMMUTATOR CONT POS**

Provides manual disabling of the console commutator during any selected position to facilitate laboratory equipment evaluation with less than five cultures. Switch 1 in the OFF position would disable channels 1, 6, and 11. Switch 2 would disable channels 2, 7, and 12, etc.

- **AMPL**

In the inhibit position, all turbidity amplifier stray light suppression current is eliminated. The control is useful in monitoring the amount of current needed to suppress the stray light background in the culture cells.

- **LAMP SUPPRESS**

In the inhibit position, all turbidity and pH commutators are disabled. All lamp regulators are also turned off, except for culture 1.

- **TEST**

Connector for cable to experiment which carries only those lines needed for prelaunch checkout of the experiment.

- **SPACECRAFT**

Connector for permanent cable to the experiment which carries power and command functions.

7.3 AUTOMATIC DATA RECORDING

The console was fitted into a portable relay rack and integrated into a data recording system provided by the University of Rochester. The assembled rack is shown in Fig. 7-4. A four-digit digital voltmeter converts the data voltage outputs from the experiment into visual presentation and binary representation. This binary information is presented to the data coupler which permits the tape punch and/or tape printer to record the information. The printed tape presents channel word identification (1 through 15) and the printed data signal level. The punched tape presents the same information plus parity check and end of line and end of scan codes to permit computer decommutation of all data. The power panel provides convenience outlets and main power turn-off. The entire rack is forced-air ventilated with two squirrel cage blowers contained behind dust filters. An accessory drawer is provided at the bottom of the rack.

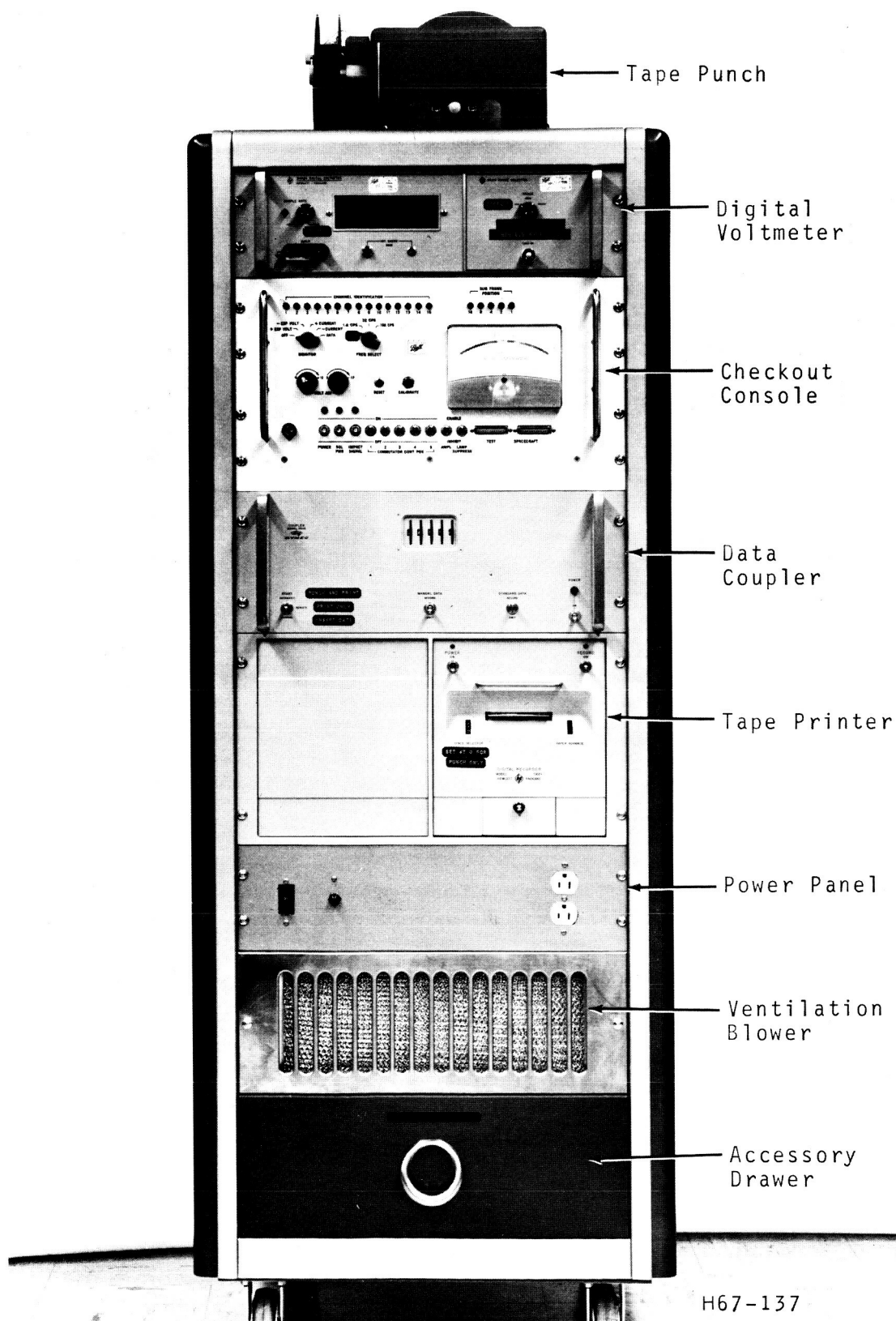
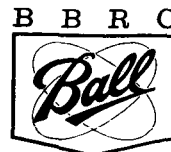


Fig. 7-4 Data Recording Rack



Section 8

SYSTEM TEST

Design specifications for the engineering model require a wide spectrum of environmental tests. Included are acceptance tests for heat sterilization, sinusoidal and random vibration, thermal vacuum endurance, impact shock, sustained acceleration, and spin. Unforeseen delays near the end of the program and funding limitations required lessening or omission of some tests. Because the device is an engineering model and is not designed for a specific mission, only those tests were performed that would show adaptability of the concept to a flight design. Resistance to heat sterilization and vibration are most important. Company experience with silicon rubber indicates that the material might not survive long-term space environment. Even though the instrument uses a number of "O" rings made from this rubber, we feel that final flight design would minimize ring sealed joints by incorporating welded joints. Survivability of the electronics system in thermal vacuum could be approximated by overstressing the system with temperature in ambient laboratory pressures. Resistance to impact shock, acceleration and spin could be approximated by results from vibration testing.

The sequence of the limited scope tests performed is as follows:

- Check total instrument functioning and measure electronic circuit parameters.
- Perform "quick look" function test.
- Perform vibration test in all three axes.
- Perform "quick look" function test.
- Perform plate count sensitivity test using E. Coli. test culture.
- Dry heat sterilize for 24 hours.
- Perform "quick look" function check.
- Repeat plate count sensitivity test.
- Recheck total instrument functioning and circuit parameters.

The automatic data system is used to gather data during the "quick look" tests and plate count sensitivity tests. Circuit parameters are measured with conventional laboratory test apparatus.



This section describes the results of all system testing performed. A brief description of test set ups is made to help the reader. These tests are described separately because the entire system was subject to both vibration test and heat sterilization. The instrument testing can best be described by function (i.e., -pH, pneumatics, electronics, etc.), which are treated in separate subsections.

8.1 COMMON ENVIRONMENTAL TESTS

The vibration test was performed on a 15,000 lb force machine programmed for acceleration input and frequency sweep rate. The instrument is shown attached into the vibration fixture in Fig. 8-1. A secure attachment of the instrument to the fixture was made with 17 peripheral high strength bolts. A monitoring accelerometer was attached to the uppermost edge of the gas reservoir mounting. The test machine was programmed for 2 g input from 5 to 2,000 Hz, and the assembly was vibrated with a frequency increase rate of 1 octave/min for a total of 8 min. This was done for all three axes. It became apparent during testing that the hopper body rather than the gas reservoir is subject to more resonance. The monitoring accelerometer was fixed to the hopper body where the indicated transmissibilities are considered to be worst case. Vibration table inputs were increased to 10 g's with the accelerometer still mounted on the hopper body. Acceleration input was limited to this value because indicated transmissibilities in the hopper area pushed the

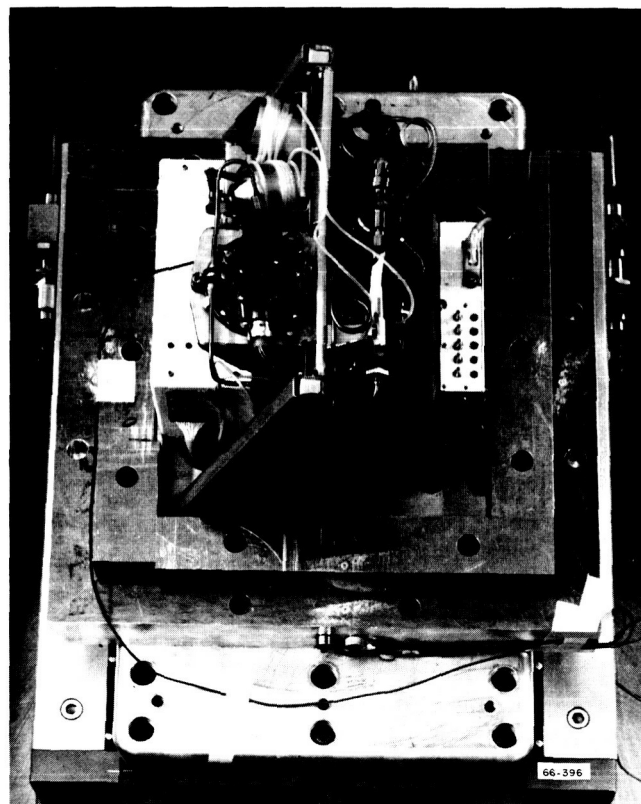
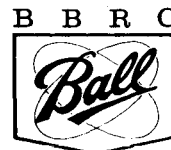


Fig. 8-1 Experiment in Vibration Test Fixture



pneumatics mounting plate stresses to their design maximum of about 200 g's. Effects on subassemblies are given in the following subsections. Acceleration input levels and transmissibility plots for all tests are shown in Appendix C.

Heat sterilization required that the instrument be maintained at 145°C for 24 consecutive hours. For testing convenience and safety, the system was tested in three parts: main electronics housing, structure, and optics; pH electronics only; and pneumatics system with charged gas reservoir. In each of the three tests, a thermal indicator was attached to the largest thermal mass included in the test. The subassemblies at ambient room temperature was inserted into preheated, forced air ovens. A typical thermal delay of 1 hour from ambient to test temperature produces a thermal rise rate of about 2°C per minute, approximately double that expected for a flight sterilization. Each assembly was maintained at 145°C for 24 consecutive hours followed by cooling to room temperature in about 2 hours. Effects of the sterilization on the subassemblies are discussed separately in the following subsections:

8.2 ELECTRONICS SYSTEM

System parameters presented herein are the same before and after environmental test except where noted. Performance of the voltage regulators and housekeeping circuitry over the extended temperature range is presented to show the circuitry survivability. Testing emphasis was placed on the anticipated operating temperature range of approximately 5° to 40°C.

8.2.1 System Power

Total system electrical power shown in Table 8-1 comes from three separate voltage sources in the console: positive 18 v supply, a negative 18 v supply, and a positive 6 v supply. The two higher voltages are regulated in the instrument to 10 v which powers all circuitry. The 6 v source supplies power for the tungsten lamps only. Indicated power consumption is for a nominal 18 and 6 v input, although the regulators would work from 16 to 21 and the lamps from 4 to 7 v.



Table 8-1
SYSTEM POWER REQUIREMENTS

Subframe (Mode)	Function	Power Source					Power X Duration (mw min)
		+18 v (mw)	-18 v (mw)	+6 v (mw)	Total (mw)	Duration (min)	
Data	Circuits	660	165	0	825	150	123,750
	Lamps	0	0	720	720	50	36,000
	#1 Lamp Stdbby	0	0	540	540	140	75,600
Zero	Circuits	570	130	0	700	5	3,500
	#1 Lamp Stdbby	0	0	540	540	5	2,700
	Solenoids	3600	0	0	3600	0.2	720
Calibrate	Circuits	810	133	0	943	5	4,715
	#1 Lamp Stdbby	0	0	540	540	5	2,700
						Total	249,685
Main Frame Average Power = $\frac{249,685 \text{ mw min}}{160 \text{ min}}$ = 1.561 w							

8.2.2 Voltage Regulators

The experiment precision regulators accepted supply input from the console between 16 and 21 v DC. Each regulator then provided a regulated 10 v output to the electronic circuits. Over an operating temperature range of -25° to +70°C and for input voltage variations from 16 to 21 v DC, the positive regulator output varied only 0.1 percent ($\pm 1\text{mv}$) for normal load currents between 22 and 47 ma. The negative regulator under the same conditions maintained voltage output within 0.2 percent (2 mv) for load currents between 7 and 15 ma.

8.2.3 Housekeeping

The thermal stability of housekeeping data over an extended temperature range is shown in Table 8-2. The nominal room temperature (20°C) output and changes from that output with temperature are shown. Synchronization outputs on channels 1 and 2 originate from a voltage divider in the precision voltage regulator and are stable with temperature. Subframe mode identification on channel 3 is derived from an operational amplifier which is not temperature compensated. However, the total drift of each indicated mode is not sufficient to change the least significant digit (1, 2, or 3) of the identification voltage. The calibrate and zero for channel 6 are shown separate from channels 7 through 10. The low change values under "Calib-Zero" indicate that the amplifier output level is shifting with temperature, but the gain remains constant. Calibrate is accomplished by injecting an additional current into the amplifier input.

Table 8-2
HOUSEKEEPING DATA TEMPERATURE STABILITY

Function	Channel No.	-25°C	+5°C	+40°C	+50°C	+70°C	+20°C ^(a)
mv change from 20°C							
Sync	1	+4	0	-1	-4	-5	3858
Sync	2	+4	0	-1	-4	-5	3844
Data Mode	3	+30	+6	-7	-14	-24	3354
Zero Mode	3	+25	+6	-6	-12	-20	2381
Calib. Mode	3	+22	+5	-6	-12	-18	1360
Calibrate	6 only	-3	-8	+7	+7	+34	1310
Zero	6 only	-10	-8	+6	+8	+34	41
Calib-Zero	6 only	+7	0	+1	-1	0	1269
Calibrate	7-10	-	-2	+3	-	-	1325
Zero	7-10	-	-3	+5	-	-	57
Calib-Zero (difference)	7-10	-	+1	-2	-	-	1262

(a) Column data output in mv.

Temperature calibration of two transistor temperature monitors is shown in Fig. 8-2. One probe is contained within the main electronics housing and has an output on channel 4. The other probe is in physical contact with middle culture cell and has an output on channel 5. Calibration curve equations for temperature calculation are given in the figure. The curves shown are plotted after 24 hours sterilization which produced an upward translation of the "before test" curves. This change is caused by heat aging of carbon resistors used in the monitor circuitry. The use of more stable metal film resistors would eliminate aging effects.

8.2.4 Turbidity Channels Temperature Variation

Even though temperature variations in the turbidity amplifier are small, system variations are considerably in excess of those anticipated when the turbidity optics and detectors are attached. To simulate typical system operation with aqueous cultures, a temperature stability test was performed with the culture cells filled with sterile, filtered distilled water. The cells were hermetically sealed, and the entire system was sealed into a plastic bag which contained activated desiccant. This was done to avoid water condensation in the turbidity optics when the test temperature reached the dew point within the optics system. The test temperature was first increased to the highest test temperature of 40.5°C, and data was taken at the end of 2 hours to assure thorough system drying. Test temperatures have been successively reduced over a total of about 12 hours.

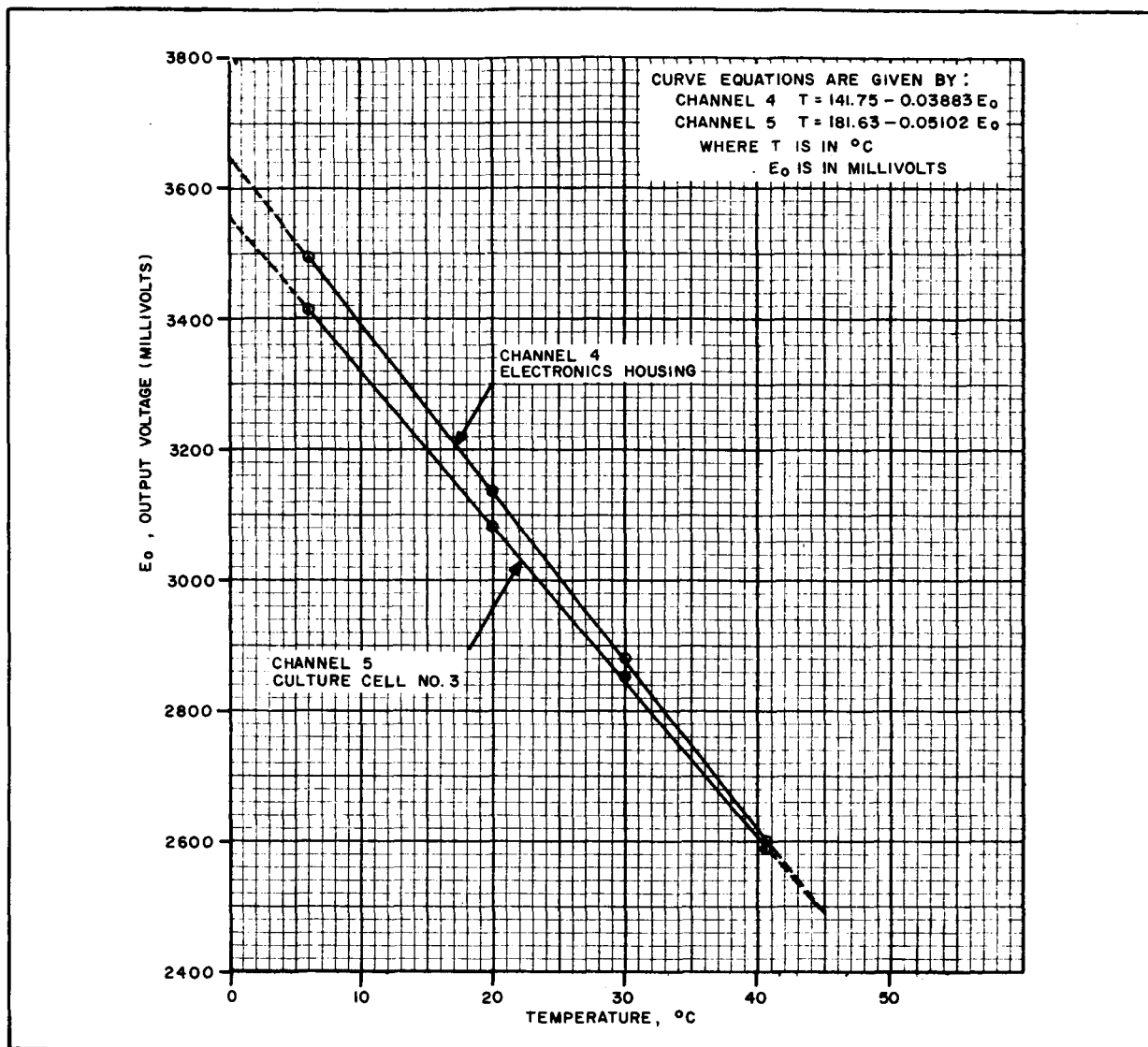


Fig. 8-2 Temperature Probe Calibration

Test results are shown in Figs. 8-3 and 8-4. The curves indicate output voltage changes from the turbidity reading at 20°C. The negative slope of all curves is caused by the light attenuation of water at 10,000 Å wavelength. With increased temperature, the spectral sensitivity of the turbidity photocell increases into the region of the water attenuation wavelength. Even though the lamp monitor photocell sensitivity at the same time increases to compensate for temperature increase, the turbidity signal is reduced by water attenuation. The net effect is the negative temperature slope shown in the figures. Straightness variations between curves are a result of individual photocell response peculiarities. Slope differences are caused by varying degrees of spectral mismatch between turbidity and monitor photocells in each optics train.

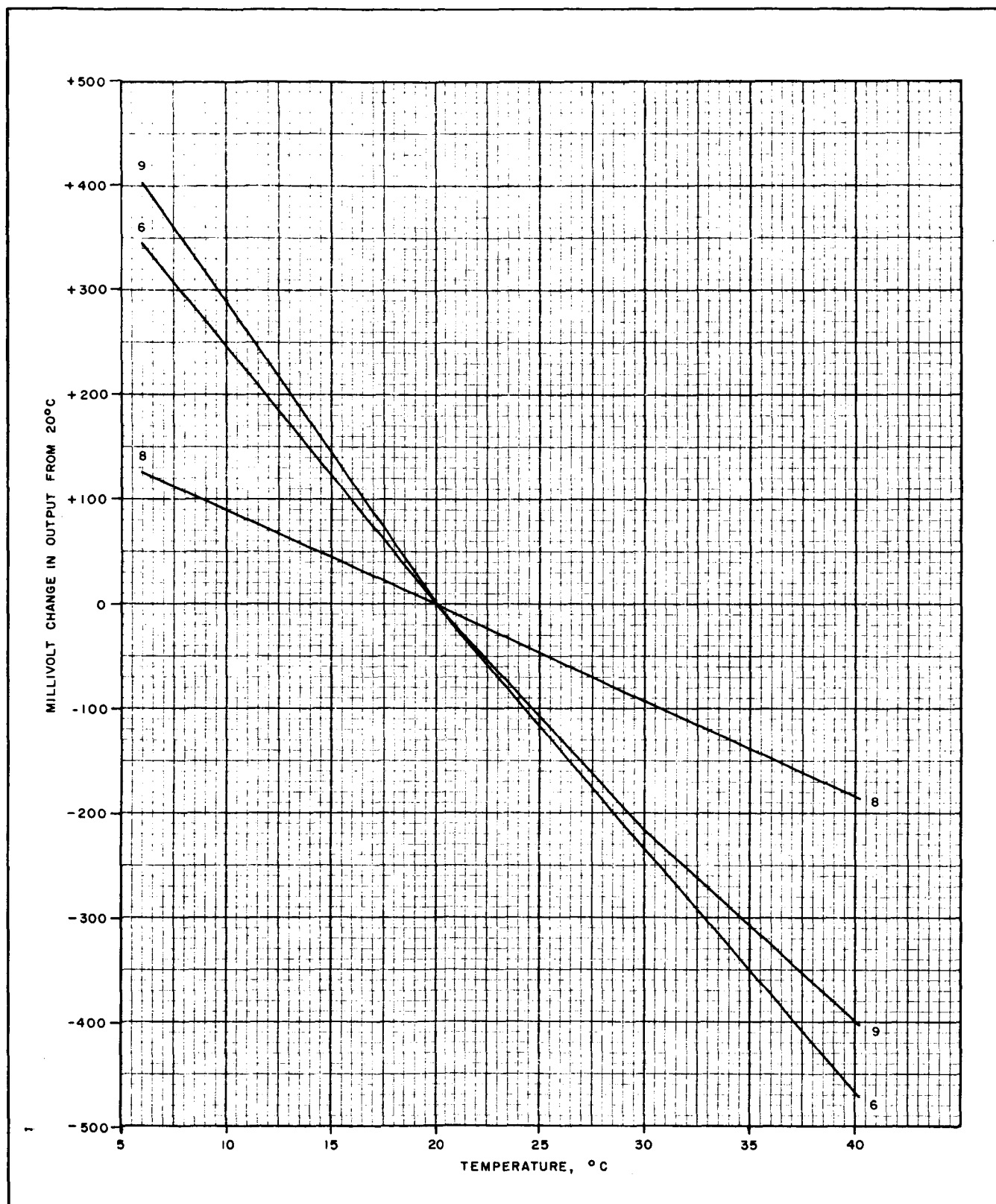


Fig. 8-3 Turbidity Channels 6, 8 and 9 Temperature Variation

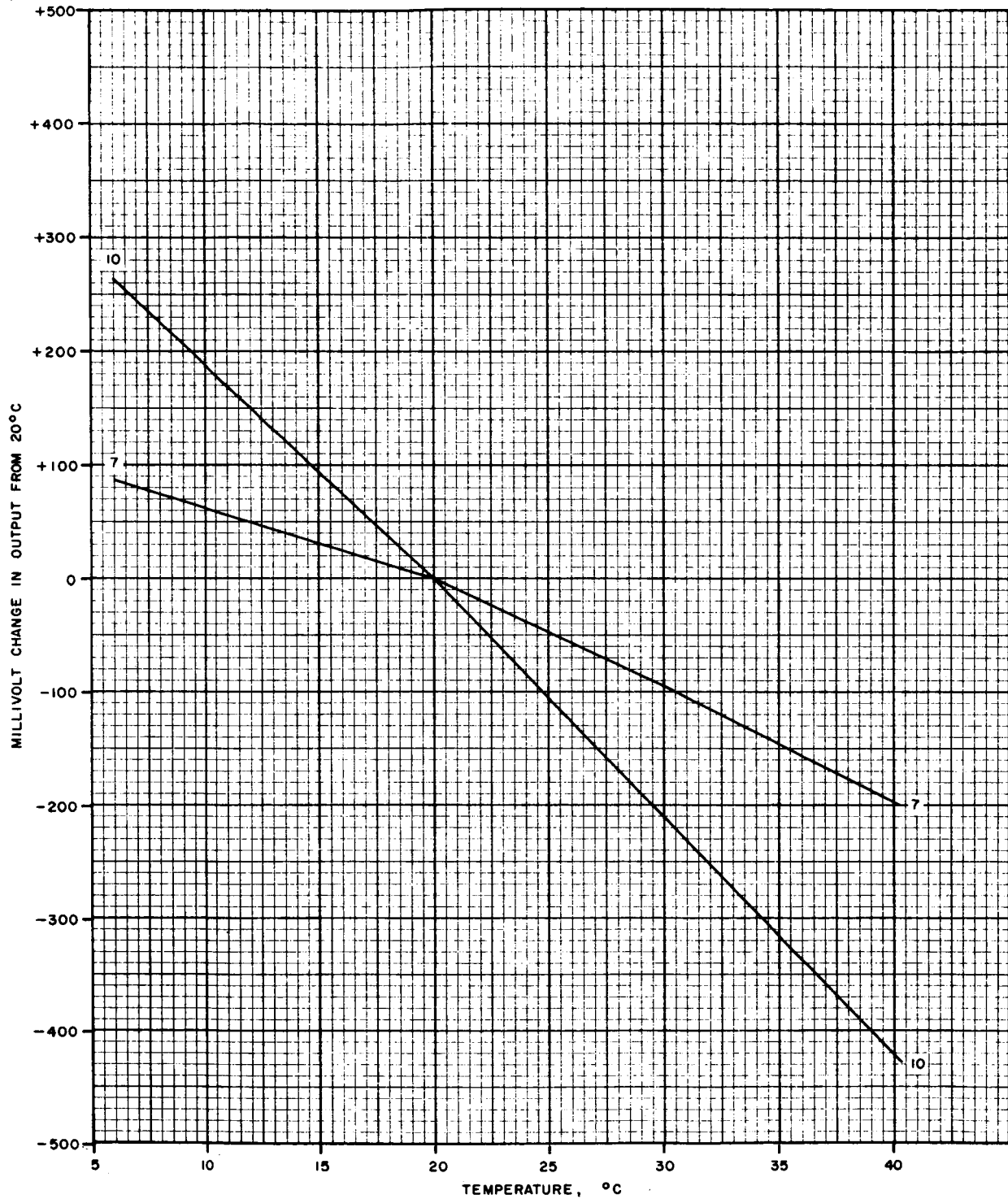


Fig. 8-4 Turbidity Channels 7 and 10 Temperature Variation

8.2.5 Environmental Test Effects

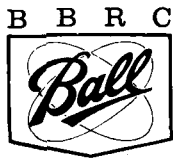
System electronics were subjected to the vibration test with power off. Before the test and between each axis test, the data rack was connected to the experiment and a "quick look" subframe, each of zero, calibrate, and data, was recorded. Five separate opaque slides with various apertures have been fabricated to produce a turbidity data output equivalent to that of a culture cell filled with sterile water. These slides were inserted and data was measured before any environmental testing, after vibration and after heat sterilization. Because the instrument sensitivity is high, insertion misalignment of the slides would cause an output uncertainty of about 25 mv. Table 8-3 shows output change caused by the testing. Changes due to vibration occurred in channels 6 and 9 only. The increased signal is attributed to movement of the occulting disc from its optimum prealigned position. Changes due to sterilization are attributed to both occulting disc translations during heat stress and to photocell degradation.

Table 8-3
 ENVIRONMENTAL TEST EFFECTS ON TURBIDITY SLIDE MEASUREMENTS

Sequence	Output Voltage (mv)				
Channel No.	6	7	8	9	10
Before test output	1708	1988	1821	1022	2162
Change after vibration	+1640	-24	+25	+871	-19
Additional change after sterilization	+200	+178	+96	-303	-10

Data recorded between vibration axis tests showed the calibrate signal from one turbidity channel missing. The signal reappeared after the succeeding test. Investigation showed that a faulty solder joint on one electrical component had momentarily opened. No changes in amplifier zero or calibrate were noticed.

The heat sterilization cycle of 24 hours was followed by a data check using the standard turbidity slides. No loss of functions was noticed, and several days of biological testing were accomplished. Subsequent to that testing, closer inspection of the electronic circuitry showed 12 imminent solder joint failures. Investigation showed two reasons for the faulty joints: a technician in error had used low temperature solder which weakened during sterilization; and thin copper interconnections on printed circuit boards had pulled loose where connected to heavier components. No component failure occurred, although one capacitor showed encapsulation cracking.



8.3 pH SYSTEM

8.3.1 Preliminary Probe Testing

Prior to the development of the pH amplifier circuitry, commercially available pH probes were tested for autoclaving effects. Two sets of Beckman Instruments No. 39167 general purpose probes were selected. Each set consisted of an electrolyte filled reference probe and hermetically sealed pH probe. The reference probes worked satisfactorily throughout nine autoclaving cycles of 30 min duration at 15 psi steam pressure. All probes were immersed in distilled water during sterilization to avoid thermal shock in the glass tips. One pH probe output dropped 25 percent at pH 4 and 56 percent at pH 10 after three autoclaving cycles. The probe failed completely after the fourth cycle because the coaxial cable insulation melted which shorted inner and outer conductors. The other probe showed a 5 percent increase at pH 4 and 10 percent increase at pH 10 after 6 cycles. The probe output was unchanged during three additional heating cycles.

From testing and from conversation with the vendor, we concluded that probe autoclaving is not a desirable way of sterilizing. Because the probe diameters are ideal for the application, shortened versions of the probe were ordered with high temperature cable insulation.

8.3.2 Amplifier Circuitry

The pH amplifier and a commutator developed for the probes were assembled on a printed circuit card. Card material is teflon impregnated glass fiber which has good temperature resistance and extremely high electrical resistance. Preliminary tests included three dry heat sterilization cycles at 150°C for 24 hours each. No electronic circuit degradation was noted although three miniature relays developed high contact resistance and had to be replaced. Immediately prior to system test, the amplifier developed a low impedance short to ground at the input. Investigation showed that accumulation of airborne dust and other contaminants had produced a 10^9 ohm leakage path between relay commutator leads. Subsequent disassembly of the circuit board weakened electrical connections enough to warrant exclusion of the pH electronics from the vibration test. The thoroughly cleaned amplifier board is coated with silicon rubber to eliminate future contaminants.

8.3.3 System Test

The pH system, which uses new miniaturized pH probes, was tested for thermal stability. Table 8-4 shows the worst case stability over the operating temperature range 0 to 50°C and uses standard buffer test solutions.

Table 8-4
 pH SYSTEM TEMPERATURE STABILITY WITH NONAUTOCLAVED PROBES

Buffer Temperature °C	pH 4		pH 7		pH 10	
	0	50	0	50	0	50
pH Units Change from 25°C	0.00	+0.11	+0.10	+0.023	+0.014	-0.05

Stability of the system zero and calibrate is shown in Table 8-5. The apparent temperature dependence is caused by the amplifier which has a built-in thermal drift to compensate for pH probe temperature changes. At the amplifier output, 1 pH unit was 600 mv.

Table 8-5
 pH SYSTEM ZERO AND CALIBRATION TEMPERATURE EFFECTS

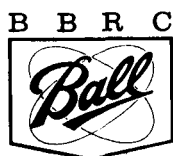
Temperature		5°C	26°C	40°C
Calibrate Zero	Channel No.	Output (v)		
	11-15	4.582	4.515	4.473
Zero	11-15	2.540	2.389	2.361

During biological testing, the pH probes were subjected to three autoclaving cycles of 15 min duration at 15 psi steam pressure. All pH probes developed a glass-to-metal seal leak which allowed the reference hydrochloric acid to leak on to the coaxial cable. The leak caused all probes to become unstable. Table 8-6 shows the resultant temperature instability of all the probes.

Table 8-6
 pH SYSTEM TEMPERATURE STABILITY WITH AUTOCLAVED PROBES^(a)

Buffer Temperature °C	pH 4		pH 7		pH 10	
	5	40	5	40	5	40
Channel						
11	--(b)	+0.40	--(b)	--(b)	--(b)	--(b)
12	+0.31	+1.40	+1.10	+1.90	+0.40	+0.91
13	-0.04	+0.91	+0.61	+1.70	+0.90	+0.34
14	-0.07	+0.96	+0.63	+1.10	+0.70	+0.37
15	-0.05	+0.94	+1.10	+1.10	+0.50	+0.35

- (a) Values given in pH units change from 25°C reading.
 (b) Too unstable.



8.4 STRUCTURE AND PNEUMATIC SYSTEM

8.4.1 Preliminary Tests

Subsystem testing prior to system testing was performed to insure correct pneumatics sequencing and component resistance to heat sterilization. Static friction of the rubber "O" rings in various valves was a problem until the valve cylinder walls were burnished with molybdenum disulphide and the "O" rings lubricated with high temperature silicon grease. Adjustment of valve spring rates and lubrication provided reliable sequencing. Immersion of the entire system in water showed no leaks in either the high pressure gas system or manifold system charged at 1.5 psig.

The bellows assembly had been proof tested by the manufacturer to an internal pressure of 300 psig. Subsystem testing at BBRC shows that the maximum operating external pressure of 210 psig produces no leakage. However, during sterilization testing with 15 cc distilled water in the assembly, the bellows material failed in a weld zone on two separate occasions. Metallurgical analysis of the rupture pointed to improper heat treatment as the failure cause. Second repair of the assembly was successful.

The nozzle assembly was tested with the arrangement shown in Fig. 8-5. Test results are shown in

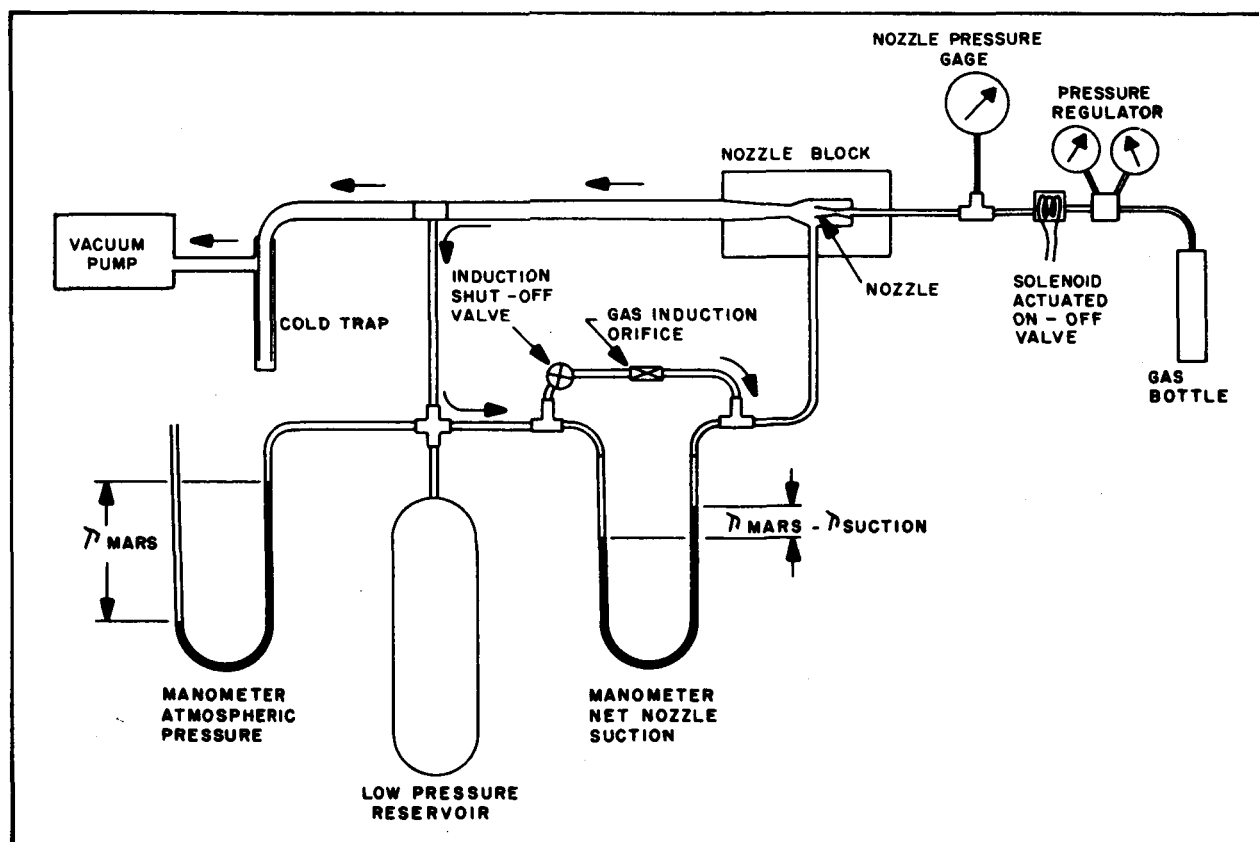


Fig. 8-5 Nozzle Assembly Test Setup

Fig. 8-6. The curve presents pressures achieved during a static operating condition, that is, with no gas induction into the low pressure taps. The particular nozzle produced an 11 mb pressure differential when operated into a 49.5 mb test pressure. By opening the gas induction orifice, the indicated pressure differential decreased to zero with an extremely large orifice. The precise effect of orifice size on induction efficiency was hard to assess because of a number of factors. Calculations indicated that an inlet gas velocity of about 200 ft/sec would transport soil particles up the tube. Gas flow would be sonically limited if the inlet orifice is too small. At the same time, the pressure differential would decrease if the inlet is too large. Gas flow friction is a function of transport tube diameter and surface smoothness. However, the curve does show the maximum attainable pressure differential and the reservoir pressure required to achieve this. Soil transportability of the system with the particular inlet orifice size and tube characteristics is shown in the following section.

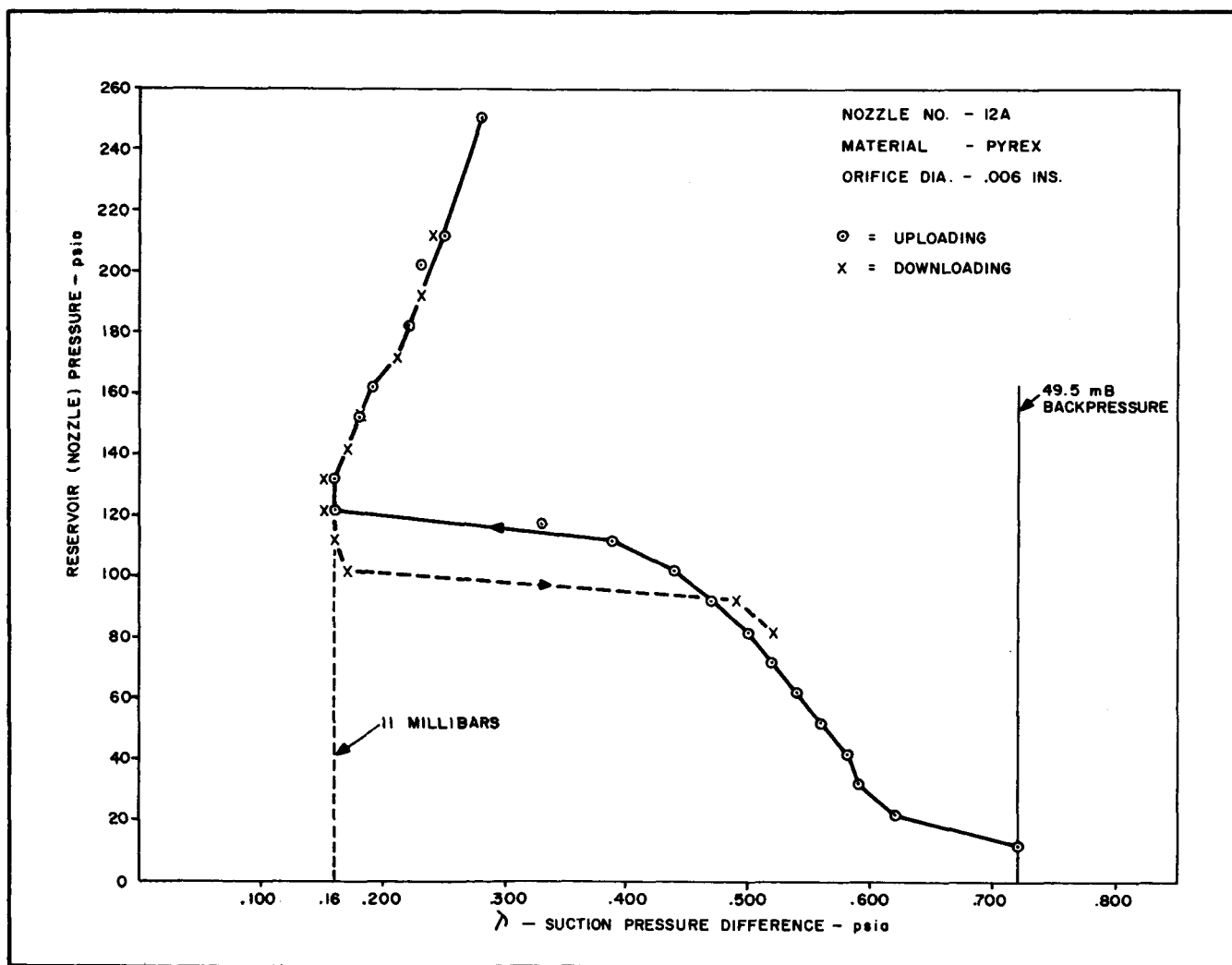
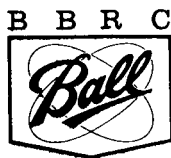


Fig. 8-6 Nozzle Test Results



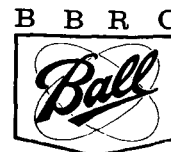
Temperatures within the nozzle assembly during operation were significantly lowered by the expanding gas. With the Mach 5 nozzle used at an ambient temperature of 70°F, the calculated nozzle throat temperature was -18°F, and the gas temperature at the nozzle efflux was -372°F. The opaque nozzle mount did not permit visual inspection of the nozzle for icing. Even though the high pressure gas used was water-pumped nitrogen, which has a dew point above the nozzle efflux temperature, icing is not considered a problem in actual operation because the induced gas would warm the nozzle. The data in Fig. 8-6 shows that the nozzle suction is dependent upon the direction the operating pressure is approached. Uploading (gradual increase of high pressure gas) produced a sharp transition into the optimum suction zone while downloading resulted in slightly better pressure differentials over a greater high pressure range. The test required about 30 min operation which did considerably cool the nozzle mount. Immediately following the test, another uploading was attempted and this resulted in a plot (not shown) above the two curves, which had a maximum suction pressure of 0.17 psia. It is possible that nozzle icing reduced the efflux diameter and changed the area ratios sufficiently to produce this effect.

8.4.2 Sample Acquisition Test

The sample acquisition was performed by placing the entire pneumatics assembly in a tall bell jar which was evacuated to a pressure of 37 mm absolute (50 mb). The gas reservoir was charged to 1,000 psi with dry nitrogen, and electrical connections were made to the gas release solenoid. A motor driven cam was arranged to allow gas turnoff at any time by depressing the latching solenoid release. The bellows assembly was filled with 15 cc of water and a new rupture diaphragm fitted for each test. The entire assembly was placed on a 16 in. high pedestal within the bell jar and the suction probes were placed at the bottom of the enclosure on beds of Lake Mead sand supplied by JPL. Total vertical lift from sand bed to nozzle assembly was 26 in. through the two 0.07 in. diameter, 4 ft long teflon tubes, which were helically coiled downward.

During the first test, the entire gas reservoir was exhausted during 6 min operation at a regulated pressure of 120 psig. Gas bubbling through the hopper liquid was more violent than at ambient laboratory atmosphere, and about 6 ml water was lost through the hopper vent valve. At gas exhaustion, the hopper vent valve closed, the pilot valve actuated, but the hopper dump valve did not open. Inspection of the assembly showed that the accelerated water evaporation during the test, coupled with the highly cooled gas bubbling through the liquid, had frozen the entire hopper assembly. Subsequent testing showed that freezing would occur in about 2 min operation.

Another test was performed in which gas was supplied for 30 sec operation. All systems functioned normally except for about 5 ml water lost through the hopper relief valve. The emergent water-sand mixture was caught in test tubes. Water measurement showed volume distribution uniformity of about 15 percent. Tests at atmospheric pressure produced greater uniformity because less water loss through the hopper vent valve permitted volumetric distribution of the water in the five manifold tubes. The



amount of sand distributed in each test tube weighed about 20 mg.

8.4.3 Vibration Test

During the vibration test described in Section 8.1, components in the pneumatics system had resonance frequencies lower than anticipated. Visual monitoring of displacement amplitudes was accomplished by using a stroboscopic light synchronized to the test vibration frequency. Predominant resonances occurred in the high pressure plumbing, the gas reservoir assembly, and the hopper assembly. The titanium tube plumbing is considered strong enough to withstand acceleration input to 20 g's. Inspection of the vibration input plots and transmissibility data of Appendix C indicated that at resonance (300 and 370 Hz), the gas bottle was subjected to 105.5 g acceleration loads. The structure was analyzed and considered capable of withstanding 200 g's, indicating that the test input could have been increased to 20 g's.

Input vibration amplitude is limited by transmissibilities encountered in the hopper assembly. A monitoring accelerometer on the hopper indicated that amplification factors of 10 times input were experienced. Since the hopper attachment plate had been stressed for 100 g's in the transverse direction, test input was limited to 10 g's, which produced the maximum local accelerations.

Damage resulting from the vibration test occurred in the nozzle assembly and gas reservoir. The glass nozzle developed a crack in the mounting flange. Repair was made by heat fusing the crack with no loss in performance. For personnel safety during close visual monitoring, the high pressure gas reservoir was not charged during testing. Internal gas pressure prevented the input ball check valve from being firmly seated, and as a result it vibrated and deformed its sealing seat. Otherwise, the assembly is leakproof if a screw-on metal cap closes the input connection.

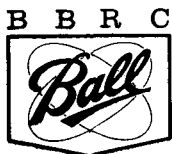
8.4.4 Sterilization Tests

The entire pneumatics assembly, except for the metal bellows which was sterilized in a separate tests, was maintained at 145°C for 24 consecutive hours. No change in performance could be detected.

8.5 BIOLOGICAL TESTING

Biological testing is performed before and after heat sterilization to determine the instrument response to microorganisms. A pure culture of E. Coli., strain K-12, was used in a medium optimum for its growth. Both inoculum and test cultures were counted on agar petri plates made from the same medium. The aqueous culture broth contained 0.5 percent sodium chloride, 1.0 percent bactotryptone, and 0.1 percent thiamine hydrochloride.

Preparation for a test first required complete disassembly of the manifold and culture cells. All parts were brush scrubbed with a laboratory detergent and triple rinsed in distilled water. The quartz end



windows were then cleaned in a solution of potassium dichromate and sulphuric acid, rinsed with distilled water, and wiped with lens tissue. The complete assembly was sterilized in a 160°C oven for 4 hours. Two milliliters of sterile medium were aseptically transferred into each of the cooled culture cells. The charged assembly then was placed in the instrument, and data was recorded during at least 4 hours allowed for particulate settling. The entire instrument was placed in a temperature oven maintained at 30°C. A 0.1 ml aliquot of prepared culture was added as an inoculum to each cell. The inoculum was taken from serial dilutions of a fresh stock culture sufficient to provide an initial organism population between 20 and 200/ml. When the turbidity data indicated a rise of at least 50 mv above a stable background, a 0.1 ml aliquot of each culture was taken and a serial dilution was made. Six petri plates were prepared for the dilutions, which cover three decades population. Each plate consisted of a thin layer of hard agar covered by another layer of soft agar, into which the dilution aliquots had been mixed. Test plates were incubated at 37°C for 17 hours before counting.

Operational problems encountered during testing resulted from poor procedural technique or from culture turbidity characteristics not completely understood. Cell assembly procedure requires inserting a quadrature rubber ring on the circumference of each end window. Both pieces then are inserted into the culture cell with a tool that seats the window against the cell body and guides the rubber ring into the annular space between window and body. The sleeve retainer then is inserted and held captive by the screw-on cap. If the window is not carefully inserted, a part of the sealing quad ring would be forced between the window and its seat. This results in an optically wedged cell which would deviate the parallel light beam from its normal path so that it misses the occulting disc. The condition appeared as a background turbidity signal that varied between tests. Other problems encountered are irregularities in turbidity data for which explanation was beyond the scope of the contract.

The most frequently occurring problem is short-term variations in turbidity data. On a plot of turbidity datum points every 5 min, the variations resembled electrical circuit noise and had peak-to-peak amplitudes of as much as 20 mv. The condition was noted in sterile media which has been filtered to remove all particulates greater than 0.4 μ diameter. Another frequently occurring problem is a sudden drop in turbidity signal when a pure culture inoculum is added to a sterile cell. The drop could be as much as 50 mv and could produce either the same plot noise as before inoculation, or could produce short-term violent fluctuations in the turbidity signals. Both effects mentioned undoubtedly had produced some uncertainty in plate count accuracies.

Plate count data for sensitivity test before and after environmental tests are shown in Table 8-7. Both inoculum and test cultures are expressed as the average of six plates counted. The tabulation of organisms per millivolt indicate that within statistical limits, vibration and sterilization have no effect on instrument performance.

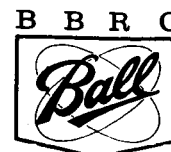
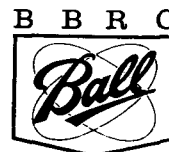


Table 8-7
BIOLOGICAL SENSITIVITY TEST RESULTS

Data	Channel No.				
	6	7	8	9	10
<u>Before Sterilization</u> (Inoculum 18 bugs/ml)					
Signal increase above background (mv)	60	39	111	303	168
Elapsed time from inoculation (min)	605	620	630	645	660
Final population count (bugs/ml)	2.16×10^6	1.99×10^6	3.91×10^6	5.01×10^6	6.65×10^6
Population to signal ratio (bugs/ml/mv)	3.6×10^4	5.1×10^4	3.52×10^4	1.65×10^4	3.73×10^4
<u>After Sterilization</u> (Inoculum 45 bugs/ml)					
Signal increase above background (mv)	150	122	87	205	129
Elapsed time from inoculation (min)	535	545	525	575	560
Final population count (bugs/ml)	2.56×10^6	3.49×10^6	1.68×10^6	5.49×10^6	3.46×10^6
Population to signal ratio (bugs/ml/mv)	1.71×10^4	2.86×10^4	1.9×10^4	2.68×10^4	2.68×10^4



Section 9

CONCLUSIONS AND RECOMMENDATIONS

9.1 CONCLUSIONS

The engineering model of the Wolf Trap represents the initial attempt to transform the concept into engineered hardware. Even though the earlier breadboard model showed that the concepts of sample acquisition and microorganism detection were feasible, the real effort of designing for a typical flight configuration must be accomplished by this phase. Broadly stated, the objectives of the program are: (1) to show how the device works operationally, and (2) to determine if the concepts are adaptable to flight hardware. Many of the operational problems encountered in testing remain unresolved, but, as a result of this program, it is now established that the turbidity detection concept can be adapted to flight mission requirements. Probably the most significant detail learned is that the basic design approaches employed are capable of withstanding dry heat sterilization.

The operational problems encountered include the maintenance of a clean turbidity system and interpretation of data. The sensitivity of the turbidity system requires that all optical components and culture cell windows be superbly clean. Conventional clean room techniques are to be employed for fabrication of mission hardware; this eliminates many of the problems encountered in the engineering model. However, the problem remains of maintaining a clean system during prelaunch biological testing. The problem of data interpretation is a result of unanticipated turbidity characteristics in the cultures. Recent developments in nephelometry instrumentation (Section 10.5) indicate that the forward scatter principles used in the Wolf Trap could be used to determine culture particulate size. This potential increase in instrument capability suggests a revised program objective which would significantly enhance the scientific value of the experiment.

Further development of subsystems and components resistant to heat sterilization is required. A dependable pH system must await development of sterilizable pH probes. Basic technological investigation currently being conducted by NASA undoubtedly will increase the number of electronic components and materials suitable for mission hardware. With the exception of carbon composition resistors, capacitors, relays, and standard printed circuit boards, all items in the engineering model have shown remarkable endurance to heating cycles. This program has also emphasized the necessity of extensive preassembly component screening of even preferred parts.

Successful vacuum cleaner acquisition of a sample on the Martian surface is quite dependent on atmospheric pressure. The venturi nozzle system offers a simple means of transporting aerosolized particles over considerably distances. A light weight extendable nozzle could acquire small particles dug up by mechanical augers and aerosolized locally by high pressure gas jets. The induced particles would then be conveniently transported back to the landed capsule in low pressure transport tubes. Potential capability



of the system would have to be proved by testing various nozzle combinations at reduced atmospheric pressures.

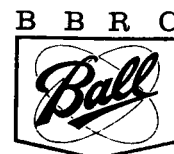
The engineering model of the Wolf Trap has shown that although the concept is adaptable to an exobiological mission, more complete turbidity data must be provided. Increased instrument capability could produce significant information about both micrororganism and soil particulate sizes. A deeper study into scattering phenomena should precede the engineering development of an extended capability device.

9.2 ENGINEERING RECOMMENDATIONS

Experience with the engineering model has shown many areas in which engineering improvements could be made. These are listed below in the principal subsystem classification used throughout the report.

9.2.1 Turbidity Detector

- The optics assembly weight could be reduced by using either a "bird cage" structure or light weight casting in place of the milled aluminum block. A greater number of cultures could be monitored with no appreciable increase in weight by using a common optics system which would rotate around a culture cell "merry-go-round" in which the cells remain stationary to avoid affecting turbidity data.
- The number of lenses could be reduced or high efficiency coatings employed to minimize light loss.
- A high intensity pulsed light source could be used to reduce average power. Recent development in injection lasers show the devices have greater reliability than tungsten incandescent sources. The extremely small size of the device could greatly simplify optics design.
- A detection scheme could be developed which would differentiate culture particle sizes (Section 10.5). Problems encountered during testing of the engineering model could conceivably be resolved by knowing if the interfering signals are due to random particulates in the culture, liquid convection currents or oddly behaving microorganisms.
- Photocells could be either better matched thermally, or temperature compensated to minimize the thermal drift.



9.2.2 Electronics System

Although the DC circuitry in the engineering model has sufficient gain and shows good resistance to heat sterilization, the use of a pulsed light source in the turbidity detector would require AC amplifiers in the electronics. Some advantages in long-term stability and greater gain could be realized by using AC amplifiers. The recommendations listed below apply to either type electronic system.

- A different calibrate system could be developed which would check both optical system and electronics performance. The present scheme injects a fixed current into the amplifier to show only circuitry stability. A preferred method would divert the illumination beam around the culture cell either by mirrors or by moving the culture cell out of the beam. This technique would show the stability of the entire turbidity system.
- An automatic background compensation circuit would be desirable. The circuit would automatically adjust the output voltage to near zero when the turbidity data reached its lowest value. Such a scheme would permit the full use of a linear output scale with increased amplifier gain to show greater resolution at low microorganism populations.
- Electronic packaging on printed circuit boards requires the use of better heat resistant materials. Problems encountered during heat sterilization include solder separation from gold plated copper strips. Recent development in sterilizable materials would help reduce problems.
- Preassembly component screening should be quite intensive for heat sensitive items. These included carbon composition resistors, capacitors, and relays. The use of relays in low current circuits should be avoided because contact resistance increases during heating.

9.2.3 pH System

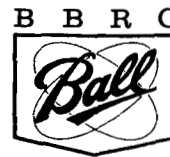
- Separate amplifiers rather than relay commutations should be used for each pH probe set to switch probes to a common amplifier. The greater the number of components in the high impedance input, the greater the chance of shunt leakage paths affecting the reading.
- Amplifier packaging in the high impedance input section should not use printed circuit material, but should employ point-to-point wiring on insulated standoffs.



9.2.4

Pneumatics and Structure

- The pneumatics mounting plate must have additional strengthening webbing in the area of the hopper mounting.
- Sample acquisition time should be shortened to about one minute to reduce the accelerated cooling of the water in the hopper.
- The hopper vent valve should be baffled to prevent water loss during sample acquisition.
- The spike pickup probe should be at least four ounces heavier to overcome the spring force of the coiled teflon tubing.



Section 10
REFERENCES

1. Ball Brothers Research Corporation, Engineering Breadboard Model- Wolf Trap Microbe Detection Device, Final Report, BBRC F65-6, Contract NsG-209AG-1, Boulder, Colorado, 8 Sep 65 (U)
2. University of Rochester (New York), Field Trials of the Wolf Trap Engineering Breadboard, by C. R. Weston, NASA N66-2386 (U)
3. H. C. van de Hulst, Light Scattering by Small Particles, New York, J. Wiley Sons, 1957
4. Roger G. Bates, "Measurement of Electromotive Force," Determination of pH: Theory and Practice, New York, J. Wiley Sons, 1964
5. J. Raymond Hodgkinson, "Particle Sizing by Means of the Forward Scattering Lobe," Applied Optics, Vol. 5, No. 5, pp. 839-843, May 66
6. H. W. Liepmann and A. E. Puckett, Introduction to Aerodynamics of a Compressible Fluid, New York, J. Wiley Sons, 1947
7. U. S. Navy Bureau of Ordnance, Handbook of Supersonic Aerodynamics Nav. Ord 1488, Vol. 2, Oct 50
8. Lee L. Evans, "Biasing FET's for Zero DC Drift, "Electro-Technology", Aug 64
9. Union Carbide Corporation, Product Bulletin No. 3: Zero Temperature Coefficient in FET's, Mountain View, Cal., May 65



Appendix A
DETERMINATION OF NOZZLE CHARACTERISTICS



Appendix A
DETERMINATION OF NOZZLE CHARACTERISTICS

A.1 TEMPERATURE AT NOZZLE THROAT (SECTION 10.7)

Gas velocity at throat is Mach 1

$$\text{Temperature ratio } \frac{T^*}{T_o} = 0.833$$

where

T^* = Absolute throat temperature

T_o = Absolute reservoir temperature

for

$$T_o = 70^\circ\text{F}$$

$$T^* = -18^\circ\text{F}$$

A.2 TEMPERATURE AT NOZZLE EXIT FOR MACH 5 NOZZLE (SECTION 10.7)

$$\frac{T}{T_o} = 0.167$$

where

T = Absolute nozzle temperature

for

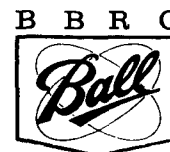
$$T_o = 70^\circ\text{F}$$

$$T = -372^\circ\text{F}$$

A.3 MASS FLOW THROUGH NOZZLE

A.3.1 From Section 10.6, gas mass flow (m) is obtained from a deviation of the compressible Bernoulli equation, namely

$$m = A \sqrt{\frac{2\gamma}{\gamma-1}} p_o \rho_o \left(\frac{p}{p_o} \right)^{2/\gamma} \left[1 - \left(\frac{p}{p_o} \right)^{\frac{\gamma-1}{\gamma}} \right] \quad (\text{A.1})$$



where

- A = Nozzle throat cross sectional area
- p_o, ρ_o = Reservoir gas pressure and density respectively
- p = Pressure of nozzle exit (for nozzle without extension)
- γ = Ratio of specific heats (equals 1.4 for nitrogen gas)

For a reservoir pressure of 130 psig (14.2 psia) and a nozzle throat diameter $d = 0.006$ in. ^(a)

$$m = 2.92 \times 10^{-6} \text{ slugs/sec}$$

A.3.2 From the above, it was deduced that

$$m = K d^2 p_o \quad (A.2)$$

where

- K = A constant
- d = Nozzle throat diameter

A.4 AREA RATIO NOZZLE

For nozzle used

$$\frac{A}{A^*} = 27.5 \text{ for Mach No. } M = 5.12$$

where

- A = Nozzle exit area
- A = Nozzle throat area

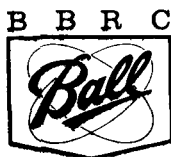
A.5 PRESSURE RATIO OF NOZZLE USED (MACH 5.12)

$$\frac{p}{p_o} = 0.00164$$

where

- p = Nozzle exit pressure
- p_o = Nozzle reservoir pressure

(a) Note that atmospheric pressure in the Boulder area approximates 12.2 psia.



for

$$\begin{aligned} p_o &= 142 \text{ psia} \\ p &= 0.233 \text{ psia} \\ p &= 16.1 \text{ mb} \end{aligned}$$

The actual nozzle used produces a calculated $M = 5.12$ and obtained peak suction is 11 mb. Discrepancies may well be due solely to an inability to measure nozzle throat or exit areas accurately enough.

A.6 DUST COLLECTION PARAMETERS

A.6.1 Analysis of the dynamics of a dust particle suspended in a vertical gas stream, based on a conservative value for drag coefficient of 1.4, and on a specific gravity of 3.0 provides a minimum vertical stream velocity, V .

$$V = 46 \text{ ft/sec}$$

In determining the induction port size, a 200 ft/sec flow velocity is considered desirable.

A.6.2 Since particle lifting forces on earth and Mars must be equal to compare relative induction performance, the forces are broken into components.

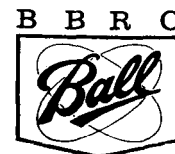
Analysis shows that

$$F \propto C_D \left(\frac{\frac{1}{2} \rho V^2}{g} \right)$$

where

$$\begin{aligned} F &= \text{Particle lifting force} \\ C_D &= \text{Drag coefficient} \\ \rho &= \text{Air or gas density} \\ V &= \text{Induced stream velocity} \\ g &= \text{Local acceleration due to gravity} \end{aligned}$$

Furthermore, in suction tests, the manometer reading "Suction Obtained", actually reads the dynamic pressure term " $\frac{1}{2} \rho V^2$ ", letting $k = \frac{1}{2} \rho V^2$ and denoting subscripts "E" for Earth characteristics and "M" for Mars respectively.



We obtain, by equating particle forces,

$$\frac{C_{D_E} k_E}{g_E} = \frac{C_{D_M} k_M}{g_m}$$

$$\text{Let } X = \frac{k_E}{k_M} = \frac{g_E}{g_m} = \frac{C_{D_M}}{C_{D_E}}$$

where X = Earth experimentation factor

Since drag coefficients depend on kinematic viscosity and Reynolds' Number, then

$$\frac{C_{D_M}}{C_{D_E}} = 1.413, \text{ and since } \frac{g_E}{g_m} = \frac{1}{0.38}$$

we have

$$\underline{X = 3.72}$$

We, therefore, conclude that the height of the mercury suction column for earth tests should be 3.72 times as high as that for actual simulated Martian tests.

At 50 mb, for nozzle pressure = 142 psia, $k_M = 2.85$ cm/sec

and

$$k_E = 3.72 \times 2.85 = 10.6 \text{ cm/sec}$$

and at earth atmosphere, this nozzle performance is achieved at 210 psig.

Finally, for 50 mb tests, the nozzle pressure must be regulated to 130 psig and for equivalent performance at earth atmosphere to 210 psig.



Appendix B
THE pH AMPLIFIER BIAS SAMPLE CALCULATION



Appendix B

THE pH AMPLIFIER BIAS SAMPLE CALCULATION

The required input drift in a junction field effect transistor required to effect the external thermal drift indicated in Section 5 is given as

$$\Delta V_{gs} = -1.0 \text{ mv}/^{\circ}\text{C}$$

where ΔV_{gs} is the change in gate-to-source voltage with temperature.

For the double diffused FET, the input coefficient for any value of drain current is given by the expression (Section 10.7).

$$\Delta V_{gs} = 2.2 \left(1 - \sqrt{\frac{I_d}{I_{do}}} \right) \quad (\text{B.1})$$

where

$$\begin{aligned} I_d &= \text{Drain current} \\ I_{do} &= \text{Drain current at zero drift} \end{aligned}$$

Solving for I_d we have

$$I_d = I_{do} \left(1 - \frac{\Delta V_{gs}}{2.2} \right)^2 \quad (\text{B.2})$$

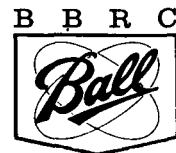
An expression relating zero bias and zero drift drain currents is given in Section 10.8 as

$$I_{do} = I_{dss} \left(\frac{K}{V_p} \right)^2 \quad (\text{B.3})$$

where I_{dss} is the zero bias drain current ($V_{gs} = 0$), V_p is the pinchoff voltage, and K is a constant for the transistor.

Parameter values for the double diffused silicon 2N3112 are

$$\begin{aligned} I_{do} &= 7 \mu\text{a} \\ I_{dss} &= 80 \mu\text{a} \\ V_p &= 1.90 \text{ v} \\ K &= 0.67 \end{aligned}$$



Substituting the parameter values into Eq. (B.3), we have

$$I_{do} = (80 \mu a) \left(\frac{0.67}{.90v} \right)^2 = 10 \mu a$$

This value of I_{do} is now substituted in Eq. (B.2) to find the value of I_d for the required ΔV_{gs} value of $-1.0 \text{ mv}/^\circ\text{C}$.

$$I_d = 10 \mu a \left(1 - \frac{-1.0}{2.2} \right)^2 = 21 \mu a$$

The bias voltage V_{gs} is calculated from the following equation taken from Section 10.7.

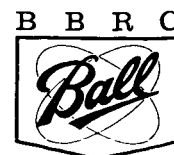
$$I_d = I_{dss} \left(1 - \frac{V_{gs}}{V_p} \right)^2 \quad (\text{B.4})$$

Solving Eq. (B.4) for V_{gs} we have

$$V_{gs} = V_p \left(1 - \sqrt{\frac{I_d}{I_{dss}}} \right) \quad (\text{B.5})$$

Substituting the calculated value of I_d and the other parameter values into Eq. (B.5), we obtain the correct transistor bias needed to produce the compensating input value of ΔV_{gs} :

$$\begin{aligned} V_{gs} &= 1.90 \left(1 - \frac{21}{80} \right) \\ &= 0.930 \text{ v} \end{aligned}$$



Appendix C
VIBRATION TEST LEVELS AND TRANSMISSIBILITIES

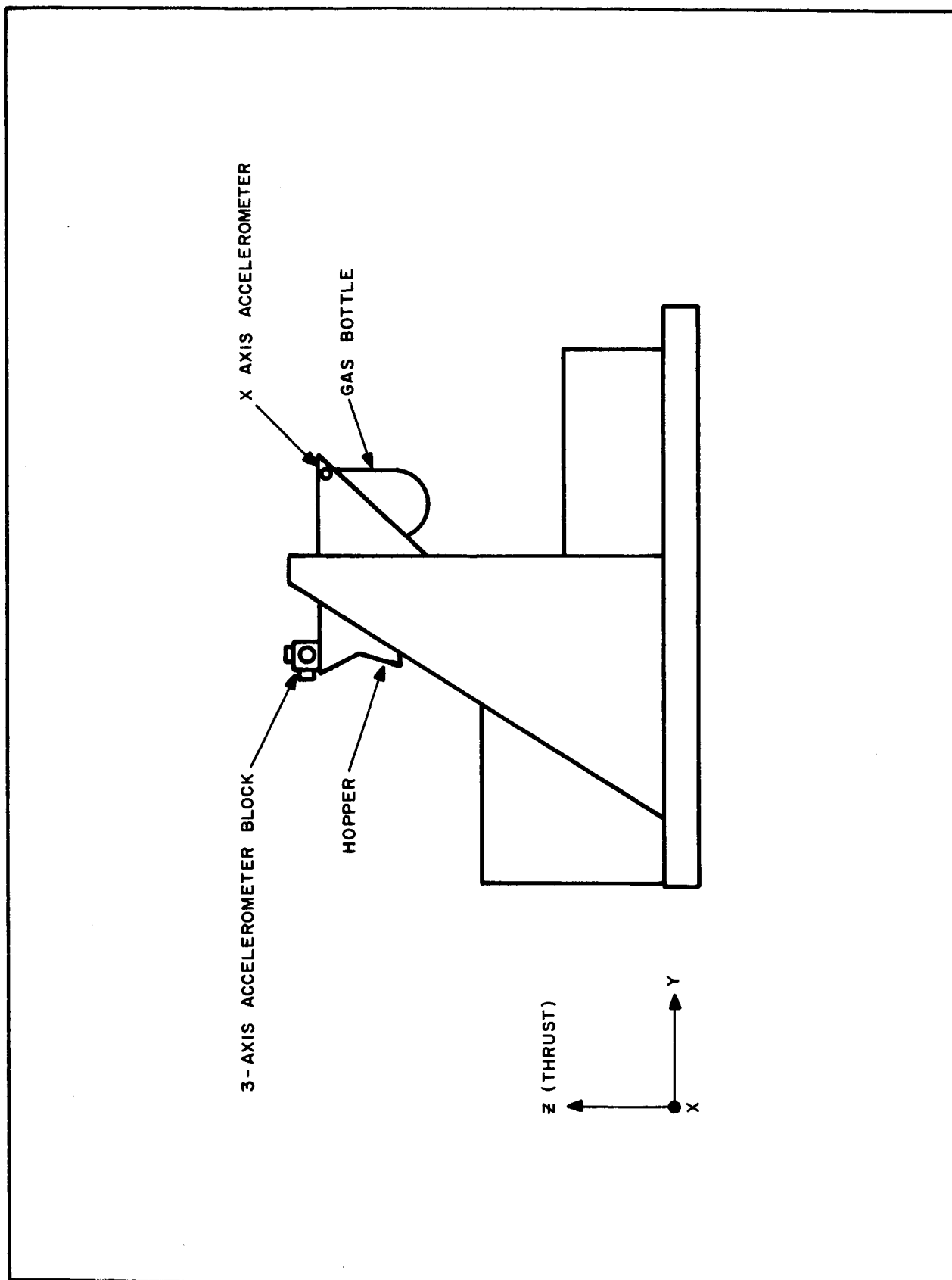


Fig. C-1 Wolf Trap Vibration Axis Notation

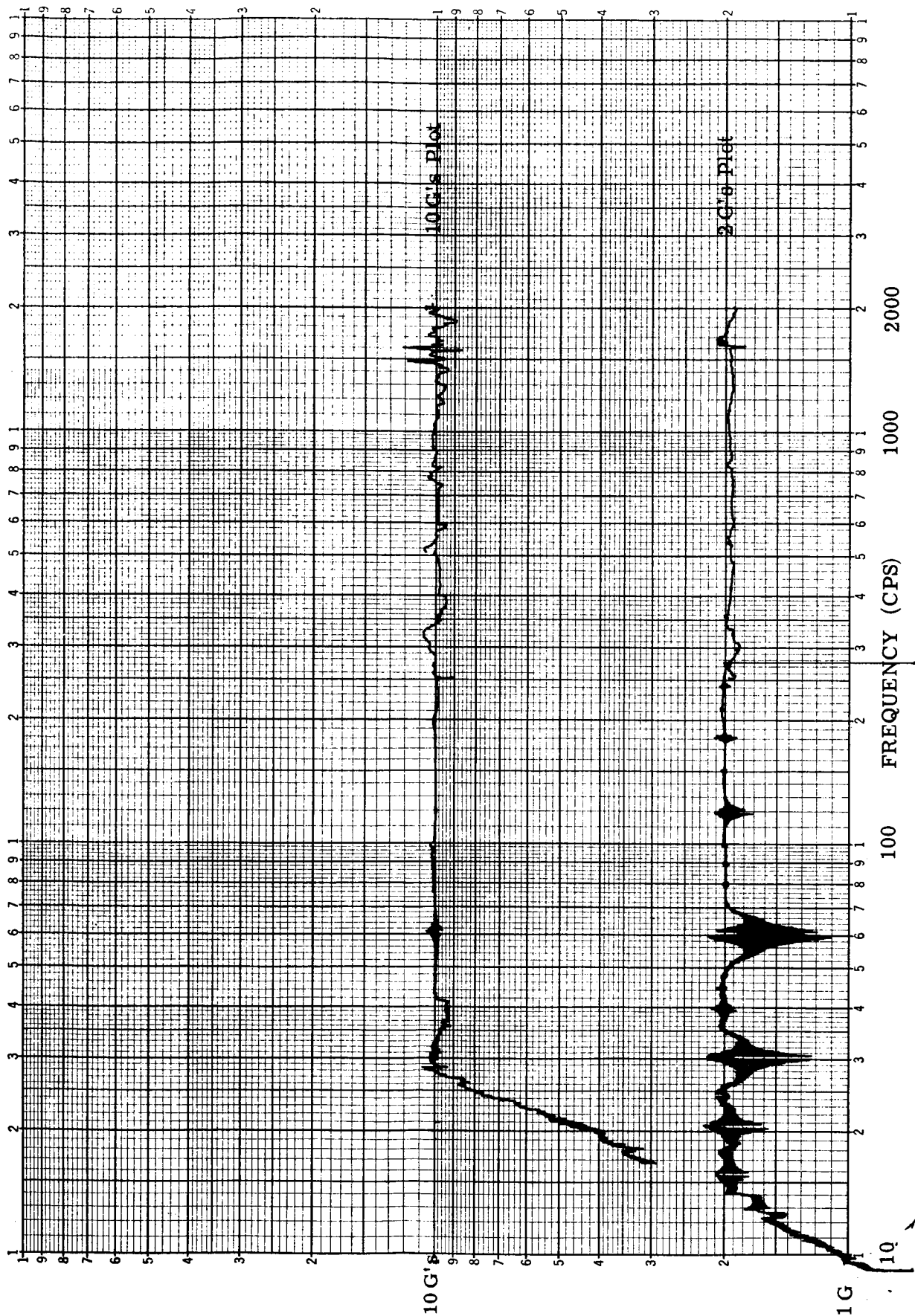


Fig. C-2 Sine Sweep Input Level to Bottle; Transverse X Axis

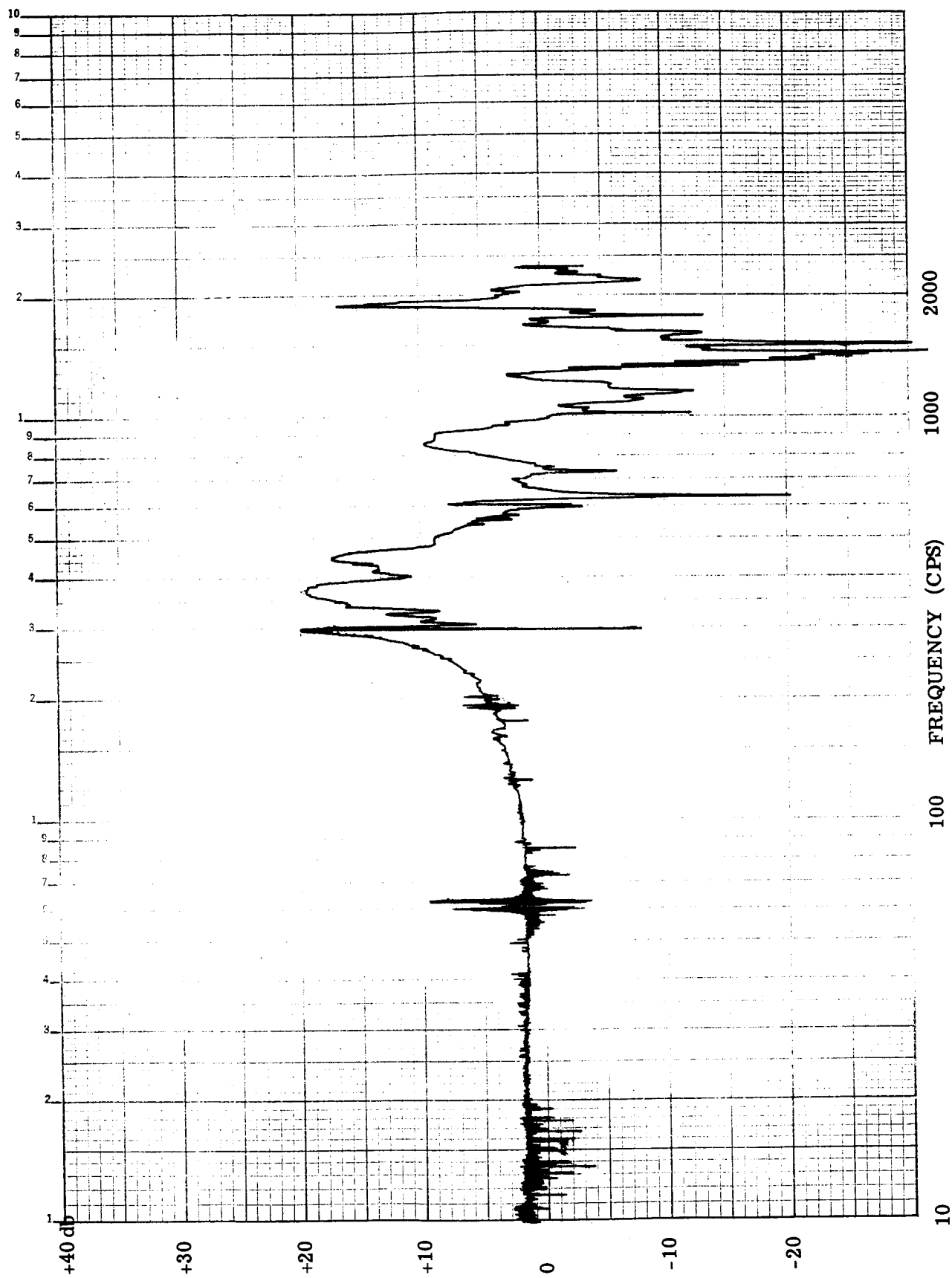
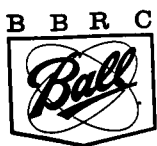


Fig. C-3 Transmissibility Plot of Bottle Bracket; Transverse X Axis; Input Level 2 g's

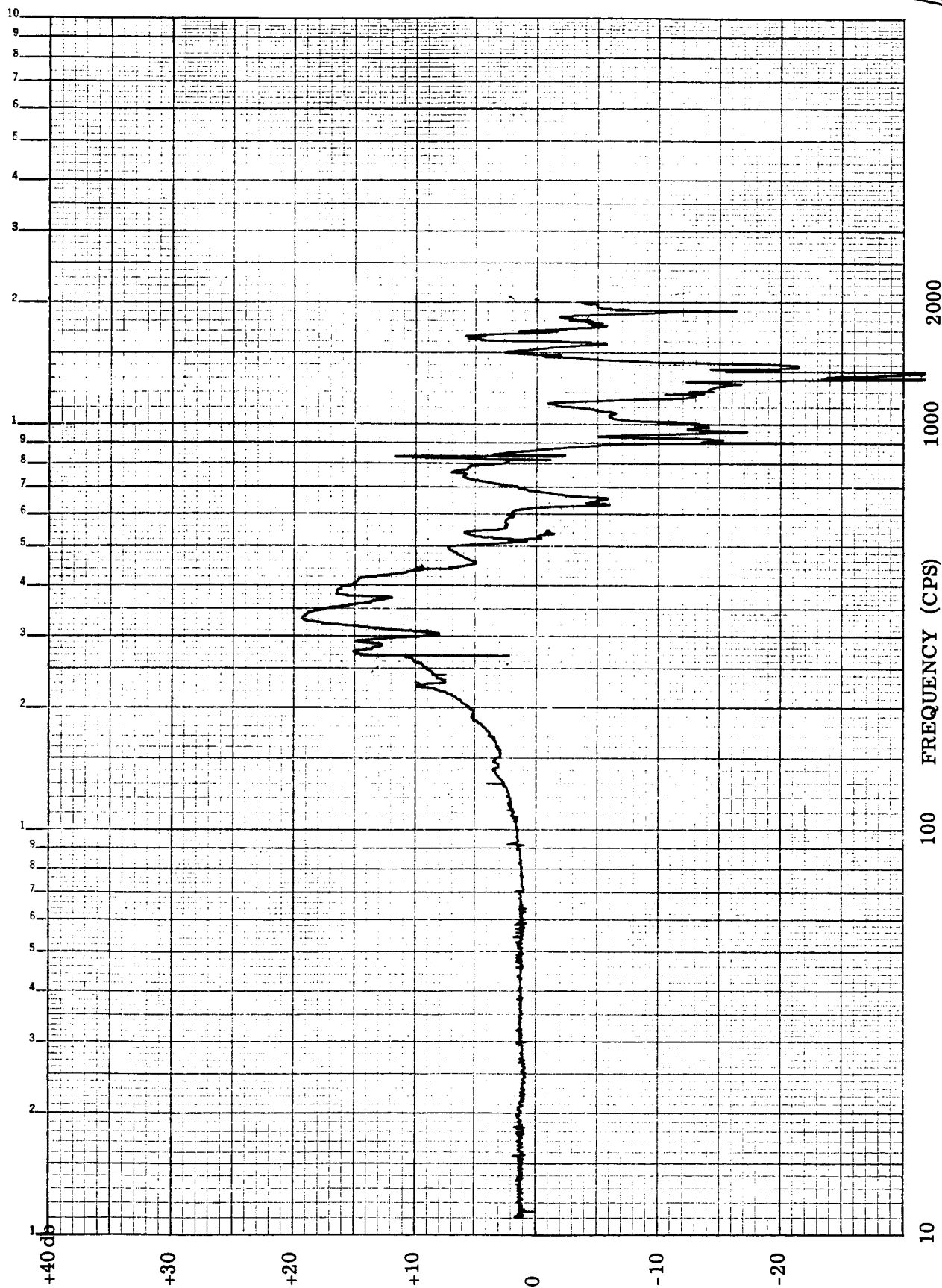


Fig. C-4 Transmissibility Plot of Bottle Bracket; Transverse X Axis; Input Level 10 g's

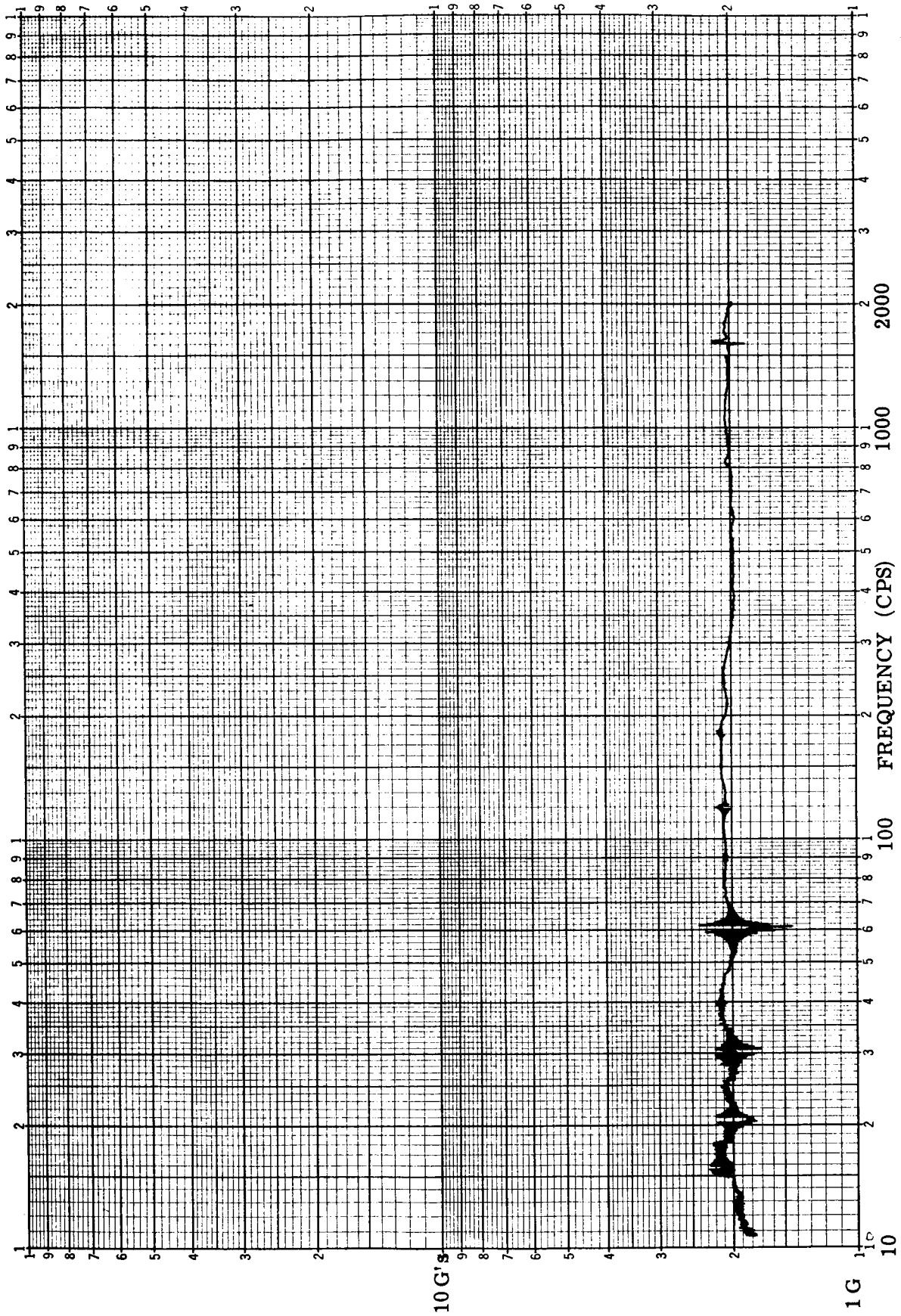


Fig. C-5 Sine Sweep Input Level to Hopper; Transverse X Axis

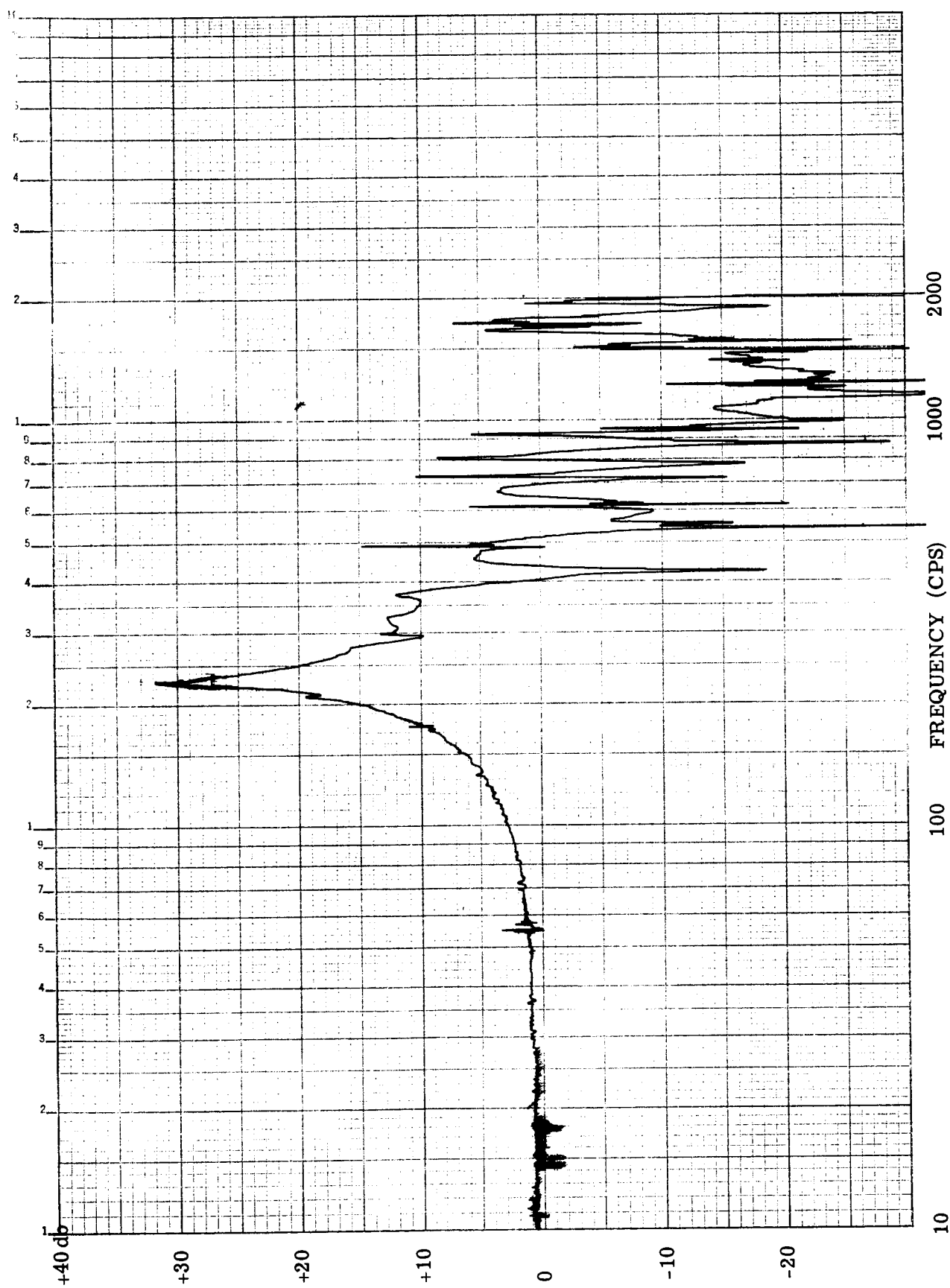


Fig. C-6 Transmissibility Plot of Hopper; Transverse X Axis; Input Level 2 g's

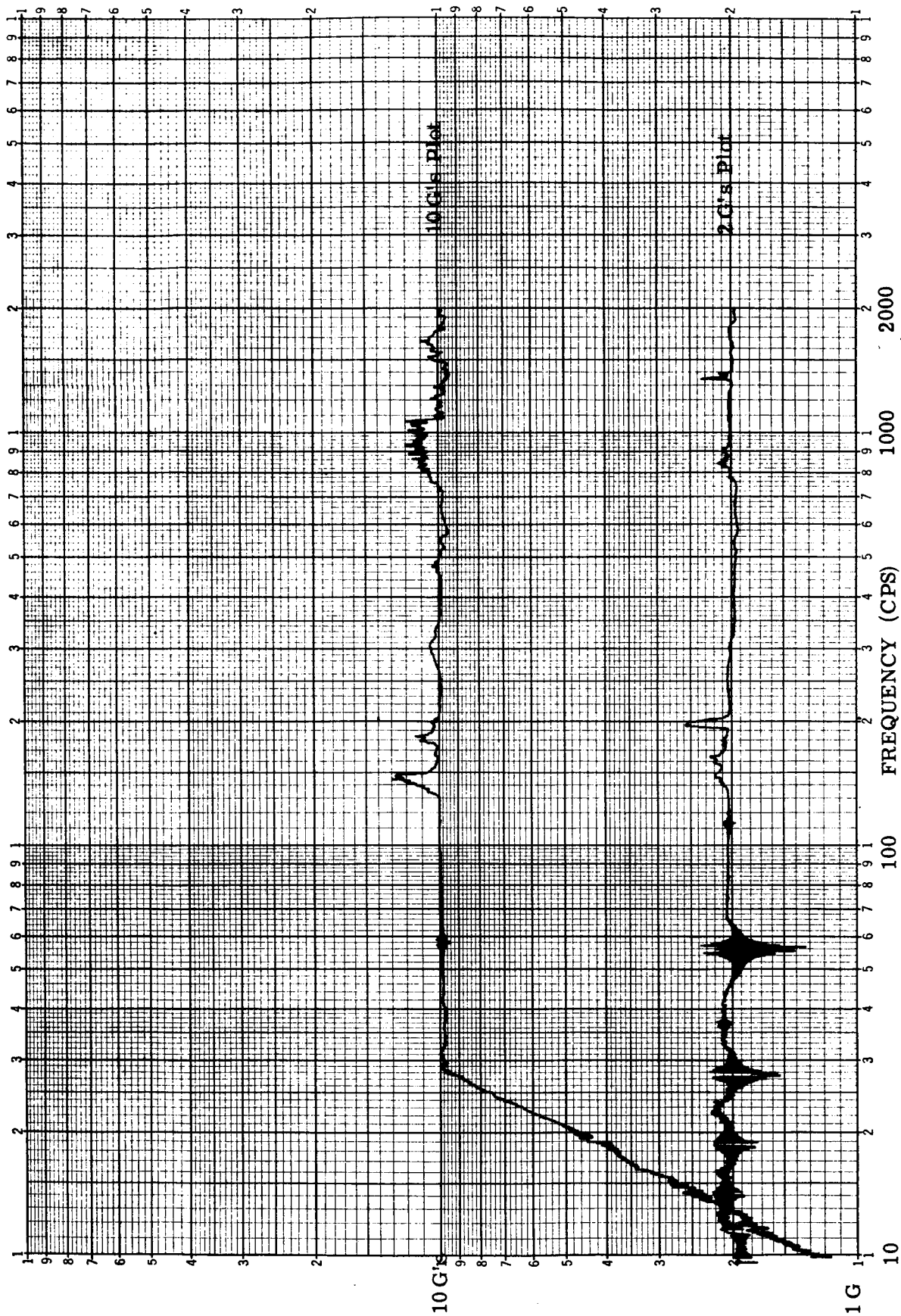


Fig. C-7 Sine Sweep Input Level to Hopper; Transverse Y Axis

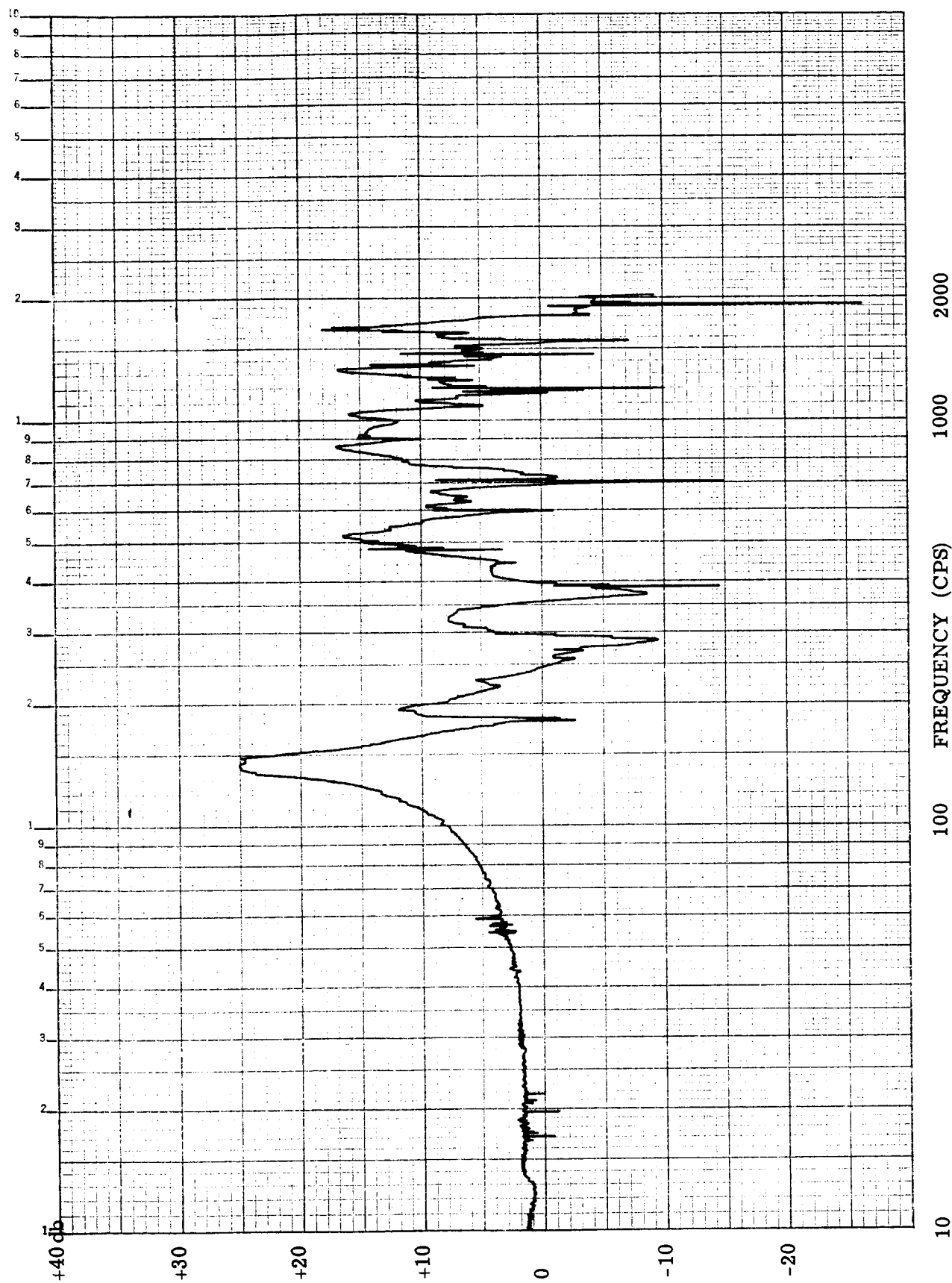


Fig. C-8 Transmissibility Plot of Hopper; Transverse Y Axis; Input Level 2 g's

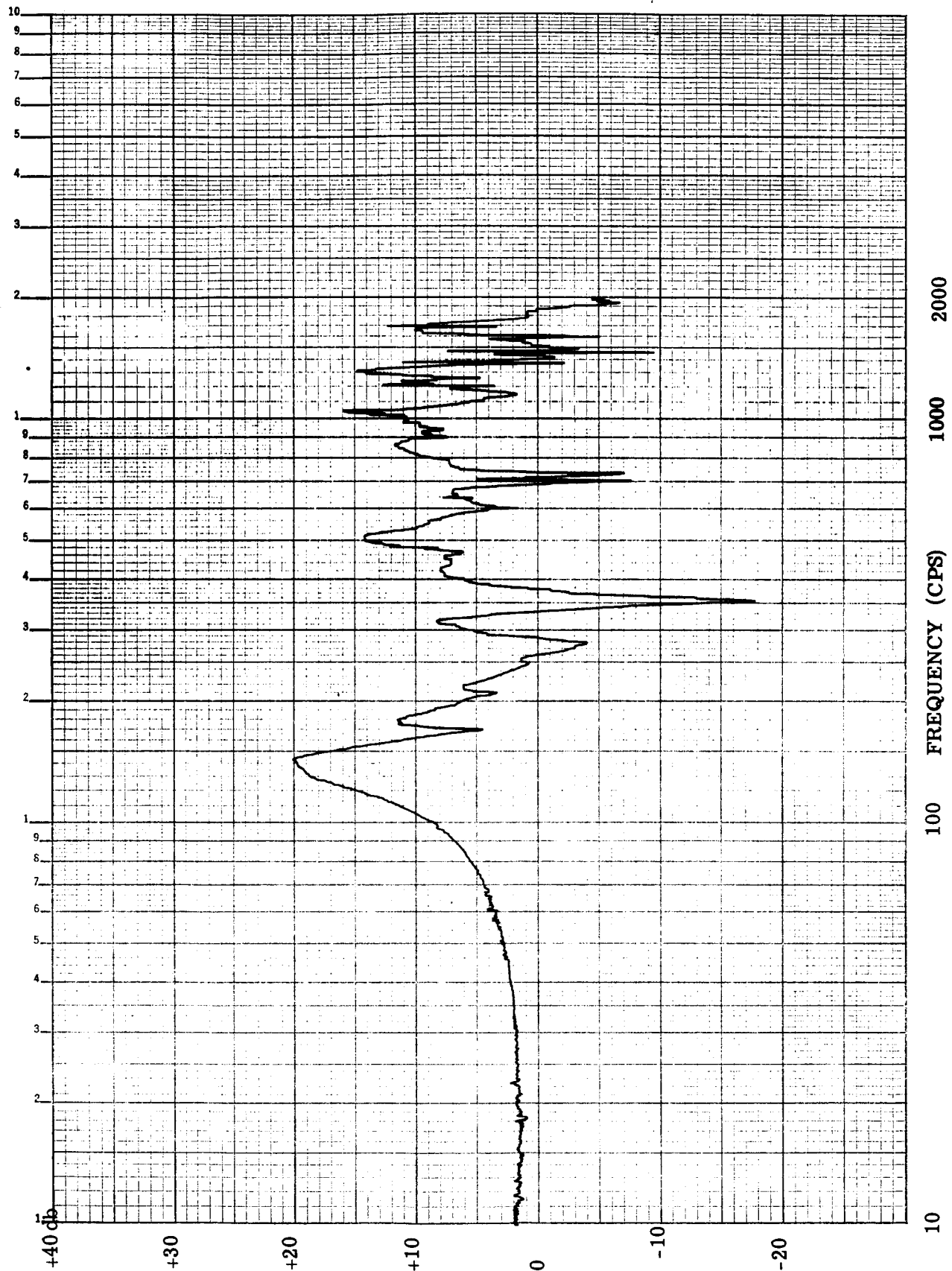


Fig. C-9 Transmissibility Plot of Hopper; Transverse Y Axis; Input Level 10 g's

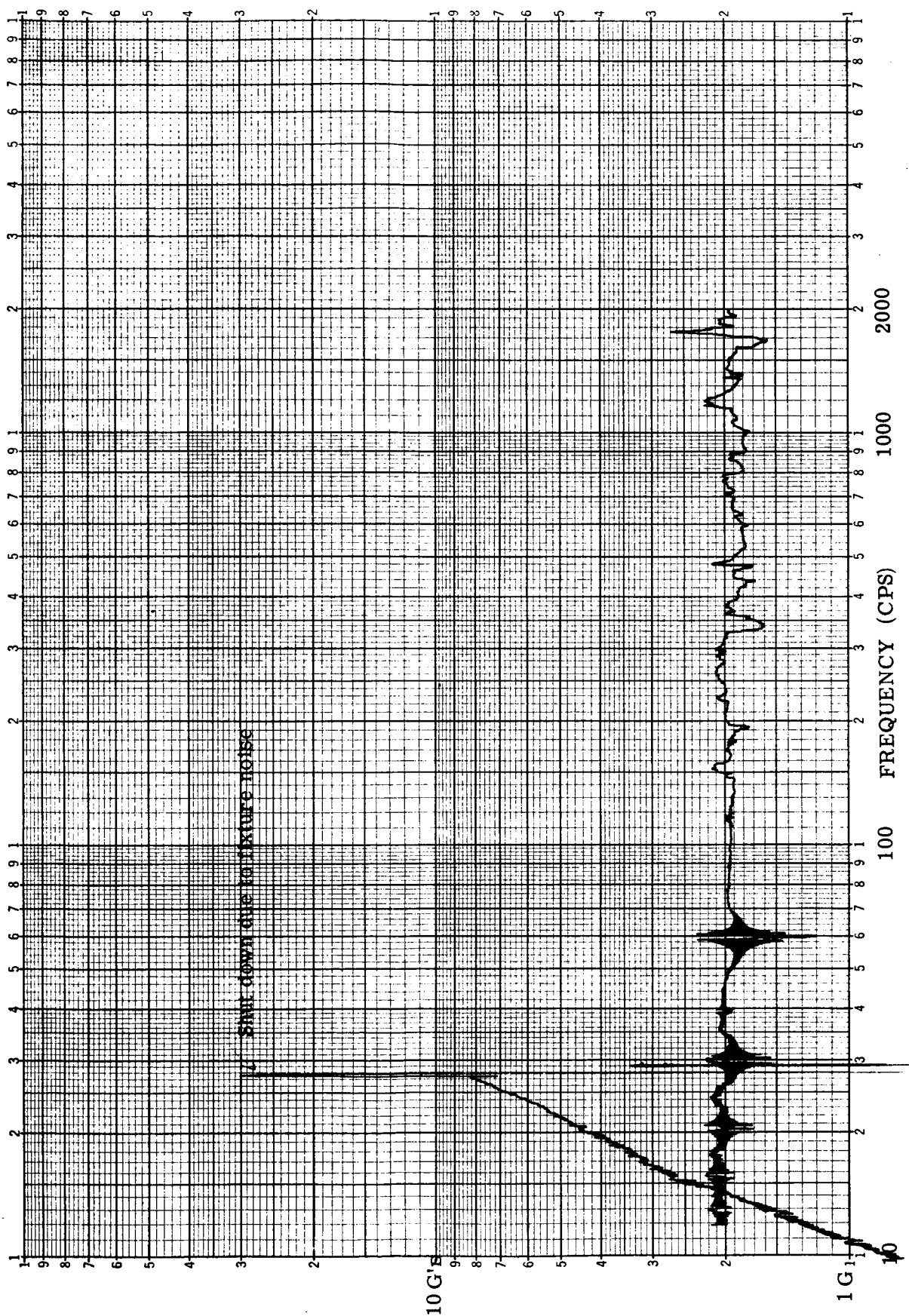


Fig. C-10 Sine Sweep Input Level to Hopper; Thrust Z Axis

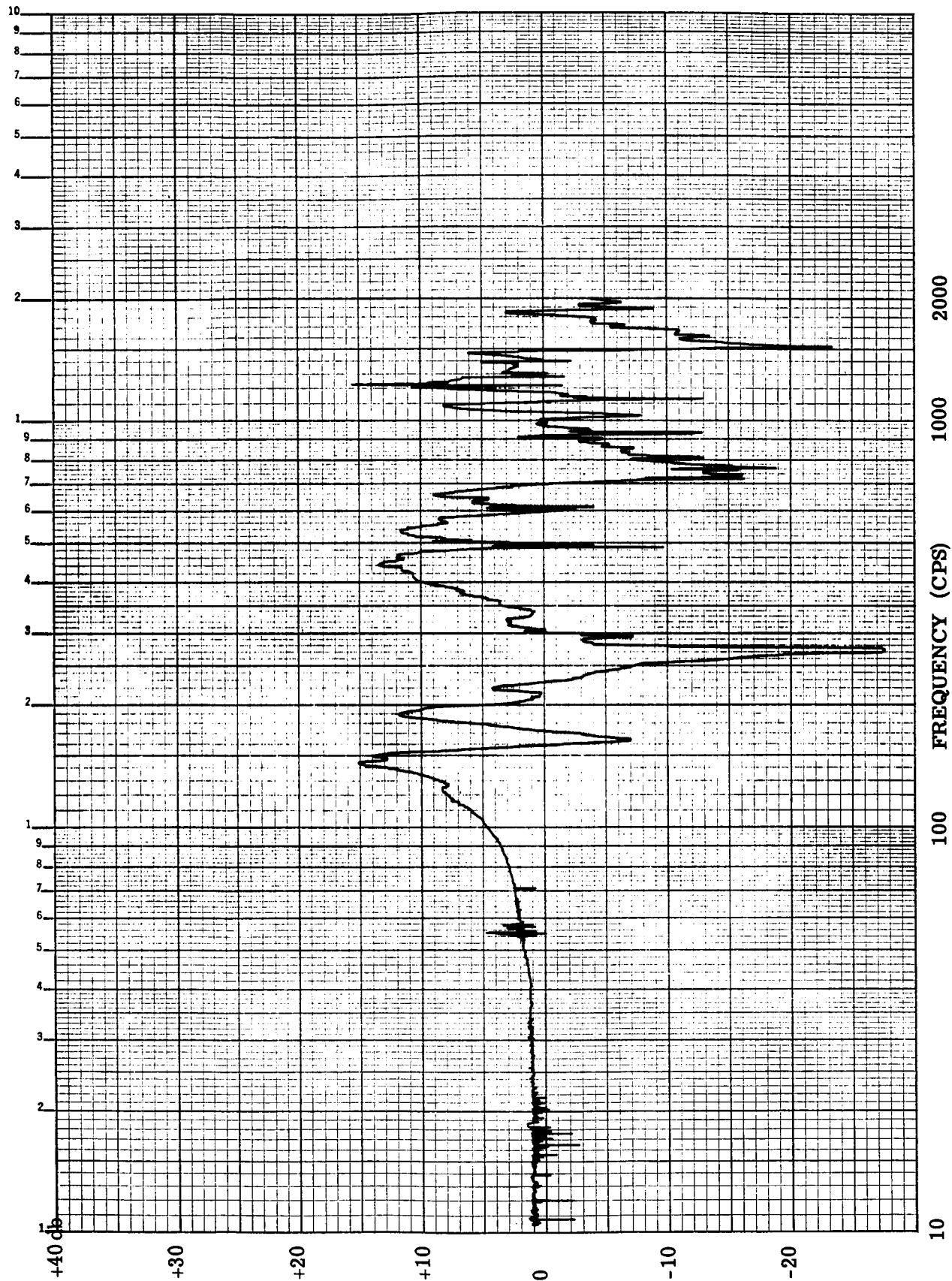


Fig. C-11 Transmissibility Plot of Hopper; Thrust Z Axis; Input Level 2 g's

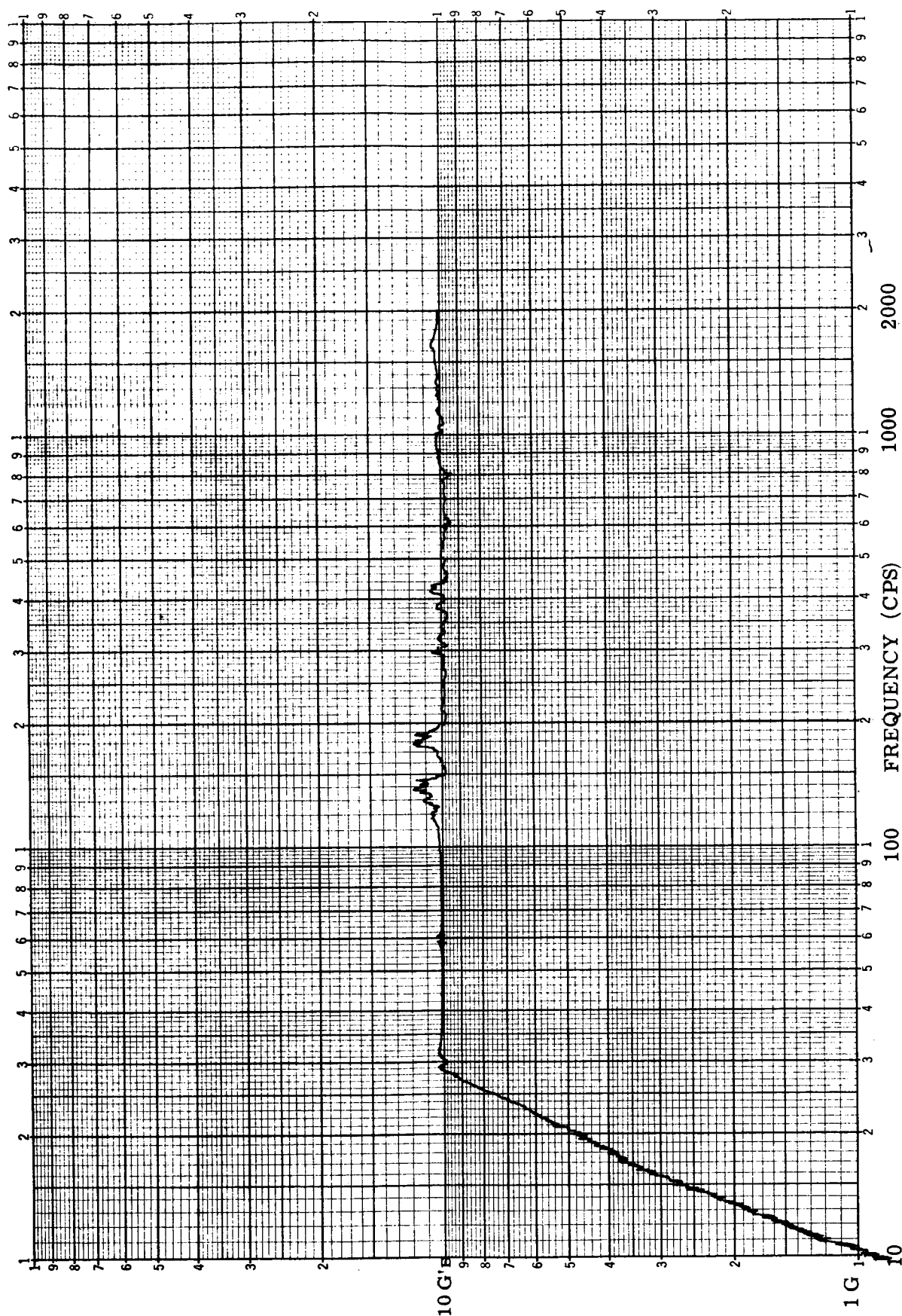


Fig. C-12 Sine Sweep Input Level to Hopper; Thrust Z Axis

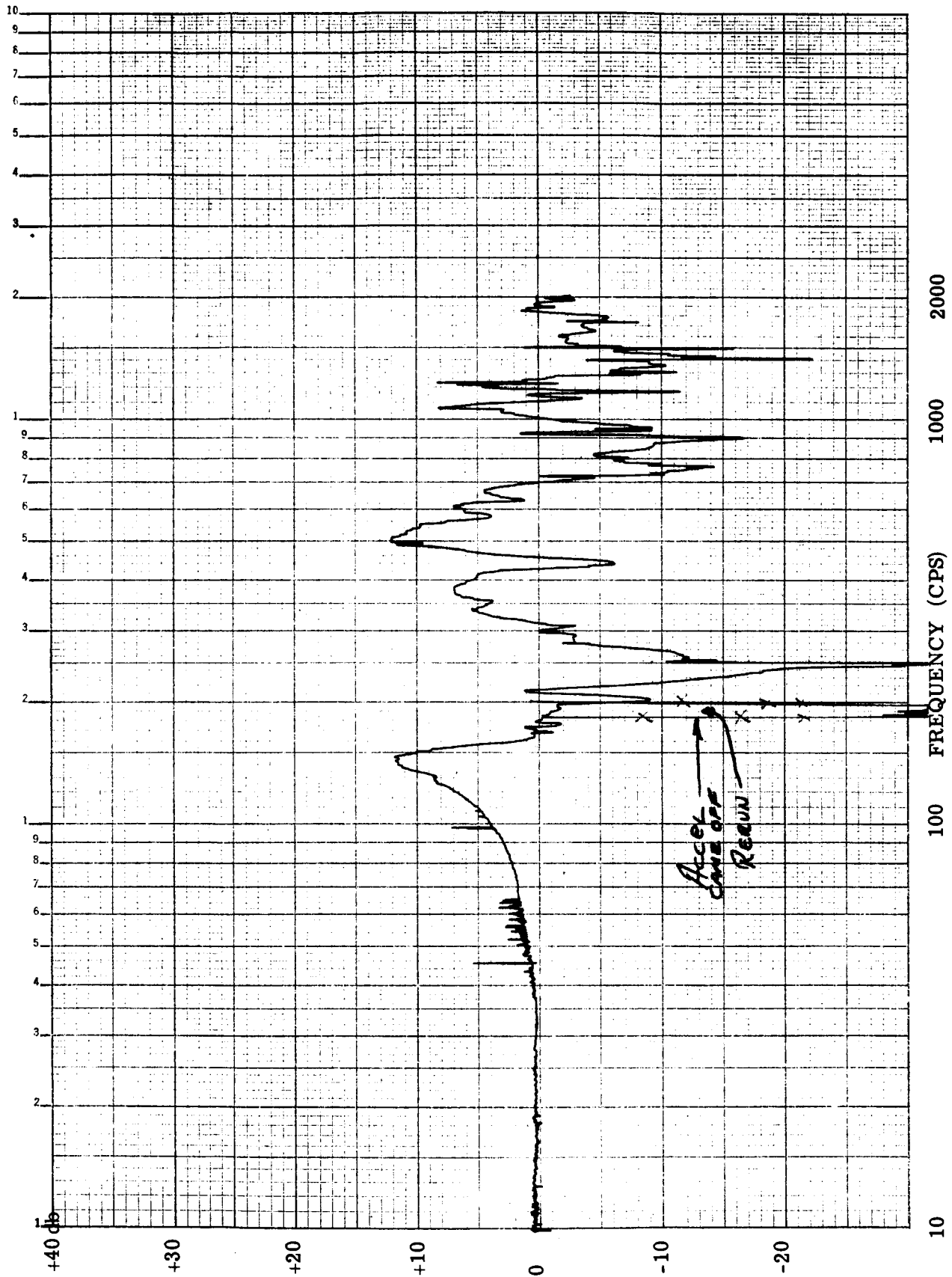


Fig. C-13 Transmissibility Plot of Hopper; Thrust Z Axis; Input Level 10 g's